Investigation of Reaction Mechanisms of OME-Fuels for Implementation in 3D-CFD Simulation of Combustion

Master Thesis in Energy Technology

Thermal Engines

Sindre Løver Hovden

University of Bergen

Geophysical Institute

Western Norway University of Applied Sciences

Department of Mechanical and Marine Engineering

Bergen, June 2019

Western Norway
University of
Applied Sciences

Investigation of Reaction Mechanisms of OME-Fuels for Implementation in 3D-CFD Simulation of Combustion

Sindre Løver Hovden

Universitetet of Bergen (UiB)
Faculty of Mathematics and Natural Sciences
Geophysical Institute
Postboks 7803
5020 Bergen, Norway

In cooperation with:
Western Norway University of Applied Sciences (HVL)
Faculty of Engineering and Science
Department of Mechanical and Marine Engineering
Postboks 7030
5020 Bergen, Norway

Norwegian title:	Undersøkelse av reaksjonsmekanismer for OME-brennstoff for bruk til implementering i 3D-CFD simulering av forbrenning
Author, student number:	Sindre Løver Hovden, 146473
Study program:	Energy technology, Thermal engines
Date:	03 June 2019
Supervisor at HVL:	Peter Edgar Koch
Supervisor at UiB:	Geir Ersland
Supervisor at LVK:	Kai Gaukel
Client:	LVK at TUM
Client's reference:	Georg Wachmesiter
Number of digital files:	1

Preface

First of all would I like to thank the people who gave me the oppurtunity to write my master thesis in Germany, at the Institute of Internal Combustion Engines at the Technical University München. Thank you Lars Magne Nerheim and Georg Wachtmeister.

Second of all would I like to thank my supervisor Kai Gaukel for offering this thesis, for providing an immense amount of supervising and support, and for being friendly. You have made my experience in Germany great.

Peter Edgar Koch and Geir Ersland has provided me with valuable feedback, thank you.

I would also like to thank my fellow students at LVK for all the lunch breaks, all the coffee breaks and all the Dönerstags.

Then I would like to thank my family for the support and for always believing in me. Last, but not least I would like to thank my partner, Ines, for always forgiving me for the late evenings at school, for all the dinners, for reading through my thesis, and finally for keeping me motivated.

Abstract

Oxymethylene ethers (OMEs) are fuels that burn virtually without soot emissions. These synthetically created fuels may someday be an important part of the diesel fuel blend, or even be a substitute for diesel fuel. The fuel is still in the development stage, and only recently investigations into the chemical kinetics of the heavier OMEs have been undertaken. Up till the publication of this thesis, five reaction mechanisms of OME_3 have been released, three of which were published in 2019. This thesis will compare the available reaction mechanisms against reaction kinetic experiments using the 0D/1D simulation software, DARS. The same reaction mechanisms will be implemented in a 3D-CFD comustion simulation using the detailed chemistry combustion model in STAR-CD. The mechanisms will then be evaluated to see if they are adequately developed to give an accurate depiction of a real combustion process using OME_3 as a fuel. The combustion of OME_1 will also be investigated.

From the results from the DARS simulations in this work it was clear that the earliest released reaction mechanism, Sun2016 (released in 2016), had poor performances in the ignition delay time simulations in DARS. The HCCI combustion simulation, also performed in DARS, also showed poor correspondence with experiments. The other three reaction mechanisms had adequate correspondence between experimental data and simulations performed in DARS.

From this work's results from the 3D-CFD combustion simulation in STAR-CD it was shown that, although the Lin2019 mechanism showed somewhat promising results during the 0D and 1D simulations, it diverged during injection in the 3D-CFD combustion simulation.The 3D-CFD combustion simulation of OME_3 using the Sun2016 performed poorly compared to the Ren2019 and the Huang2019 mechanisms both in terms of computational cost and in terms of realistic results. However, the Ren2019 and Huang2019 mechanisms were nevertheless found to create an unrealistic representation of the combustion using OME_3 as fuel. The Sun2016, Huang2019 mechanism were unsuccessful in providing an accurate depiction of the experimental data in the combustion of OME_1. The Ren2019 mechanism did not ignite properly, and the Lin2019 mechanism did not contain OME_1.The ECFM combustion model showed more physically realistic results, thus being more recommended than the detailed chemistry combustion model for simulating the combustion of OME_1.

The OME_3 mechanisms evaluated in this thesis were not adequately developed to give an realistic depiction of the combustion of OME_3. However, since a comparison between experimental data of OME_3 combustion could not be achieved, this needs to be comfirmed through engine tests. The mechanisms did also fail to provide a physically accurate depiction of the combustion of OME_1.

Sammendrag

Oxymetylene etere (OME) er brennstoff som brenner så og si uten utslipp av sot. Disse syntetisk skapte brennstoffene kan spille en viktig rolle i diesel miksen en dag, og kanskje til og med et surrogat for diesel. Brennstoffet er enda i utviklingsstadium, og inntil nylig hadde det ikke blitt utført undersøkelser av den kjemiske kinetikken til de tyngre OMEene. Opptil publiseringen av denne masteroppgaven var det fem kjemiske mekanismer for OME_3 som hadde blitt publisert, der tre av de var utgitt i 2019. Denne oppgaven skal sammenligne de tilgjengelige kjemiske mekanismene mot reaksjonskinetiske eksperiment ved bruk av det 0D/1D simulasjons-programvaren, DARS. De samme kjemiske mekanismene blir så implementert i en 3D-CFD forbrenningsimulasjon ved bruk av den detaljerte kjemi forbrenningsmodellen i STAR-CD. De kjemiske mekanismene vil så bli evaluert for å se om de er utviklet nok til å gi en nøyaktig fremstiling av en real forbrenningsprosess av OME_3 som brennstoff.

Fra resultatene i DARS fra dette arbeidet ble det funnet ut at den første kjemiske mekanismen som ble utgitt, Sun2016 (utgutt i 2016), hadde dårlig overensstemmelse mellom simulering av tenningsforsinkelse og eksperiment. Simulasjonen av HCCI forbrenning, også utført i DARS, viste også dårlig overenstemmelse med eksperiment. De tre andre mekansimene som ble undersøkt viste tilstrekkelig samsvar mellom eksperiment og simulasjoner utført i DARS.

Fra dette arbeidet sine resultater fra 3D-CFD simuleringen av forbrenning bel det vist at, selv om Lin2019 mekanismen viste noenlunde lovende resultater under 0D og 1D simuleringene, divergerte den under injeksjonen i 3D-CFD forbenningsimulasjonen. 3D-CFD simulasjonen forbrenningssimulasjonen av OME_3 utført ved bruk av Sun2016 mekanismen fremviste dårlige resultat med tanke på både beregningstid og realistiske resultat, sammenlignet med Ren2019 og Huang2019 mekanismene. Ren2019 og Huang2019 mekanismene fremviste imildertid urealistiske representasjoner av forbrenningen av OME_3 som brennstoff. Sun2016 og Huang2019 mekanismene gav heller ikke en nøyaktig fremstilling av forbrenningen av OME_1 i sammenligning med eksperimentell data. Ren2019 mekanismen tente ikke, og Lin2019 mekanismen inneholdt ikke OME_1. ECFM-3Z forbrenningsmodellen viste en mer realistiske resultat, og derfor er den anbefalt fremfor den "detaljerte kjemi" forbrenningsmodellen for simulering av forbrenningen av OME_1.

OME_3 mekanismene som ble evaluert i denne oppgaven er ikke utviklet nok til å gi en realistisk fremstilling av forbrenningen av OME_3. Dette må riktignok bekreftes ved å utføre motor tester der OME_3 bli brukt som brennstoff. OME_3 mekanismene klarte heller ikke å gi en fysisk nøyaktig fremstilling av forbrenningen av OME_1.

Table of Contents

List of Acronyms

CFD - Computational Fluid Dynamics

EGR - Exhaust Gas Recirculation

OME - Oxymethyl Ether

ECFM-3Z - 3-Zones Extended Coherent Flame Model

DMZ - Dynamic Multi-Zone

POMDME/PODE - Polyoxymethylene dimethyl ethers

PM - Particulate Matter

HVO - Hydrogenated Vegetable Oil

RCM - Rapid Compression Machine

HCCI - Homogeneous Charge Compression Ignition

PRF - Primary Reference Fuel

CNG - Compressed Natural Gas

UHC - Unburnt Hydrocarbons

C3 - Hydrocarbons with three carbonatoms

CV - Control Volume

SIMPLE - Semi-Implicit Method for Pressure Linked Equations

PISO - Pressure-Implicit with Splitting of Operators

SI - Spark Ignition

DI - Direct Injection

MDF - Mass Density Function

CAD - Crank Angle Degrees

DNS - Direct Numerical Simulation

NIST - National Institute of Standards and Technology

RoHR - Rate of Heat Release

List of Figures

List of Tables

1 Introduction

1.1 Background

To limit global warming, improve air quality in cities and reduce the dependency of fossil fuels, the consumption of fossil fuels needs to be reduced. These fuels are the main energy source of the world and will have to be reduced to reach the different climate goals, like the Paris Agreement or the goals set by the European Commission. The European Commission has set a target for 2050 to reduce the greenhouse gas emissions of 80-95% compared to the greenhouse gas emission levels in 1990. Due to an ever-growing energy demand, this is a huge challenge. The total electricity demand in Germany in 2050 could increase by a factor of 1.1 to 3 compared to the total electricity demand in Germany today, and a factor 3 to 4.5 in the EU-28[1].

This increase in power demand, coupled with the formidable greenhous gas reduction goals, will greatly impact the transport sector. To meet these goals, W. Maus and E. Jacob [2] postulated five hierachically graded criterions of future mobility:

1. CO_2 neutrality
2. Sustainable availability
3. Minimal emissions
4. Cost-effectivness
5. Functionality

This means that fossil fuels used in the transport sector will have to be replaced by electric vechicles and alternative fuels. The alternative fuels can be synthezised from methanol, which can be synthesized using the CO_2 produced in industry and H_2 produced from renewable sources. The alternativ fuel is thus sustainable and CO_2-neutral. Synthetic fuels are expected to have around the same mobility cost as battery electric vechicles[3]. Where the mobility costs include the costs for the production and distribution of the energy carrier as well as the depreciation costs for the acquisition of the vehicle.

For the alternative fuel to be permissible, it needs to have emissions lower than the emission legislations. Fuels without Carbon-Carbon bonds produce a very small amount of soot, and as the oxygen content in the fuel increases, the soot production

decreases. As a result, the NOx-soot trade-off is improved[4]. OME fuels are alternative fuels that have these characterics. They are relatively new and are currently being researched. Investigation of the reaction kinetics of OME can provide insight into the combustion process and allow for opimalization.

The reaction kintics of OME_3 were first investigated in 2016, and five reaction mechanisms have been published where four of them are available online. This thesis will validate the available mechanisms against published chemical kinetic experimental data, and compare them. Later the mechanisms will be implemented in the 3D-CFD comustion simulation of the fuels OME_1 and OME_3. The results will then be compared against the pressure curve, the temperature profile, and the heat release data from an engine using OME_1 (with an additive) as fuel. The original description of this work can be found in appendix C. Although DME and OME_1 is mentioned, the focus was mostly put on OME_3 and some focus was put on OME_1.

1.2 Fuels

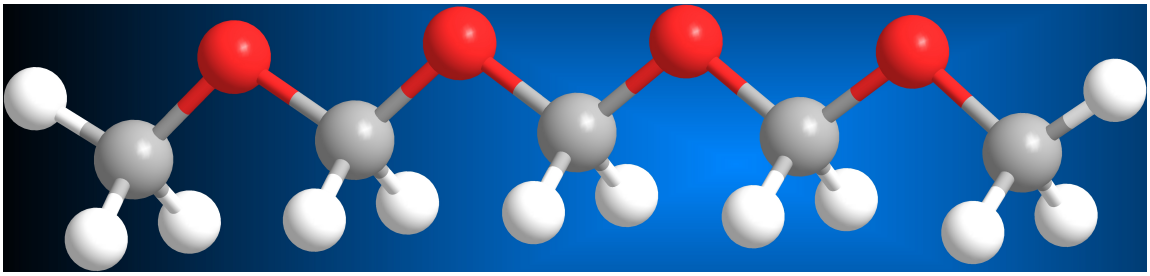

Figure 1.1: 3D model of OME_3. Red dots are oxygen atoms, white dots are hydrogen atoms, and grey dots are carbon atoms. This molecule has three CH_2O groups and is therefore named OME_3.

Oxymethylene ethers (OMEn), short for Polyoxymethylene dimethyl ethers (POMDMEn), are dimethyl ethers (DME) connected with groups of polyoxymethylene (POM). The general formula of OMEn is CH_3-O-(CH_2-O)n-CH_3, where n is the number of oxymethylene groups. Oxymethylene ethers are created synthetically from methanol, and thus may be produced from sustainable raw materials[5]. The properties of OMEn depend on the number of POM groups; OME_0, also known as dimethyl ether (DME), is gaseous at standard conditions, whereas OME_1 to OME_6 are liquid under standard conditions. OMEn with n ranging from $n = 0$ to $n = 6$ are suitable for use as fuels in the diesel engine due to their good ignitability[6].

The most interesting part of the OME fuels is the soot production, or rather the lack of it. The lack of Carbon-Carbon bonds in the molecular structure and high oxygen

content inhibits the production of soot precursors like C_2H_2, C_2H_4 and polycyclic-aromatic hydrocarbons (PAH). OMEn can also be mixed with diesel in any ratio.[7] Another attractive property of OMEs is that they are without toxic properties[8].

Table showing properties of OMEs:[9]

Table 1.1: Properties of OMEn

OMEn	OME_1	OME_2	OME_3	OME_4	OME_5	OME_6
Molecular formula	$C_3H_8O_2$	$C_4H_{10}O_3$	$C_5H_{12}O_4$	$C_6H_{14}O_5$	$C_7H_{16}O_6$	$C_8H_{18}O_7$
Oxygen content [wt%]	42.1	45.2	47.0	48.1	48.9	49.5
Boiling point [°C]	42	105	156	202	242	273
Melting point [°C]	-105	-70	-43	-10	18	38
Cetane number	29	63	67	76	90	unknown
Lower heating value [MJ/kg]	22.4	20.6	19.4	18.7	18.1	17.7
Density [kg/m^3]	0.86	0.98	1.03	1.07	1.11	1.14

As the number of oxymethylene groups increases, the oxygen content increases and as a result the lower heating value decreases. However, the heating value with respect to volume almost stays constant because the density also increases. The cetane number also increases as the number of oxymethylene groups increases, the same do the freezing point and boiling point. Due to the low viscosity and poor lubrication properties, OME_1 should have a lubricity enhancer added when used as a neat fuel in order to avoid engine damage[10]. For OME_3 and higher, the lubricity is satisfactory without lubricity enhancers.

The flash point of OME_2 has been measured to be 17.4 °C , this is far below the Norwegian standard of > 55 °C for diesel fuels[11]. This makes OMEn with $n < 3$ a flammable liquid like petrol, and may lead to some safety complications. The high vapor pressure of OME_1 makes vapor lock likely to occur [12]; this can be prevented by a pressurized fuel system. For OMEs with $n > 1$ the vapor pressure is lower and the viscosity is higher so there is no need for a pressurized fuel tank system[13]. However, the low freezing point of OMEs with $n > 3$ makes blends with high contents of these OMEs less suitable for cold conditions. Thus the most suited OME for use

as a neat fuel is OME_3. However, the most probable scenario would be a blend of OMEs. And then OME_3 and OME_4 would be the most desired OMEs to be blended with diesel[14]. $OME_{3\text{-}5}$ blended with diesel with an $OME_{3\text{-}5}$ volume fraction of more than 10–12% cannot be used in non-dedicated engines[15] .

A blend of OME_{3-6} is already available in large scale production, and as can be seen from figure 1.2, it can be made cheaper than diesel fuel on a volume basis. The price of OME_{3-6} depends on the price of methanol and the OME synthesis-process. However, diesel fuel has almost twice the heating value on volume basis of that of OME_{3-6}, thus making OME_{3-6} more expensive than diesel.

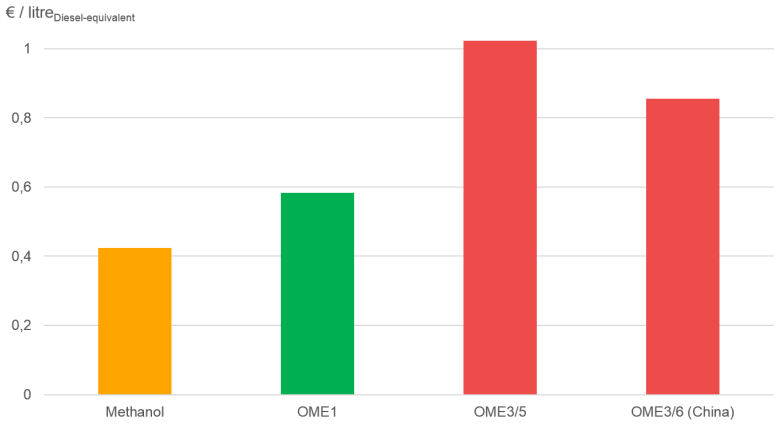

Figure 1.2: The cost of C1-based fuels compared to diesel[8].

1.3 Literature survey

The soot inhibiting properties of DME and OME_1 have long been known. And the first detailed reaction kinetic model for OME_1 was developed in 2001 by Daly et al.[16]. Using ab initio quantum chemistry and statistical methods, thermochemical data and kinetics of the ($O\text{-}CH_2\text{-}O$) group, that is important in OMEs, was calculated by Kopp et al. in 2018[17]. Based in this study, the most recent detailed reaction mechanism for OME_1 was created by Jacobs et al.[18] in 2019.

However, the first engine tests proving the soot inhibiting properties of POMDME, was performed by T.H Fleisch and R.A Sills in 2004[19]. They tested a blend of $OME_{3\text{-}8}$ with diesel and observed dramatic reductions in soot (particle matter) emissions and some reduction in NOx and UHC emissions. Lump et al.[20] tested blends of B7 diesel with 10% and 20% volume fraction of $OME_{3\text{-}4}$ in 2011. The results were a reduction of 40-50% PM emissions and 50-60% soot emissions with

the 20 % $OME_{3\text{-}4}$ blend, and a reduction of over 40% PM emissions and 30-40% soot emissions with the 10% $OME_{3\text{-}4}$ blend.

Pellegrini et al.[15] performed engine tests in a Euro-3 engine using a neat $OME_{3\text{-}5}$ blend in 2012. Results showed that Euro 5 emission limits were reached without a diesel particle filter. In 2013, Pellegrini et al.[21] also performed engine tests with vehicle with a Euro-2 engine using the same $OME_{3\text{-}5}$ neat blend in the New European Driving Cycle (NEDC) test. They observed a reduction in PM emissions by 77% compared to diesel fuel emissions. However, they also observed an increase of 34.5% in UHC + NOx emissions and an increase of 60% in CO emissions.

Until 2014, OMEn (n=3,4,5) had only been available in small samples, but this changed as an OMEn production site in China with a capacity of 10 kton/year opened in 2014, with a production cost close to that of diesel.[22] This made OMEn (n=3,4,5) cheaper and more available for experiments. In 2015, Liu et al.[23] performed engine tests with OME/diesel blends where the OME mainly consisted of OME_3 with a mass distribution of $OME_2/OME_3/OME_4$ = 2.553%/88.9% /8.48%. The volume fraction of the OME in the OME/diesel blend was 10% and 20%. More than 90% reduction in soot emissions, compared to emissions from regular diesel combustion, was observed with the 20% OME blend. Also here an increase in NOx emissions was observed; overall the NOx emissions were increased by 16% in the 20% OME blend. However, with the same blend the CO-emissions were 90% lower than those of regular diesel combustion.

In 2017, Härtl et al.[9] performed engine tests of HVO, OME_1 with additives, and an $OME_{3\text{-}6}$ blend in a heavy-duty single-cylinder research engine. The engine was equipped with a diesel oxidation catalyst (DOC) and exhaust gas recirculation (EGR) was performed at different operating points. The results showed very low emissions of particles and unburnt components for the combustion of OME_1 with the additives and the $OME_{3\text{-}6}$ blend. However, an increase in methane emissions was observed close to stoichiometric conditions. By using EGR, the NOx-soot tradeoff was avoided.

In 2016, the first reaction mechanism developed for OME_3, termed Sun2016 in this thesis, was proposed by Sun et al.[24]. The mechanism was developed based on the first investigations of the chemical kinetics of OME_3 also performed by Sun et al. The investigatioms focused on the high temperature region for OME_3 and was used to validate the mechanism. These experiments consisted of species concentration from a laminar premixed burner, and laminar flame speed from a freely propagating flame.

Based on the Sun2016 mechanism, He et al.[25] published a comprehensive combustion mechanism for OME_3 in 2018, termed He2018 in this paper. He et al. focused on the low- and intermediate temperature region. This region is important when simulating diesel engine combustion, it is in this region the fuel is injected in and

ignition occurs. Therefore, a mechanism accurately describing this region is essential in the simulation of the combustion process of OMEs. In the study, He et al. used a rapid compression machine (RCM) to perform ignition delay time experiments were performed in the temp range (conditions). HCCI combustion experiments performed by Wang et al.[22] in 2016 were also validated against the pressure profile and rate of heat release. The detailed OME_3 mechanism consisted of 225 species and 1082 reactions.

In 2017, the detailed OME_3 mechanism, He2018, was combined with a reduced diesel/gasoline mechanism created by Ren et al.[26]. This detailed PRF-OME_3 (Primary reference fuel) mechanism[27] was then validated against a combustion of a OME_3/gasoline/diesel blend (30% OME, 35% gasoline, 35% diesel) in a DICI engine. The merged mechanism contained 354 species and 943 reactions.

To improve compatibility with 3D-CFD simulation, Ren et al.[28] created a reduced mechanism for diesel/gasoline/OME_3 blend in 2019. The base mechanism was taken from earlier work[26]. The sub-mechanism for OME_3 was based on the detailed He2018 mechanism. This sub-mechanism was reduced using an iterative reduction procedure which included direct relation graph with error propagation, sensitivity analysis and finally isomer lumping. This newly developed mechanism was validated against the experiments from Sun et al.[24], He et al.[25] and Wang et al.[22]. The final version of the reduced mechanism contained 145 species and 585 reactions, including PAH and NOx sub-mechanisms.

Lin et al.[29] created a new mechanism consisting of skeletal sub-mechanisms of various fuels integrated with a reduced C2-C3 mechanism and detailed H2/CO/C1 mechanism 2019. This mechanism consisted of a newly developed PRF mechanism and a skeleton sub-mechanism for PODE. The PRF mechanism was based on the work of Chang et al.[30] and Liu[31]. The OME_3 sub-mechanism of He2018 was reduced using sensitivity analysis. The reduced OME_3 sub-mechanism was then integrated into the PRF main-mechanism utilizing the decoupling methodology. The mechanism was validated against the experiments from Sun et al.[24], He et al.[25] and Wang et al.[22]. The final size of the PRF-PODE3 mechanism contained 61 species and 190 reactions, of which the OME_3 sub-mechanism contained 11 species and 19 reactions. Emission prediction was left out of the mechanism, to make the mechanism more compact. OME_1 and OME_2 was not included in the mechanism.

Motivated by the experimental studies on OME_n/CNG and diesel/CNG conducted by Song et al.[32] , the first OME_n/NG (Natural gas) dual fuel mechanism was developed by Huang et al.[33] in 2019. This mechanism was based on the detailed OME_3 mechanism devopled by He2018 and a reduced natural gas mechanism devolped by Huang et al.[34] in 2019. The detailed OME_3 mechanism created by He et al.[25] was reduced using direct relation graph, direct relation graph with error propagation, rate of production, and sensitivity analysis. The reduced OME_3 mechanism

was then combined with the reduced natural gas mechanism. The final version of the combined mechanism for PODEn/NG contained 124 species and 650 reactions.

An overview of the mechanisms compared in this work

Table 1.2: Overview of the OME_3 mechanisms

Mechanism	Number of species	Number of reactions	Base mechanism	Includes OME_1
Lin2019	61	190	PRF	no
Ren2019	145	585	PRF	yes
Sun2016	274	1674	OME_3	yes
Huang2019	124	650	NG	yes

2 Theory

This chapter will present the fundamental theory behind the software used. Chapter 2.1 introduces chemical kinetics which describes how reactions take place. Chapter 2.2 introduces the governing equations of fluid flow, the finite volume method, and how these can be used in computational software. Finally, the software used in this thesis will be presented in chapter 2.3.

2.1 Chemical Kinetics

After knowing the initial stage of a reactive mix, chemical thermodynamics can be used to determine the final state after chemical and thermal equilibrium have been established. However, chemical thermodynamics is not able to determine how the reactive mix got to the final stage and how long it took. Using chemical kinetics, it is possible to predict the path a reactive mix takes to the final state.

Chemical kinetics is the study of the elementary reactions and their rates. And is a specialized field of physical chemistry. Chemical kinetics is used in many different scientific fields that require precise knowledge of a reaction mechanism, like for example combustion. In many combustion processes, chemical reaction rates control the rate of combustion, and, in essentially all combustion processes, chemical rates determine pollutant formation and destruction. Also, ignition and flame extinction are intimately related to chemical processes. Understanding chemical kinetics, combustion processes can be better understood and optimized.

2.1.1 Rates

The rate of a chemical reaction is the change in the amount of reactants or products per unit time. Reaction rates are therefore determined by measuring the time dependency of some property that can be related to the number of reactants or products, this property is usually the concentration c [moles/volume]. The rate of change, ω, in the molar concentration of species i is given by equation 2.1.

$$\omega = \frac{dc_i}{dt} = k \cdot c_i^n \tag{2.1}$$

This rate of change is quantified by the reaction rate coefficient, k. The units of k depend on the overall reaction order. The reaction order, denoted by n, is the relationship between the concentrations of species and the rate of a reaction, it is found by doing experiments.

The Arrhenius law

In general, the rate of a chemical reaction is accelerated by an increase in temperature. The modified Arrhenius equation (2.2) relates the chemical reaction rate constant to the temperature.

$$k = A \cdot T^b exp\left(\frac{-E_A}{R}\right) \tag{2.2}$$

Where A is called the pre-exponential factor and is related to molecular collision, and R is a gas constant. b is an exponent used to fit rate data with experimental data.

2.1.1.1 Global reactions

The overall reaction of fuel with an oxidizer to form combustion products can be expressed by the global reaction mechanism shown in equation 2.3.

$$Fuel + Oxidizer \rightarrow Products \tag{2.3}$$

The use of global reaction to express the chemistry in a specific problem could be called a "black box" approach. This approach does not provide a basis for understanding what is actually happening chemically in a system. The reaction (2.3) indicates that the process is a one-step process and happens instantaneous. In reality, many succeeding processes can occur involving many intermediate species. These succeeding processes are called elementary reactions.

2.1.1.2 Elementary reactions

An elementary reaction is a single step reaction with a single transition state and no intermediates. The elementary reactions express how molecules and ions are actually reacting with each other. There are different types of elementary reactions based on the molecularity of the reaction. The molecularity is the number of atoms or species that interact with each other at the molecular level. There are three types of elementary reactions: unimolecular reactions, bimolecular reaction, and termolecular reactions.

Unimolecular reactions

Unimolecular reactions describe the chemical process in which a reactant undergoes decomposition or rearrangement to produce one or more products. This is expressed in equation 2.4.

$$Reactants \rightarrow Products \tag{2.4}$$

The reaction rate of a unimolecular reaction is expressed by equation 2.5. The units of k is [1/s].

$$\frac{dc_A}{dt} = k \cdot c_A \tag{2.5}$$

Bimolecular reactions

Most elementary reactions of interest in combustion are bimolecular; that is, two molecules collide and react to form two different molecules. Thus, a comprehensive understanding of bimolecular reactions is very important in seeking to comprehend chemical kinetics. All elementary bimolecular reactions are overall second order, being first order with respect to each of the reacting species. An arbitrary bimolecular reaction may be expressed by equation 2.6.

$$A + BC \rightarrow AB + C \tag{2.6}$$

A reaction rate of a bimolecular reaction is expressed by equation 2.7. The units of k is [1/cs]

$$\frac{dc_A}{dt} = k \cdot c_A c_B \tag{2.7}$$

Termolecular reactions

Termolecular reactions involve the collision three reactant species. Three molecules collide at an instant is rare, but occasionally these are some of the ways reactions take place. Termolecular reactions are third order. An example of how a termolecular reaction may look is given in equation 2.8

$$A + B + C \rightarrow AB + C \tag{2.8}$$

A reaction rate of a termolecular reaction is expressed by equation 2.9. The units of k is [1/c^2s]

$$\frac{dc_A}{dt} = k \cdot c_A c_B c_C \tag{2.9}$$

2.1.2 Collision theory

The collision theory is based on the kinetic theory of gases and explains how chemical reactions occur when molecules with sufficient kinetic energy collide. In order for the reaction to occur the particles must collide with sufficient energy and correct orientation. The orientation of the molecules depends on a geometrical factor that is called the steric factor, p. The steric factor, also called probability factor, takes into account the geometry of collisions between A and BC. The minimum energy that the colliding molecules must possess to overcome the repulsive and bonding forces of the reactants is called the activation energy, (E_A). These factors may not be determined by collision theory. However, these factors may be determined using a more advanced theory.

2.1.3 Transition state theory

During a collision, a highly energized unstable molecule called the activated complex is formed. This activated complex is also called the transition state and is described by the transition state theory. The transition state theory of reaction rates examines the state of the activated complex and its influence on the reaction rate. Transition state theory makes two essential postulates, which may be summarized as follows:

1. During the reaction of A with BC, there will exist a configuration of the atoms that can cause the activated complex to spontaneously undergo a reaction, either to the reaction products or back to the reactants.
2. The activated complex is assumed to be in effective equilibrium with the reactants.

These postulates may be summarized in equation 2.10. The transition state is represented by the symbol, ‡.

$$A + AB \rightleftharpoons ABC^{\ddagger} \rightarrow AB + C \tag{2.10}$$

The thermodynamic and statistical properties can be specified using the transition state theory, and ultimately the activation energy and the steric factor may be determined.

2.1.4 Reaction mechanisms

The collection of elementary reactions necessary to describe an overall reaction is called a reaction mechanism. Reaction mechanisms consists of step by step descriptions of what happens at molecular level in chemical reactions. Each step of the

reaction mechanism consists of elementary reactions. The number of steps in a reaction mechanism may only be a few steps, or even as many as several hundred. A reaction mechanism is only a rationalization from which a rate law that agrees with the observed rate laws can be worked out. Therefore, although a mechanism explains the experimental results, it is not a proof that the mechanism is correct.

Chemical kinetic modelling

A lot of progress has been made to define the detailed chemical pathways leading from reactants to products, and to measure or calculate their associated rates. Chemical kinetic models are made from this knowledge and are used to simulate reacting systems. The fundamental principles of kinetic modelling are based on the conversion of chemical reaction mechanisms into the constituting differential equations, applying the law of mass action. The law of mass action states that the rate of a chemical reaction is proportional to the product of the concentrations of the reactants. The sets of differential equations describing the rates of formation and destruction of each species are then numerically integrated. The computed concentrations of reactants, intermediates and products are compared to experimental data. Experimental data may be obtained using various experimental techniques, these techniques must fulfil the following criteria:

- bring the reactants together, mix them and initiate the reaction on a timescale that is negligible compared to that of the reaction.
- measure the concentration of reactants or products as a function of time after initiation.
- accurately measure and control the temperature (and for some reactions, the pressure) at which the reaction occurs.

These criteria are relatively easily fulfilled for reactions occurring on timescales of minutes and hours. However, the combustion of diesel at 3000 RPM is occurring on a timescale of a few milliseconds. Thus, making it hard to measure the various combustion characteristics. Examples of techniques used for performing reaction kinetic experiments are: rapid compression machines, premixed flat burners, freely propagating flame, and shock tubes.

Model reduction

Detailed reaction mechanisms may involve more than hundreds of chemical species, resulting in more than a hundred partial differential equations. These chemical species react with anywhere from hundreds to more than a thousand of elementary reactions. These kinetic processes cover time scales from nanoseconds to seconds. If detailed reaction mechanisms are coupled with CFD models tremendous computational resources are required. Therefore, there is a desire for reduction in size of the detailed reaction mechanisms.

Reduced reaction mechanisms contain only the critical elements of the full mechanism. However, these models are still large when used in detailed CFD calculations. Skeleton models consists of only a few generalized reactions and species, and is based on chain-branching reactions. Chain-branching reactions involve the formation of two radical species from a reaction that consumes only one radical. Skeleton models are more suitable for detailed CFD calculations. However, at the cost of accuracy. Simplification of reaction mechanisms, which are valid for the combustion problems, are therefore an important part of kinetic modelling. The aim of model reduction is the development of models, which are as simple as possible in the sense of an efficient description, and also as detailed as necessary in the sense of reliability.

The goal of model reduction is to find the best compromise between computational efficiency and reliability. The model should be as reduced as possible to reduce the computational cost, but also as detailed as possible to give reliable predictions. Example of reduction methods are: sensitivity analysis, reaction flow analysis, and lifetime analysis. These methods are briefly described below:

- Sensitivty analysis identifies the species and reactions that are are sensitive to the governing parameters. The unsensitive species and the unsensitive reactions are unimportant and can be removed.
- Reaction flow analysis identifies the major and minor pathways the reactants take to the products. By combining sensitivity analysis and reaction flow analysis, ne the skeleton mechanism can be created.
- Lifetime analysis considers the time a species exist. If a species has a much slower prodcution rate than consumption rate, it is short lived. Quasi-steady state can then be assumed to simplify the system.

2.2 Computational Fluid Dynamics

Computational fluid dynamics (CFD) is the analysis of systems involving fluid flow, heat transfer and associated phenomena such as chemical reactions by means of computer-based simulation[35]. CFD modelling is a very useful tool that has become an essential part of the optimization and design of modern combustion engines. Processes such as the fuel injection, the spray propagation, evaporation and mixing with charge air, turbulent combustion and auto-ignition can be simulated using CFD models. However, typical applications often involve complex three-dimensional geometries, and turbulent flow characteristics. When combustion is to be modelled, the chemistry of the system also must be taken into consideration, complicating the simulation further. Usually chemical accuracy is sacrificed for accuracy in the calculation of flow or the geometry. Reduced mechanisms are used instead to smooth the

calculation time, and to maintain the chemical accuracy to an extinct.

CFD software are usually expensive, but it can replace the need for an expensive experimental facility. Furthermore, CFD can be used in areas where traditional experiments cannot, e.g., systems where controlled experiments are hard to perform, systems where the environment is hazardous.

CFD codes contain three elements: a pre-processor, a solver, and a post-processor.

- The Pre-processor is where the problem is set up. Here the geometry and the fluid properties are defined, the grid is generated, the physical and chemical phenomena are selected, and the boundary conditions are specified.
- The solver is where the problem is solved. Here the governing equations of fluid flow (continuity, momentum, and energy equations) are integrated over finite control volumes. The control volumes are then discretized, and the integral equations are turned into algebraic equations which are solved by an iterative method.
- The postprocessor is where the problem is analyzed. Here the solution to the problem can be exported and visualized by the use of graphs, particle tracking and animations.

2.2.1 Governing equations of fluid flow

From the basic conservation principles – conservation of mass, energy and momentum, the governing equations of fluid flow can be derived. For a viscous flow, these equations are also called the complete set of Navier-Stokes equations[36]. The complete set of Navier-Stokes equations consist of the continuity equation (2.11), the energy equation (written in total enthalpy form) (2.12), and the momentum equations (2.13)

The complete set of Navier-Stokes equations assume that the fluid is a continuum and is not made up of discrete particles. These equations are a connected system of non-linear partial differential equations, and very hard to solve without using numerical methods. To simulate fluid flow, these equations must be solved. These equations are listed below.

$$\frac{\partial \rho}{\partial t} + \nabla \cdot (\rho \vec{u}) = 0 \tag{2.11}$$

$$\frac{\partial(\rho H)}{\partial t} + \nabla \cdot (\rho H \vec{u}) = \nabla \cdot (\lambda \nabla T) + \frac{\partial p}{\partial t} + \left[\frac{\partial u\tau_{xx}}{\partial x} + \frac{\partial u\tau_{yx}}{\partial y} + \frac{\partial u\tau_{zx}}{\partial z} + \frac{\partial v\tau_{xy}}{\partial x} + \frac{\partial v\tau_{yy}}{\partial y} + \frac{\partial v\tau_{zy}}{\partial z} + \frac{\partial w\tau_{xz}}{\partial x} + \frac{\partial w\tau_{yz}}{\partial y} + \frac{\partial w\tau_{zz}}{\partial z} \right] + S_h \quad (2.12)$$

$$\frac{\partial(\rho u)}{\partial t} + \nabla \cdot (\rho u \vec{u}) = -\frac{\partial p}{\partial x} + \frac{\partial \tau_{xx}}{\partial x} + \frac{\partial \tau_{yx}}{\partial y} + \frac{\partial \tau_{zx}}{\partial z} + S_{Mx} \quad (2.13)$$

$$\frac{\partial(\rho v)}{\partial t} + \nabla \cdot (\rho v \vec{u}) = -\frac{\partial p}{\partial y} + \frac{\partial \tau_{xy}}{\partial x} + \frac{\partial \tau_{yy}}{\partial y} + \frac{\partial \tau_{zy}}{\partial z} + S_{My}$$

$$\frac{\partial(\rho w)}{\partial t} + \nabla \cdot (\rho w \vec{u}) = -\frac{\partial p}{\partial z} + \frac{\partial \tau_{xz}}{\partial x} + \frac{\partial \tau_{yz}}{\partial y} + \frac{\partial \tau_{zx}}{\partial z} + S_{Mz}$$

Where $\vec{u}$ is the velocity field in Cartesian coordinates and is give by: $\vec{u} = u\vec{i}+v\vec{j}+w\vec{k}$. $\vec{i}$, $\vec{j}$, and $\vec{k}$ are the unit vectors along the x,y, and z axes. The components of velocty for x,y,z are u,v, and w respectively. H is total enthalpy and is defined as: $H = U + \frac{p}{\rho} + \frac{1}{2}(u^2 + v^2 + w^2)$. U is internal energy, ρ denotes density, t is time, λ is thermal conductivity, τ is the shear stress and S is the source term.

The complete set of Navier-Stokes equations contains a few unknowns. Four of the unknowns are thermodynamic variables that can calculated under the assumption of thermodynamic equilibrium, i.e. the fluid adjusts itself to new conditions, so the changes are considered to be instantaneous. By using the equations of state (2.14), the state of a substance under thermodynamic equilibrium can be described by knowing two variables, density, ρ, and temperature, T.

$$p = p(\rho, T) \qquad U = U(\rho, T)) \quad (2.14)$$

In compressible fluids the equations of state can link the energy equation and the momentum, and the conservation of mass equations. However, this is not possible for incompressible fluids, as there is no density variation. Therefore, only the mass conservation and momentum equations are needed to solve flow fields in incompressible flows, apart from heat transfer problems where the energy equation also is needed.

There are now seven equations with seven unknowns. Because the number of equations is the same as the number of unknowns, the system is mathematically closed. This means that the system can be solved if initial and boundary conditions are provided.

A general variable Φ is introduced to generalize the conservative form of the governing equations. The generalized form can be written as:

$$\frac{\partial}{\partial t}(\rho\Phi) + \nabla \cdot (\rho \vec{u} \Phi) = \nabla \cdot (\Gamma \nabla \Phi) + S_\Phi \quad (2.15)$$

This equation is called the transport equation and consists of the following terms: rate of change and convection on the left side, and diffusion and the source term on the right side. Γ is a diffusion coefficient.

2.2.2 Finite volume method

The finite volume method is used to convert the partial differential equations into algebraic equations. the first step of the finite volume method is the mesh generation; The continuous fluid domain is divided into discrete control volumes called cells. The mesh cells are discrete approximations of the larger domain and the finer (smaller sized cells) the more accurate these approximations are. However, the computation cost also increases, so the mesh should be finest at the sections with the most variation, and coarser at the less variation.

The next step is to integrate the transport equation over the control volume (CV):

$$\int_{CV} \frac{\partial(\rho\Phi)}{\partial t} dV + \int_{CV} \nabla \cdot (\rho\Phi\vec{u}) dV = \int_{CV} \nabla \cdot (\Gamma\nabla\Phi) dV + \int_{CV} S_\Phi dV \tag{2.16}$$

By applying Gauss's Divergence term, equation 2.16 can be rewritten to equation 2.17

$$\frac{\partial}{\partial t}\left(\int_{CV} \Phi\rho dV \right) + \int_A \mathbf{n} \cdot (\rho\Phi\vec{u}) dA = \int_A \mathbf{n} \cdot (\Gamma\nabla\Phi) dA + \int_{CV} S_\Phi dV \tag{2.17}$$

In transient problems, equation 2.17 is integrated with respect to t over a time step Δt. The new equation is the most integrated form of the transport equation:

$$\int_{\Delta t} \frac{\partial}{\partial t}\left(\int_{CV} \rho\rho dV \right) dt + \int_{\Delta t}\int_A \mathbf{n} \cdot (\rho\Phi\vec{u}) dA dt = \int_{\Delta t}\int_A \mathbf{n} \cdot (\Gamma\nabla\Phi) dA dt + \int_{\Delta t}\int_{CV} S_\Phi dV dt \tag{2.18}$$

The transport equation is then converted from its differential form into a solvable algebraic form. This is done using a discretization scheme. The discretization scheme approximates the values for each of the terms in the transport equation. The general algebraic form for 3-dimentional problems is:

$$a_P\Phi_P = \sum_{nb} a_{nb}\Phi_{nb} + B_P\Phi_P^o + s$$

With

$$B_P = \frac{(\rho_P V)^o}{\delta t}$$

a_P represents the effects of diffusion and/or convection, Φ denotes a conserved variable (momentum, energy, species etc.), F is the massflux, the subscript P is the nodal point in the current cell, the subscript nb are nodes in the neighboring cells, and s is the source term.

The final step in the finite volume method is to solve the equations. The discretized equation, 2.2.2, are set up at each nodal point in every computational cell (modified where necessary, to include boundary conditions). The number of equation-sets such as 2.2.2 is the same as the dependent variables. After the equations have been set up they are solved to find the distribution of the property Φ at the nodal points.

There are two types of solution techniques for solving the linear algebraic equations: indirect/iterative methods, and direct methods. Iterative methods are preferred for larger systems of equations, while direct methods are usually used for smaller systems of equations.

2.2.3 SIMPLE and PISO

The convection of scalar /phi is dependent on the velocity field. The solution of the transport equation introduces two problems:

1. The complete set of Navier-Stokes equations are coupled because every velocity component appears in every equation. And there is no transport equation for pressure in the momentum equations.
2. The momentum equations contain non-linear variables. This is not a problem for compressible flows due to the equation of state (2.14). However, for incompressible flows this is not possible. This means that in order for the velocity field to satisfy continuity, the correct pressure field must applied.

Semi-implicit Method for Pressure Linked Equations (SIMPLE) and Pressure-Implicit with Splitting Operators (PISO) are solution algorithms that are used to solve the transport equations. The SIMPLE algorithm is an iterative pricedure and PISO is non-iterative procedure. Both procedures calculate the pressure- and velocity fields.

2.3 Software

Experimental results are always preferred over results from numerical simulations since experiments represent the real behavior of the measured thing in the real world, and numerical simulations are based on theoretical models based on the observed behavior of the measured thing. However, experiments may require expensive experimental facilities or experimental equipment, and the experimental set-up may be a

time consuming process. Numerical simulations on the other hand only require the software, the computational power and time to perform the simulations. Therefore, it is often a more economical substitute for experiments.

CFD simulations coupled with chemical kinetics have been playing an increasingly significant role in the engine design[37]. However, even without the chemical kinetics, the complex physics that occurs on short timescales and within a moving geometry makes in-cylinder analysis of internal combustion engines very challenging. Detailed chemistry has even shorter timescales than the turbulence, and the implementation of detailed chemistry introduces a large set of non-linear ordinary differential equations which complicates the computation further. Due to these scaling problems the detailed simulation of three-dimensional turbulent flows in practical systems using detailed kinetics is beyond the capacity of even today's super-computer[37]. Therefore, reduced versions of detailed reaction mechanism are desired.

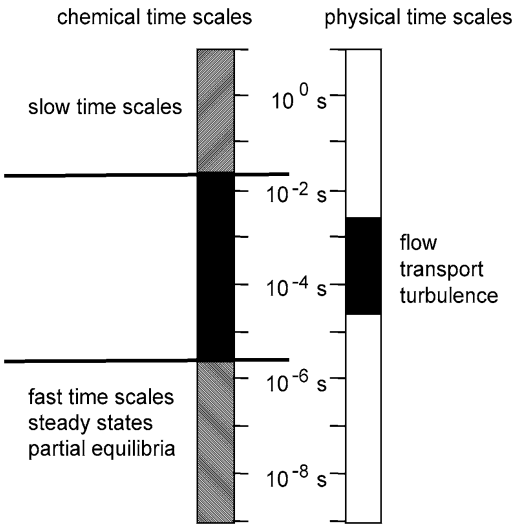

Figure 2.1: The different timescales that govern a chemically reacting flow[37].Used with permission from Springer Link.

2.3.1 DARS

DARS is visual programming simulation tool which is used to study the progression of reactions without taking flow into consideration. This allows for less use of computational power, which is very time-saving as only the chemistry of a system is to be examined. It is developed by CD-adapco, the same company that developed STAR-CD, and can be implemented in Star-CD. DARS uses transient, 0D and 1D models to study various properties of interest to combustion such as species concentration,

laminar flame speed, ignition delay, emissions. These models are sophisticated ideal reactors such as constant volume reactor, constant pressure reactor, perfectly stirred reactor, plug flow reactor. DARS also contains HCCI/SI engine models, HCCI/SI/DI stochastic engine models, and different flame models. DARS also has a mechanism reduction module. This module utilizes sensitivity analysis, reaction flow analysis and lifetime analysis to reduce mechanisms.

2.3.1.1 Mechanism files

DARS uses the CHEMKIN format for the mechanism input files and all mechanisms files must be on this format. Accurate thermodynamic and transport properties of the species involved in the reaction mechanism are necessary for an accurate simulation using the reaction mechanism. Values for these properties are calculated from the data in the molecular input files. DARS offers analysis of surface reactions with 1D models. For this, solid state phase data is needed as an input file. However, this is not needed for the DARS models used in this thesis. The following data are needed in a reaction mechanism:

Gas phase reactions: Specified in a mechanism file, typically called the ".mech" file. This input file determines the species and the reactions that are active in the mechanism. The mechanism file contains three variables that are used to calculate the reaction rate from the modified Arrhenius equation (equation 2.2): A (pre-exponential factor), b (rate fitting exponent), and E_A (Activation energy). An example of a mechanism file is attached in the supplementary appendix B.1.

Molecular data: Specified in transport file, typically called the ".tran" file. This input file defines the transport properties: viscosity, diffusion, thermal diffusion, and thermal conductivity. These transport properties describes the transport of physical properties due to movements in the gas is described. These properties are calculated from the molecular data supplied in the transport file. The transport file contains seven variables: The chemical name, an index for the structure of the species (0 = atom, 1 = linear molecule, 2 = non-linear molecule), well depth divided by Boltzmann's constant, collision diameter, the bond dipole moment, the polarizability, and the rotational collision number at 298 K. An example of a transport file is attached in the supplementary appendix B.2.

State function data: Specified in a thermochemical file, typically called the ".therm" file. This input file defines the heat capacity and the state functions enthalpy and entropy. These properties need to be specified for each species because they are species specific. The 7-coefficient NASA polynomials (2.19,2.20 and 2.21) are used to calculate these functions and derive all other state functions. These polynomials only depend on the temperature, and are given in two temperature ranges. An

example of a therm file is given in the appendix B.3.

$$\frac{C_{p,i}}{R_0} = a_{1,i} + a_{2,i}T + a_{3,i}T^2 + a_{4,i}T^3 + a_{5,i}T^4 \tag{2.19}$$

$$\frac{H_i}{R_0 T} = a_{1,i} + \frac{a_{2,i}}{2}T + \frac{a_{3,i}}{3}T^2 + \frac{a_{4,i}}{4}T^3 + \frac{a_{5,i}}{5}T^4 + \frac{a_{6,i}}{T} \tag{2.20}$$

$$\frac{s_i}{R_0} = a_{1,i}ln(T) + a_{2,i}T + \frac{a_{3,i}}{2}T^2 + \frac{a_{4,i}}{3}T^3 + \frac{a_{5,i}}{4}T^4 + a_{7,i} \tag{2.21}$$

Where $C_{p,i}$ is the heat capacity, T is the temperature, a_1, a_2, a_3, a_4, a_5, a_6, and a_7 are numerical coefficients, H is the enthalpy, s is the entropy, R_0 is the universal gas constant, and the subscript i denotes the species.

2.3.1.2 Governing Balance Equations

Each combustion simulation in DARS must consider the laws of thermodynamics. Therefore the balance equations for energy, mass, and momentum need to be solved. These balance equations are all based on the Navier-Stokes equations for reactive flows. The balance equations used in DARS are presented below.

The balance of mass equation:

$$\frac{\partial m_i}{\partial t} = \sum_{l}^{N_{in}} \dot{m}_{i,l} - \sum_{k}^{N_{out}} \dot{m}_{i,k} + \omega_i M_i \tag{2.22}$$

Where m is the mass, ω is the reaction rate, M is the molar weigth, the subscripts i, l, and k denotes the species, inlet, and outlet, respectively.

The balance of species mass fraction equation:

$$\frac{\partial Y_i}{\partial t} = \sum_{l}^{N_{in}} \frac{\dot{m}_l}{m}(Y_{i,l} - Y_i) + \frac{\omega_i W_i}{\rho} \tag{2.23}$$

Where Y_i is the mass fraction.

The balance of energy equation with respect to internal energy:

$$\rho C_v \frac{dT}{dt} = \sum_{l}^{N_{in}} \frac{\dot{m}_l}{V} \sum_{i}^{N_s} Y_{i,l}(U_{i,l} - U_i) - \sum_{i}^{N_s} \omega_i U_i + \sum_{l}^{N_{in}} \frac{\dot{m}_l}{V} \frac{R_0 T_l}{\overline{M}_l} - \sum_{k}^{N_{out}} \frac{\dot{m}_k}{V} \frac{R_0 T}{\overline{M}} + \frac{h_c A}{V}(T - T_w) + \sigma\epsilon \frac{A}{V}(T^4 - T_w^4) \quad (2.24)$$

Where C_v is specific heat at constant volume, $\overline{M}$ is average molar weight, σ is Stefan-Boltzmann's constant, h_c is the heat transfer coefficient, and ϵ is the emissivity

The balance of energy equation with respect to specific entahlpy:

$$\rho c_p \frac{dT}{dt} = \sum_{l}^{N_{in}} \frac{\dot{m}_l}{V} \sum_{i}^{N_s} Y_{i,l}(h_{i,l} - h_i) - \sum_{i}^{N_s} \omega_i H_i + \frac{h_c A}{V}(T - T_w) + \sigma\epsilon \frac{A}{V}(T^4 - T_w^4) \quad (2.25)$$

The balance of momentum equation:

$$-\frac{dp}{dx} = \rho v \frac{dv}{dx} \quad (2.26)$$

2.3.1.3 EGR

There are two options for simulating EGR in DARS: looping over simulation cycles, and artificial EGR. By looping over cycles, the outlet gas composition is used as the inlet gas composition for the next cycle. The first cycle is run without EGR, unless the composition is read from an input file. The output gas composition from this first cycle is then used in the next cycle and so on. The number of cycle and the EGR rate must be specified by the user. It is also possible to simulate high pressure EGR injection with the *boost EGR* option.

The artificial EGR option is appropriate when it is assumed that the exhaust gas is cooled, so that there are no radicals when the recirculated gas is injected into the cylinder. This EGR option assumes that the combustion is complete, and the only species considered in the EGR are CO2, H2O, N2, and excess oxygen or fuel. A user-specified blend may also be used.

2.3.1.4 General Model options

There are some panels that are used in every model used in DARS; these are presented in this subchapter. There are also unique panels that will be presented later.

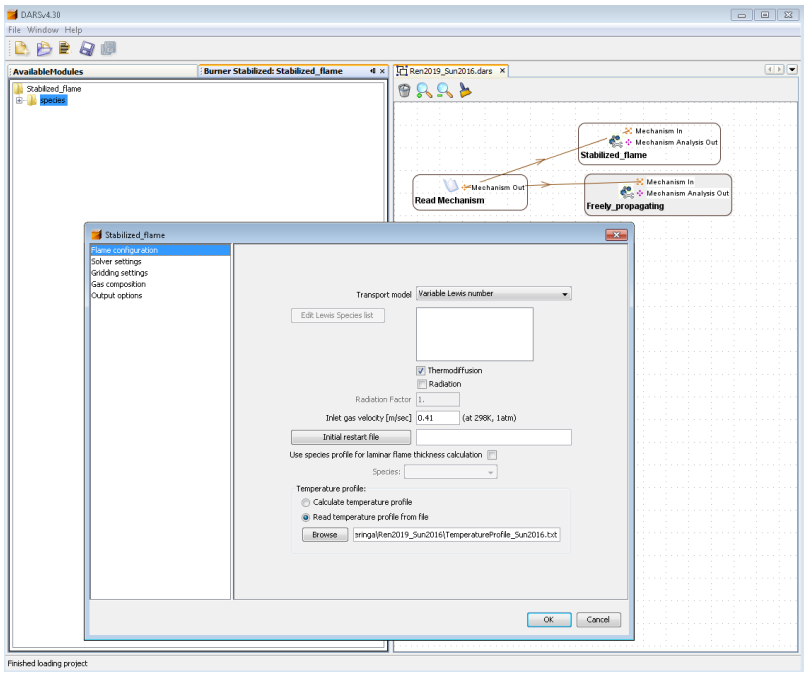

Figure 2.2: The available panels for the premixed flame burner stabilzed in DARS.

General parameters panel

This panel is used to select if radiation, chemical reactions should be calculated. If radiation is activated, a radiation factor that calculates heat losses caused by radiation needs to be specified. Some model have the option of including initial files e.g. a temperature profile, this is done in this panel. There are three options for the temperature profile: *calculate temperature profile*, *use constant temperature*, and *read temperature from file*.

Gas composition panel

In this panel the initial temperature, pressure, the composition, and/or EGR rate of the gas are specified. When the case is a multi-run, the parameters can be specified as range of different conditions. The gas can either be defined as a mixture or as a fuel and oxidizer. In the case of a fuel and oxidizer, the composition of the oxidizer may assigned as air or be customized. The equivalence ratio must also be specified in the case of a fuel and oxidizer. If the gas is defined as a mixture, the equivalence ratio cannot be specified.

Solver panel

This is where options for the solver is chosen. Not every option listed below is available for every model.

Analytical Jacobian: This option improves the computational performance and makes the solver converge more easily.

Spare Jacobian: This option is a simplification of the Analytical Jacobian calculation, and can either result in less computational time or cause problems with the convergence.

Spare Solver: This option uses the special structure of the Jacobian to decrease the computational time. It is dependent in the number of species that react, and is recommended for mechanisms containing 200 species or more.

Filter negative mass fractions: Here one of four following options must be selected: *Allow negative mass fractions*, *filter negative mass fractions from the output* , *filter negative mass fractions from the solver*, and *filter negative mass fractions from the solver with accuracy control*. Negative mass fractions can appear during calculations even though they are not correct physically, either a reduction in computational time or hindering of convergence may occur by temporary allowing this. The standard (and recommended) option is *filter negative mass fractions in the solver*.

The time step algorithm in DARS is customizable, here the maximum number of time steps, and the minimum and maximum time step size can be specified.

The Maximum number of full iteration steps: When a new gradient (Jacobian) is calculated when solving the continuity equations, it is defined as a full iteration step. The Maximum number of full iteration steps that are allowed are specified in this option.

Maximum number of damping levels for converging solution: The process of reducing the step size in order to find a solution is called damping. This is performed when a higher error than the previous error is given by an iteration step. The maximum number of damping levels for converging solution is specified in this option.

Maximum number of detailed Newtion steps: This option defines how many times a gradient can be re-used before a full iteration step is performed.

Convergence velocity: The convergence velocity determines the requirements on convergence for each new solution. When convergence velocity is 1, each new solution has to approach the exact solution. Equation 2.27 is the criterion used to check convergence.

$$n_s = f_s x_s \tag{2.27}$$

Where n_s is the value of the solution, f_s is the solution error, and x_s is the distance between two sequential iteration steps. If $\mathrm{N}_{s+1} < \mathrm{N}_s \cdot C$, where C is the convergence velocity, N_{s+1} is accepted as the solution.

Limit reaction rates: When this option is activated, the computation of reaction rates will be based on the actual concentration of the reactants instead of only the

Arrhenius expressions. This option is used when the chemical mechanisms are stiff and convergence is difficult to reach, and will lead to longer simulation times.

Analytical Jacobian: This option improves the computational performance and makes the solver converge more easily.

Maximum number of detailed Newton steps: Defines how many times a gradient can be re-used before a new full iteration step is performed.

Output options panel

This panel controls the output data. The user can choose between the profiles of species concentration, density, mole fraction and mass fraction. Two analysis tools can be used; Sensitivity analysis and reaction flow analysis. NOx and soot calculations can also be performed if the mechanism supports the simulation of these pollutants. The Number of output data points defines the resolution of the output data profiles.

2.3.1.5 Constant volume reactor model

The constant volume reactor model is a closed rigid vessel, where during combustion the volume is kept constant at 1 dm^3. It is assumed that the system is homogenous and stationary. Because the system is closed, the balance equations are simplified to conservation equations. The model is based on the following conservation equations: Mass conservation:

$$\frac{\partial m}{\partial t} = 0 \tag{2.28}$$

The conservation of species:

$$\frac{\partial Y_i}{\partial t} = \frac{\omega_i M_i}{\rho} \tag{2.29}$$

Due to the volume being constant, the internal energy conservation equation is used to express the conservation of energy. As $u_{i,in} = u_{i,out}$, this can be simplified to:

$$\rho c_v \frac{dT}{dt} = \sigma \epsilon \frac{A}{V}(T^4 - T_w^4) - \sum_l^{N_s} \omega_i U_i \tag{2.30}$$

The momentum is zero because of the assumptions that the system is homogenous and stationary.

General parameters

Calculations of chemical reactions can be deactivated, by deselecting the *calculate with chemical reactions* box.

Solver settings

The solver settings of the constant volume reactor model contain the regular time stepping algorithm, with the exception that an initial time and a final time have to be specified. The following solver options are available: Analytical Jacobian, Spare Jacobian, and Spare Solver. Filter negative mass fractions is also available.

Gas composition

The constant volume reactor model allows specification of either initial pressure or initial fuel mass in the gas composition panel.

Output options

Number of data points are available for specification.

2.3.1.6 HCCI reactor models

There are two different types of engine models in DARS; homogeneous and stochastic. The main difference between these two models is that the stochastic reactor model can capture the effects of in-homogeneities and turbulence, while the homogeneous reactor work under the assumption that there are homogeneous conditions within the cylinder at all times. Another big difference is the computational time as seen in the validation of HCCI combustion.

HCCI Stochastic Reactor Model

The stochastic reactor models in DARS use a probability density function approach to simulate reaction systems. These models can capture the effects of in-homogeneities and turbulence at a low computational cost. While CFD resolves the scalars spatially, DARS's stochastic reactor models describe the scalars with a probability density function. The probability function of the gas mixture in the engine is discretized by mass into a number of "particles", denoted by N. These particles represent the discretized mass density function and they act as a gas cluster. The mass density function (MDF) is defined as

$$F_{\Theta}(\Psi_1, ..., \Psi_{S+1}, t) \tag{2.31}$$

where F is the MDF, $\Theta(t) = (\Theta_1, ...\Theta_N; t)$ is the vector of the scalars in the particle distribution, Ψ is the space variables of this space vector. Under the assumption of statistical homogeneity, the MDF after a certain time is given by the following equation:

$$\frac{\partial}{\partial t}F_{\Theta}(\Psi, t)+\frac{\partial}{\partial \Psi_i}(G_i(\Psi)F_{\Theta}(\Psi, t))+\frac{\partial}{\partial \Psi_{i+1}}(U(\Psi_{x+1})F_{\Theta}(\Psi, t)) = mixingterm \tag{2.32}$$

Where

$$U = \frac{h_g A}{mC_p}(T - T_w) \tag{2.33}$$

$$G_i = \frac{M_i}{\rho}\omega_{ij} \qquad i = 1, ..., x \qquad j = 1, ..., r \tag{2.34}$$

$$G_{x+1} = \frac{1}{C_p}\sum_{i=1}^{x} h_i \frac{M_i}{\rho}\omega_{ij} - V\frac{1}{C_p}\frac{dp}{dt} \tag{2.35}$$

h_g is the Woschni heat transfer coefficient,M_i is the molar mass of species i, ω is the global reaction rate, A is the area, m is the mass, c_p is the heat capacity, T_w is the temperature of the wall, T is the temperature of the flow, j is a given reaction, ρ is the density of the fluid, V is the volume in the combustion chamber. The third term in 2.32 is replaced by a finite difference scheme to introduce a fluctuation. If $U(\Psi_{S+1}) < 0$, equation 2.36 is used.

$$\frac{1}{h}[U(\Psi_{S+1})F(\Psi, t) - U(\Psi_{S+1} - h)F(\Psi_1, ..., \Psi_S, \Psi_{S+1} + h, t)] \tag{2.36}$$

If $U(\Psi_{S+1}) > 0$, equation 2.37 is used.

$$\frac{1}{h}[U(\Psi_{S+1})F(\Psi, t) - U(\Psi_{S+1} + h)F(\Psi_1, ..., \Psi_S, \Psi_{S+1} + h, t)] \tag{2.37}$$

Equation 2.32 is simplified into equation 2.38 by using an operator splitting loop approach. This equation describes the change of MDF with respect to piston movement, mixing, chemical reactions, and heat transfer.

$$\begin{aligned}
\frac{\partial}{\partial t}F_\Theta(\Psi, t) = {} & \frac{\partial}{\partial \Psi_{S+1}}\left(V\frac{1}{Cp}\frac{dp}{dt}_{\Delta V}F_\Theta(\Psi, t)\right) \\
& + \frac{C_\Theta \beta}{\tau}\left[\int_{\Delta\Theta} F_\Theta(\Psi - \Delta\Psi, t)F_\Theta(\Psi + \Delta\Psi)d(\Delta\Psi) - F_\Theta(\Psi, t)\right] \\
& + \frac{\partial}{\partial t}F_\Theta(\Psi, t)\left(V\frac{1}{Cp}\frac{dp}{dt}_{mix}F_\Theta(\Psi, t)\right) \\
& - \left(\frac{\partial}{\partial \Psi_{S+1}}\left(\frac{1}{C_p}\sum_{i=1}^{S} h_i\frac{M_i}{\rho}\omega(\Theta)F_\Theta(\Psi, t)\right) - \sum_{i=1}^{S}\frac{\partial}{\partial \Psi_i}\left(\frac{M_i}{\rho}\omega(\Theta)F_\Theta(\Psi, t)\right)\right) \\
& + \frac{\partial}{\partial \Psi_{S+1}}\left(V\frac{1}{Cp}\frac{dp}{dt}_{chem}F_\Theta(\Psi, t)\right) \\
& - \frac{\partial}{\partial \Psi_{S+1}}\left(\frac{h_g A}{C_p}(\Psi_{S+1} - T_w)F_\Theta(\Psi, t)\right) + \frac{\partial}{\partial \Psi_{s+1}}\left(V\frac{1}{Cp}\frac{dp}{dt}_{heattransfer}F_\Theta(\Psi, t)\right)
\end{aligned} \tag{2.38}$$

Where C_Φ is a proportionality constant, β is a curl mixing model constant, Using equation 2.38 introduces a small error at each step due to an assumption of constant pressure. This is corrected by performing a pressure correction calculation at the end of each step.

The turbulence is modelled by the use of mixing models. Turbulence as well as mixing are stochastic processes that are not easy to model. However, by the use of direct numerical simulation (DNS), the flow fields can be determined.

The following mixing models are available in DARS: The interaction by exchange with the mean model (IEM)[38][39], the multi weighted coalescene/dispersal model (C/D)[40], and the modified C/D model[41][42]. These models use simplified approaches to simulated turbulence. When using these models, the turbulence mixing time, a measure of mixing or turbulence intensity, needs to be specified. The turbulent mixing time, τ, is defined in equation 2.39.

$$\tau = \frac{l_I}{\overline{\overline{U}}} \qquad or \qquad \tau = \frac{l_I}{u'} \tag{2.39}$$

Where l_I is the integral length scale, which is a measure of the largest scale structure in the flow field, U is the mean velocity of the gas, and u' is the turbulence intensity defined as

$$u' = \lim_{t->\infty} \left(\frac{1}{t} \int_{t0}^{t0+t} u^2 dt \right)$$

The chemical composition of the model is calculated by equation 2.40 This equation is solved using a standard backward differential equation along with a Newton algorithm.

$$\begin{aligned} \frac{\partial}{\partial t} F_\Theta = \frac{\partial}{\partial \Psi_{S+1}} \left(\frac{1}{C_p} \sum_{i=1}^{S} h_i \frac{M_i}{\rho} \omega(\Theta) F_\Theta(\Psi, t) \right) - \\ \sum_{i=1}^{S} \frac{\partial}{\partial \Psi_i} \left(\frac{M_i}{\rho} \omega(\Theta) F_\Theta(\Psi, t) \right) \sum_{i=1}^{S} h_i \frac{M_i}{\rho} \omega(\Theta) F_\Theta(\Psi, t) \Bigg) - \sum_{i=1}^{S} \frac{\partial}{\partial} \end{aligned} \tag{2.40}$$

Woschni's heat transfer model[43] is used with a stochastic approach to determine the total amount of heat transfer and the distribution of the heat transfer of over the particles. In the stochastic HCCI engine model, heat release rate is defined as the total heat release from each particle divided by the time step. This can be seen in equation 2.41

$$HRR = \sum_{n=1}^{Npart} \frac{m_n (H_n^f - H_n^i)}{\Delta CAD} \tag{2.41}$$

where H^f is the enthalpy of the particle after the chemistry step, H^i is the enthalpy of the particle before the chemistry step m is the mass of the particle, and n is the particle indicator.

HCCI Homogeneous Reactor Model

The homogeneous reactor models in DARS are based on the assumption that there are homogeneous conditions in the cylinder at all times. The homogeneous reactor models are faster than the stochastic reactor models. However, maximum pressure rates and maximum temperatures have a tendency to get overpredicted. This is a consequence of the homogeneous reactor models only consisting of one single homogeneous volume. The numerical model is made up of a set of 0-D transient differential equations that describes the conservation of energy and the balance of species[44]. Newtons's method is used to solve the system of conservation equations, and backward differential formulas are used to solve the time.

The pressure is dependent on the piston movement and the pressure increase caused by chemical reactions, and is simply calculated by using the equation of state: $p = \rho\frac{RT}{M}$.

The instantaneous volume, V is given by equation 2.42:

$$V = V_c + \frac{\pi B^2}{4}\left(L_{cr} + R_C - L_{cr}cos(\theta) + \sqrt{L_{cr}^2 - R_c^2 sin^2(\theta)}\right) \tag{2.42}$$

Where B is the bore, V_c the clearance volume, L_{cr} the length of the connecting rod, and R_{ct} the crank radius.

Closed system is assumed as combustion occurs during the closed valve period. Thus the conservation equations for chemical species are therefore:

$$\frac{dY_i}{dt} = \frac{M_i}{\rho}\sum_{j=1}^{Nr} v_{i,j}k_j \tag{2.43}$$

And the energy equation:

$$m\sum_{i=1}^{Ns}\left(u_i\frac{M_i}{\rho}\sum_{k=1}^{Nr} v_{i,k}r_k\right) + h_g A_{wall}(T - T_{wall}) + \rho\frac{dV}{dt} + mC_v\frac{dT}{dt} = 0 \tag{2.44}$$

Where $v_{j,k}$ is the stoichiometric coefficient for the species i in reaction j and k_j is the reaction rate of j. h_g is the heat transfer coefficient. The Woschni heat transfer model[43] is used to model heat transfer:

$$h_g = 3.26B^{-0.2}p^{0.8}T^{-0.53}w^{0.8} \tag{2.45}$$

$$w = C_1 c_m + C_2 \frac{V_s T_1}{p_1 V_1}(p - p_0)$$

Where c_m is the mean piston speed, Vs is the swept volume, po is the motoring pressure, and C1 and C2 are constants.

Clustering (stochastic reactor model only)

Particle clustering may be used to speed up the simulation. Particles with similar conditions e.g. temperature, equivalence ratio, or mixture fraction will then be calculated together under the chemstry step. A tolerance level must be specified for each parameter, this can either be defined as a relative value or an absolute value. This value determines how far away from average of the cluster a particle can be in order to be considered to belong to the cluster.

The average of the cluster is recalculated every time a new particle is added. All particles are assigned a deviation measurement, D, at the end of every clustering step. This deviation measurement describes the position of the particle relative to the average of the cluster, as shown in equation 2.46 :

$$D(par, scalar) = \frac{C(cluster, scalar) - \Theta(par, scalar)}{C(cluster, scalar)} \tag{2.46}$$

Θ is the scalar of the particle, and C is the average scalar of the cluster.

After the cluster step, only the chemistry of the clusters are solved by the chemistry solver. The particles' distance from the cluster is assumed to be conserved during the chemistry step. The particles within a cluster is assumed to have the same trajectory as the average of the cluster. As a result, the solution of the average of the cluster is applied to each particle within the cluster, but the deviation measurement is also considered:

$$\Theta'(par) = C(cluster)(1 - D(par)) \tag{2.47}$$

Engine data

The engine data panel is where the engine parameters are specified. Here the engine speed, the geometry of the engine, the wall temperature, the swirl ratio, the compression ratio, and the initial and final crank angle are specified. Woschni wall heat transfer model may be selected and some of the constants can be modified.

There are two options for EGR; cycle-to-cycle EGR, and artificial EGR. In the engine data cycle-to-cycle EGR may be selected, if this is selected the EGR percentage and the number of EGR cycles must be specified. Cycle-to-cycle EGR can be defined with or without the fuel and one mass or mole basis.

Stochastic data (stochastic reactor model only)

At each time step, the volume work of the piston movement, the mixing of the particle's scalars, the chemical reactions and heat transfer are solved one after the other with a pressure correction calculation being applied at the end of the time step. The pressure correction is described below.

Solver settings

The only difference in the solver settings from the general model options are that instead of specifying the maximum number of time steps, the time step size in CAD is to be specified.

Gas composition

This panel is similar to other models. Artificial EGR is also available.

Output options

This panel is similar to other models.

2.3.1.7 Premixed flame models

DARS defines a flame as a self-sustaining propagation of a localized combustion zone at subsonic velocities (deflagration). DARS has two different types of premixed flame models; burner stabilized and freely propagating. Both flames are calculated at constant pressure, and they are one-dimensional with the z-axis perpendicular to the flame front.

The premixed flame models are based on the following conservation equations:

The contiuity equation:

$$\frac{d(\rho u)}{dz} = 0 \tag{2.48}$$

The conservation of energy:

$$\rho u c_p \left(\frac{dT}{dz}\right) = \left(\frac{d}{dz}\right)\left(\lambda\left(\frac{dT}{dz}\right) - \right) - \sum_{i=1}^{N_S} h_i \omega_i - \sum_{i=1}^{N_S} c_p D_i \frac{dT}{dz} - 4\alpha\sigma(T^4 - T_0^4) V f_r \tag{2.49}$$

The conservation of species:

$$\rho u \left(\frac{dY_i}{dz}\right) = -\left(\frac{dD_i}{dz}\right) + \omega_i \tag{2.50}$$

Where ρ is the density, u is the gas velocity component, Y_i is the mass fraction of species i, D_i is the diffusion flux, ω is the production rate of species, c_p is the heat capacity at constant pressure, λ is the thermal conductivity, h_i is the specific enthalpy of species i and N_s is the number of species. α is Planck's constant, σ the Stefan Boltzmann constant, T_0 the temperature of the surroundings and f_r a radiation factor.

Premixed flame burner stabilized model

This model is based on the conservation equations listed earlier. The burner consists of many small holes from which the premixed flame originates from. At the surface of the burner, Z=0. The radical recombination of the radical species O, OH, HO2 and H are included at Z=0.

Premixed flame freely propagating model

This model is based on the conservation equations listed earlier. However, a mixture of burnt and unburnt gases exists in the flame zone. The temperature of the burnt gases is higher than the unburnt gases; the density is lower for the hot gases. As the density decreases, the velocity increases. By integrating the continuity equation (2.48), the following equation is obtained:

$$\rho_u u_u = \rho_u S_L = \rho_b u_b \tag{2.51}$$

S_L is the laminar flame speed, the subscript u is unburnt gas, and the subscript b is the burnt gas. This equation is used to calculate the laminar flame speed.

Flame configuration panel

This panel is unique to the flame models in DARS. Here the flame settings are configured. Three different transport models are available in DARS; *Variable Lewis number*, *Constant Lewis number*, and *Unity Lewis number*.

The *Variable Lewis number* option calculates the diffusion coefficients. *Constant Lewis number* allows the user to specify the Lewis numbers of the species. *Unity Lewis number* sets the Lewis number of all species to 1.0. The transport model that was chosen was *Variable Lewis number*.

When Variable Lewis number is selected, the thermodiffusion option can be selected. When this option is chosen, the third term in the energy equation (2.49) is calculated.

Another option in flame configuration panel is the radiation box. When this is activated, a radiation factor can be chosen. This factor is the volume fraction of burned gas at high temperature to unburned gas at low temperature. When the flame front is infinite, the fraction is 0.5, which is also the default value.

Initial restart file allows the user to specify a start profile for the flame by choosing a file that contains the solution of another flame, this option helps the solution converge.

Normally the laminar flame thickness is computed from the temperature profile. However, there is also an option to calculate the laminar flame thickness from a species profile instead.

Inlet gas velocity: This option is unique for the premixed flame burner stabilized model. Here the inlet velocity of the gas at 298 K and 1 atm is specified.

Use flame stepping: This option uses the solution of a previously computed flame to choose the start profile, this speed up the calculations. If this option is not selected "Use cold start" has to be selected, the flame is then calculated from scratch.

Gridding settings panel

The flames are calculated on a grid, this panel specifies the fineness of the grid.

Number of grid points: The resolution of the flame is modified by this number. A higher number leads to a more smooth solution, but also leads to a higher computational time. The grid of the flame is modified by the minimum and maximum dicretization size.

The importance given to resolving curvature and gradients is defined by the maximum number of grid points per curvature and gradient options. These options affect the grid refinement in regions of large first and second derivative value of the solved parameters.

Grid smoothness: This number modifies the smoothness of the grid. The small the number is, the smoother the grid becomes.

Maximum number of grid readaptations during steady state: This option species the maximum number the grid is readapted after convergence is reached to verify the solution's quality.

Solver settings

The premixed flame models have standard solver options, with the exception of the "maximum number of time step" option.

Gas composition

The gas composition options for premixed flames are standard.

Output options

Species concentration/density/mole fraction/mass fraction profile can be written as output data. Sensitivity and reaction flow analysis, and NOx and soot calculation

can also be undertaken.

2.3.2 STAR-CD

STAR-CD is a CFD program developed by CD-adapco, now owned by Siemens. By the use of the finite volume method, flow problems involving turbulence, chemical reactions, and heat transfer are solved. The software consists of three parts:

1. ES-ICE (expert system – internal combustion engine), this program is used for pre-processing, setting up and run moving mesh problems for internal combustion engines.
2. pro-STAR, this program loads the model setup created in ES-ICE. This program is used for pre-processing too, but also post-processing. Although the main set up is done in ES-ICE, a small portion of the set-up is done in pro-STAR.
3. STAR, this program is the solver. Here the transport equations are solved.

2.3.2.1 Models in STAR-CD

Combustion model

STAR-CD offers a variety of combustion models. The 3-Zones Extended Coherent Flame Model (ECFM-3Z)[45] is generally recommended for both diesel and gasoline engine simulation. However, the Detailed Chemistry model is of interest in this thesis. This combustion model incorporates chemical kinetics into the CFD. Transport equations are solved for all species by the use of a reaction mechanism.

Spray model

The fuel spray is a comlicated process that involves many physical phenomena e.g multi-phase flow and atomization. STAR-CD uses a Langranian/Eulerian approach of observing fluids. The fuel spray is customizable via many submodels and options. The spray options and different models are listed below.

Courant number – controls the number of time steps needed to trace a fuel droplet through a cell, this determines the accuracy of the trajectory calculations. The value for the Courant number is in the range of $0 < C < 1$. When $C = 1$, one time step is used. For $C = 0.5$ two time steps are used.

Under-relaxation for sources – reduces solution oscillations and helps to keep the computation stable/helps the computation converge by choosing a factor

that regulates the corrector steps in the PISO algorithm. The range of this factor is [0,1].

Turbulent dispersion – The process of when a droplet in a turbulent flow experiences a randomly-varying velocity field to which it responds according to its inertia, is modelled in STAR by a stochastic approach.

Interpolation method – Specifies the interpolation method used for evaluating the continuous-phase temperature, velocity and species mass fraction at droplet locations. The two options are vertex interpolation and gradient interpolation. The vertex method applies only for the velocity calculations for hexahedral cells. The gradient method applies for all other variables and cell shapes.

Spray definition method – Chooses the method which specifies the initial droplets conditions. Three options are available:

1. *Spray injection with atomization*: All initial conditions are calculated on the basis of built-in spray models using data entered into the "Spray models and injectors" panel.
2. *Explicitly defined parcel injectors*: Injection conditions such as droplet velocities, injection rates, diameters, etc. are specified in the "Explicit injection" panel.
3. *User subroutine*: Both the injection conditions and injection locations are specified by a user subroutine.

Liquid film: Activates a model for predicting the dynamic characteristics of wall liquid films.

Droplet type and properties – Defines the fuel droplet type used in the simulation by specifying its name and physical properties. It is possible to choose droplet properties from STAR-CD's internally calculated values, from STAR-CD's NIST database, or from a user subroutine.

The droplet controls: Control the post-processing size and the overall Langrangian simulation process.

Break-up model: Chooses the break-up model used in the simulation. Three options are available; no droplet break up,the Reitz model[46], and the KHRT model[47].

Wall interaction

There are three different outcomes that are possible when a droplet impacts a wall: deposition/spread, rebound, and splashing. The behaviour after a droplet has collided with a wall will have to be specified by the use of a wall interaction model.

STAR-CD offers a couple of wall interaction models, e.g. Bai's spray impingement model[48], the Bai-Onera droplet-wall interaction model[48][49], and the Senda droplet-wall interaction model[50][51][52].

Turbulence models

Turbulence is still to this day not a completely understood phenomenon. However, through experiments turbulence models have arose, these turbulence models are inexact, but still the best representations we have. Four categories of turbulence models are offered in STAR-CD: Eddy Viscosity models, Reynolds stress models, LES (Large Eddy Simulation) models, and Detached Eddy Simulation models. STAR-CD offers a couple of turbulence models for each of these four categories.

DMZ

Using the dynamic multi-zone method[53], the computational time could be substantially reduced. This method creates groups of cells with similar thermo-chemical states. These groups are then solved instead of each single cell being solved.

2.3.2.2 Governing equations

The complete set of Navier Stokes equations are given in STAR-CD using Cartesian coordinates on tensor form. Where equation 2.52 is the continuity equation, equation 2.53 is the momentum equation, and equation 2.54 is the energy equation (on total enthalpy form).

$$\frac{\partial \rho}{\partial t} + \frac{\partial}{\partial x_j}(\rho u_j) = S_m \tag{2.52}$$

$$\frac{\partial \rho u_i}{\partial t} + \frac{\partial}{\partial x_j}(\rho u_j u_i - \tau_{ij}) = -\frac{\partial p}{\partial x_i} + S_i \tag{2.53}$$

$$\frac{\partial \rho H}{\partial t} + \frac{\partial}{\partial x_j}(\rho u_j H + F_{h,j} - u_i \tau_{ij}) = \frac{\partial p}{\partial t} + u_i S_i + S_h \tag{2.54}$$

Where $H = \frac{1}{2}u_i u_i + h$, $\quad p = p_s - \rho_0 g_m x_m$, and $\quad h = \bar{C}_p T - C_p^0 T_0 + \sum Y_m H_m$. Time is denoted by t, x_j is cartesian coordinate, u_i is fluid velocity component in x_i direction, p is the piezometric pressure, ρ_0 is the reference density, g_m are the gravitational acceleration components, x_m are coordinates relative to the reference point where ρ_0 is defined, τ_{ij} are stress tensor components, $F_{h,j}$ is the diffusional energy flux in direction x_j, H is the total enthalpy, h is the static enthalphy, $\bar{C}_p$ is the average heat capacity at constant pressure, C_p^0 is the heat capacity at temperature T_0, Y_m is the mass fraction of the mixture m, H_m is the heat of formation constituent m, S_m is a mass source, S_i is a momentum source, S_h is an energy source.

These equations are discretised by the finite volume method. STAR-CD offers the following discretization schemes: upwind differencing (UD), linear upwind differencing (LUD), central differencing, monotone advection and reconstruction scheme (MARS), and blended differencing. The algebraic equations created using one of the discretization schemes are then solved using implicit methods. Two implicit methods are available in STAR-CD: the PISO and the SIMPLE algorithms.

3 Methodology

This chapter will present the procedure of aquiring the results in chapter 4. The methodology is divided in two section; Methodology in DARS, 3.1, and Methodology in STAR-CD 3.2. Both section will describe the models and the settings used in the simulation. The computational time will also be presented.

3.1 Methodology in DARS

The mechanisms validated in this thesis have been validated before in their reports [24][28][29][33]. However, this validation process has only been undertaken by the use of the CHEMKIN software. This thesis used DARS for the validation of the mechanisms against various reaction kinetic experiments and also compare the different mechanisms with respect to their combustion characteristics.

The published experimental data consists of laminar flame speeds, species concentrations, ignition delay times, and HCCI combustion data. Most of the mechanisms investigated also include another fuel mechanism. However, only the reaction mechanism of OME is of interest in this thesis. Thus, the other fuels will not be validated. All the simulations are performed in DARS. The computer used for the simulations in DARS is a regular Windows 7 PC with 8 cores.

The validation of the mechanisms gives insight to under which conditions the mechanisms give satisfactory predictions and not. A well-validated oxidation model is one which can simulate a fuel's oxidation over a wide range of physical conditions including mixture compositions, temperatures and pressures [54]. However, a mechanism may perform well under the experimental conditions and underperform under real engine conditions.

3.1.1 Species concentration validation

The species concentration experiment premixed flat burner performed by Sun2016. Sun et al.[24] was the first to measure the species profile of a laminar premixed flame using OME_3 as fuel. They used a McKenna burner with a diameter of 60mm to produce the flame. The stoichiometric premixed flame of OME_3 was burning at a constant pressure of 3333 Pa with a flow rate of 2 standard liters per minute. Argon

was used as a dilution gas and the flow rate of argon was 1 standard liter per minute. O2 was used as oxidizer and the flow rate of O2 was 0.857 standard liters per minute.

For the validation of species concentration, the Premixed Stabilized Flame Model in DARS was used with the following set up:

Flame configuration

Variable Lewis number and thermodiffusion were selected. The radiation option was left out as the simulations did not converge and the fraction was not known. The gas inlet velocity at was set to 0.41m/s. As no previous flame calculation was available, Initial restart file was left blank. The temperature profile from the sun2016 experiment was selected. The option "Use species profile for laminar flame thickness calculation" was not selected as the temperature profile was given.

Solver settings

Table 3.1: Premixed Stabilized Flame Model: Solver settings

Maximum number of time steps:	50
Minimum time step size[s]:	1.0E-7
Maximum time step size[s]:	0.1
Relative tolerance limit:	1.0e-5
Maximum number of full iteration steps:	50
Maximum number of damping levels for converging solution:	10
Maximum number of detailed Newtion steps:	20
Convergence velocity:	1.01
Limit reaction rates:	Not selected
Use Analytical Jocobian:	Not selected

Gridding settings

Table 3.2: Premixed Stabilized Flame Model: Gridding settings

Number of grid points:	300
Minimum discretization size[s]:	1.0E-9
Maximum discretization size[s]:	0.1
Maximum number of grid points per unit curvature:	1
Maximum number of grid points per unit gradient:	1.5
Grid smoothnes:	0.05
Maximum number of grid readaptations during steady state:	5

Gas composition

The value of the initial temperature was unimportant because the temperature profile is used. However, this value was set to 293 K. The pressure was set to 3333 Pa. And the mole fraction of the mixture was: 50% argon as a dilute, 42.85% O2 as oxidizer, and 7.15% OME_3 as fuel.

Output options

The "write mole fraction profile" was activated, before the case was run.

Computational time

One case was run with one process. The computational time is given in table 3.3. The overview of the mechanisms and their sizes are found in table 1.2.

Table 3.3: Premixed Stabilized Flame Model:Computational time

Mechanism	Total time used
Lin2019	59 s
Huang2019	53 s
Ren2019	389 s
Sun2016	1335 s

3.1.2 Laminar flame speed validation

The only published study of the laminar flame speed of OME_3 was performed by Sun et al.[24]. They conducted an experiment using a constant volume combustion vessel along with a high-speed camera to measure the laminar flame speed of different OME_3/air mixtures. The combustion vessel had an initial temperature of 408K and a pressure of 1 atm. The equivalence ratio ranged from 0.7 to 1.6, with a step size of 0.1. For the validation of the laminar flame speed of OME_3, the Premixed Freely Propagating Flame Model in DARS was used with the following settings:

Flame configuration

Variable Lewis number was chosen as the transport model, with thermodiffusion activated. The radiation was not selected. Cold start was used as there no available previous flame simulation that was similar to this case. The option *Use species profile for laminar flame thickness calculatio* was not selected. The option *calculate temperature profile* was chosen, as there was no temperature profile available.

Solver settings

Table 3.4: Premixed Freely Propagating Flame Model: Solver settings

Maximum number of time steps:	100
Minimum time step size[s]:	1.0E-10
Maximum time step size[s]:	0.1
Relative tolerance limit:	1.0e-5
Maximum number of full iteration steps:	50
Maximum number of damping levels for converging solution:	10
Maximum number of detailed Newtion steps:	20
Convergence velocity:	1.01
Limit reaction rates:	Not selected
Use Analytical Jocobian:	Not selected

Gridding settings

Table 3.5: Premixed Freely Propagating Flame Model: Gridding settings

Number of grid points:	350
Minimum discretization size[s]:	1.0E-6
Maximum discretization size[s]:	0.1
Maximum number of grid points per unit curvature:	0.1
Maximum number of grid points per unit gradient:	0.1
Grid smoothnes:	0.05
Maximum number of grid readaptations during steady state:	4

Gas composition

The initial temperature was set to 403 K. The pressure was set to 1 atm. And fuel was defined as fuel and oxidizer, where OME_3 was the fuel, and air was the oxidizer. The equivalence ratio range was set from 0.7 to 1.6. In order to create a smoother graph, the equivalence ratio step size was set to 0.05.

Output options

The *write mole fraction profile* was activated, before the case was run.

Computational time

Five cases were each run with one process at the same time. The computational time is given in table 3.6.

Table 3.6: Premixed Freely Propagating Flame Model: Computational time

Mechanism	Total time used	Time in hours
Lin2019	5299 s	1.5 h
Huang2019	33251 s	9.2 h
Ren2019	29402 s	8.2 h
Sun2016	60092 s	16.7 h

3.1.3 Ignition delay time validation

He et al.[25] were the first to measure the ignition delay time of OME_3. They used the Tsinghua University rapid compression machine[55] to simulate a compression stroke, and measured the ignition delay time under various conditions. The Tsinghua University rapid compression machine's compression ratio was adjustable; this was used to specify the end gas temperature and the pressure. The mixture in the test section could be compressed to a high pressure and a high temperature within 25–30 ms. The experiments were performed under six different conditions, where the pressure was 10 bar or 15 bar, and the equivalence ratio was 0.5, 1.0, or 1.5. The gas was diluted depending on its equivalence ratio as shown in table 3.7.

Table 3.7: Ignition delay time experiment: Dilution ratio

Equivalence ratio	Dilution ratio (N:O)
0.5	1:8
1.0	15:1
1.5	20:1

General parameters

The temperature profile were calculated. Calculations of chemical reactions were activated. Radiation was not activated.

Solver settings

Table 3.8: Constant Volume Model: Solver settings

Minimum time step size[s]:	1.0E-10
Maximum time step size[s]:	1e-5
Final time [s]:	0.15
Maximum order of the bdf method:	5
Absolute tolerance limit:	1e-12
Relative tolerance limit:	1e-6
Maximum number of full iteration steps:	10
Maximum number of damping levels for converging solution:	3
Maximum number of detailed Newtion steps:	20
Convergence velocity:	1.0
Limit reaction rates:	Not selected
Use Analytical Jocobian:	Not selected

Negative mass fractions was chosen to be filtered in the solver. The final time was increased to 0.25 s for the Sun2016 mechanism because the mechanism had problem igniting. The computational time however, is calculated with the final time set to 0.15 s.

Gas composition

The fuel was defined as a mixture of OME_3, N_2 and O_2. So for each equivalence ratio, the fuel mass fraction was changed. The fuel mass fraction is given in table 3.9. There are two different initial pressures: 10 bars and 15 bars. The initial temperature is varied from 588 K (=1.7 [1000/K]) to 1112 K (=0.9 [1000/K]). The temperature step size was set to 2 K to create a smooth graph.

Table 3.9: Ignition delay time experiment: Mass fraction of the different cases

Species	Massfraction		
	$\phi = 0.5$	$\phi = 1.0$	$\phi = 1.5$
OME_3	0.0424	0.0478	0.0544
O_2	0.1064	0.595	0.0450
N_2	0.8512	0.8927	0.9006

Output options

The Number of output data points was set to be 5000.

Computational time

Three cases were each run with three processes at the same time. The computational time is given in table 3.10.

Table 3.10: Constant Volume Model: Computational time

Mechanism	Total time used	Time in hours
Lin2019	2488 s	0.7 h
Huang2019	8554 s	2.4 h
Ren2019	8280 s	2.3 h
Sun2016	29502 s	8.2 h

3.1.4 HCCI combustion validation

The characteristics of OME_3 HCCI combustion were investigated by Wang et al[22]. The purpose of the study was to help with the understanding of POMDME fuel-blends, and to help with the development of chemical mechanisms for OME_3. In this experiment a blend of OME2, OME_3 and OME4 with a respective mass fraction of 2.6%, 88.9% and 8.5% was used to represent OME_3. This blend was then used in a HCCI engine operating under a different range of equivalence ratios, and EGR rates. The EGR in the was cooled so that the outlet temperature of the EGR was around 30 /degree C. Experimental data of the pressure diagram and the rate of heat release were published and used in the validation of the different mechanisms.

For the validation of HCCI combustion without EGR, the stochastic HCCI reactor model in DARS was used. The homogeneous model tended to overpredict the heat release rate, so this model was not used without EGR. However, the EGR in the SRM model is assumed to be perfectly mixed with the incoming air, this means that EGR mass is spread equally over all particles. This idealization led to an underprediction of both the heat release and the pressure diagram when EGR was included. The homogeneous HCCI engine model was found to be more suitable as it did not use the same assumptions, so it was used to validate the EGR experiments.

Engine settings

The engine settings were mutual for the two engine models. The engine specifications is given in table 3.11

Table 3.11: HCCI engine data

Bore [mm]	83.1
Stroke [mm]	92.0
Connecting rod [mm]	145.8
Compression Ratio	16.7
Engine speed [RPM]	1600
Swirl ratio	1.7

These specifications were inserted into the engine data panel in the stochastic HCCI model. The initial crank angle of the simulation was set to -60 degrees before top dead center, and the final crank angle was set to 40 degrees after top dead center. Woschni wall heat transfer model[43] was used without changing the constants. As the coolant and oil temperatures were maintained at 80 °C ± 2 °C, the same temperature where used to specify the wall temperature.

Stochastic HCCI Reactor Model solver settings

Table 3.12: Stochastic HCCI Reactor Model: Solver settings

ime step size in CAD:	0.05
Minimum time step size[s]:	1.0E-10
Maximum time step size[s]:	1e-3
Absolute tolerance limit:	1e-10
Relative tolerance limit:	1e-6
Maximum number of full iteration steps:	20
Maximum number of damping levels for converging solution:	6
Maximum number of detailed Newtion steps:	40
Convergence velocity:	1.0
Limit reaction rates:	Not selected

Negative mass fractions was chosen to be filtered in the solver.

Stochastic HCCI reactor model stochastic data

Table 3.13: Stochastic HCCI Reactor Model: Solver settings

Mixing model:	IEM
Mixing time [s]:	5.E-4
Variable mixing time:	Not selected
Stochastic constant:	23
Number of particles:	800
Maximum number of particles:	9000
Number of EGR particles:	0

Stochastic HCCI reactor model gas composition

The fuel was defined as a fuel and oxidizer, with OME_3 as the fuel and air as the oxidizer. The initial temperature was set to 511.8 K, and the initial pressure was set to 387333 Pa. The six equivalence ratios were specified in the equivalence ratio tab.

Stochastic HCCI reactor model clustering

The standard clustering options were used.

Homogeneous HCCI reactor model solver settings

Table 3.14: Homogenous HCCI Reactor Model: Solver settings

Minimum time step size[s]:	1.0E-10
Maximum time step size[s]:	1e-3
Maximum order of the bdf method:	5
Absolute tolerance limit:	1e-10
Relative tolerance limit:	1e-6
Maximum number of full iteration steps:	10
Maximum number of damping levels for converging solution:	3
Maximum number of detailed Newtion steps:	20
Convergence velocity:	1.0
Limit reaction rates:	Not selected

Negative mass fractions was chosen to be filtered in the solver.

Homogeneous HCCI reactor model gas composition

The same fuel definition, inlet temperature, and inlet pressure of the stochastic HCCI reactor model were used. However, the equivalence ratio was set at $\phi = 0.34$. The artificial EGR was chosen because the EGR was cooled. The artificial EGR consisted of CO_2, O_2, N_2, and H_2O with a ratio of 26%, 42%, and 52%.

Homogeneous HCCI reactor model output options

Number of data points were 1000.

Homogeneous HCCI reactor model computational time

Three cases were each run with one process. The computational time is given in table 3.15.

Table 3.15: Homogenous HCCI Reactor Model:Computational time

Mechanism	Total time used
Lin2019	0.4 s
Huang2019	1.5 s
Ren2019	1.5 s
Sun2016	3.1 s

Stochastic HCCI reactor model computational time

Three cases were each run with three processes at the same time. The computational time is given in table 3.16.

Table 3.16: Stochastic HCCI Reactor Mode: Computational time

Mechanism	Total time used	
Lin2019	2805 s	0.8 h
Huang2019	15487 s	4.3 h
Ren2019	18229 s	5.1 h
Sun2016	83051 s	23.1 h

3.2 Methodology in STAR-CD

The 3D-CFD simulations of combustion using OME_3 as fuel, was performed in the CFD software STAR-CD using the Lagrangian approach. This section describes the methodology in STAR-CD and the models and submodels used are displayed.

An experiment using an engine with the same engine data as given in table 3.18 were performed using an additized OME_1 blend, denoted as $OME1_{1b}$. The experimental data with OME_1b is included for the sake of showing how the combustion behaviour of OME_3 fuel is different than that of OME_1b. Some of the properties of $OME1_{1b}$ is given in table 3.17 along with the properties of a hydrogenated vegetable oil corresponding to EN 15940 (paraffinic diesel fuel), regular OME_1 and regular OME_3.

Table 3.17: Properties of HVO, OME_1, OME_{1b}, OME_3

Fuel	Paraffinic diesel EN 15940	OME_1	OME_{1b}	OME_3
Lower heating value [MJ/kg]	43.8	22.4	22.5	19.4
Density at 15°C [kg/m^3]	0.78	0.86	0.87	1.03
Oxygen content [wt%]	0	42.1	42.1	48.1
Boiling point [°C]	210-302	42	42	156
Cetane number	79.8	29.3	40	67

3.2.1 Set-up in ES-ICE

The geometry mesh

The geometry mesh model was provided by Kai Gaukel, my supervisor in Germany. This was a moving hexahedral mesh of the pistonbowl in the cylinder. The mesh resolution was a compromise between a reasonable calculation time and fineness. Planar symmetry was used to reduce the total mesh size by a factor of eigth. The final size of the mesh contained 774110 cells.

Engine data

Table 3.18: Engine data of the DI diesel engine

Bore [mm]	120
Stroke [mm]	155
Connecting rod [mm]	251
Piston pin offset	0.6
Piston Stroke length [mm]	155
Compression Ratio	16.998
Engine speed [RPM]	1200

3.2.1.1 Star controls (star set-up)

Combustion options

The combustion model was set to detailed chemistry with either $C_3H_8O_2$ or $C_5H_{12}O_4$ injected as the user defined fuel, depending on the case. The mixture option was specified as 1.63. EGR was set to 0% and residuals were set to 7%. The detailed chemistry was set to start at 711 degree crank angle. The Flame propagation factor and the reaction rate scale factor were both left at 1.0. Due to problems with the mechanisms igniting early in the project, DMZ was turned off, soot and dynamic mechanism reduction were also deactivated.

The Spray

The number of injection holes was 8 and the azimuthal cone angle was 30°. The following spray options were selected:

Table 3.19: Spray options

Courant number	0.35
Under-relaxation for sources	0.15
Turbulent dispersion	activated
Interpolation method	Vertex data
Spray definition method	Spray injection with atomization
Liquid film	deactivated

The liquid film was deactivated to simplify the model thus reducing the computational cost. To accurately simulate the spray, the thermophysical properties of the droplets should be as correct as possible. However, es-ice does not include the droplet properties of OME_3 and a database of the thermo-physio properties of OME_3 is not

Table 3.22: Break up model options

Break up model	KHRT
KHB0	0.61
KHB1	40.0
RTC3	0.1
RTCT	1.0

Table 3.23: Nozzle options

CD	0.9
L/D	4.04
Contraction	0.9
Roughness	1.0e-6

currently available. Therefore, the properties of the droplet in the spray had to be supplied by a userfile. This file is placed in a folder called "ufile" in the working folder. Userfiles for OME_1 and OME_3 that were made at the The Technical University of Munich were used.

The following tables show the droplet controls, the break-up model, the nozzle options, and the wall interaction model.

Table 3.20: Droplet controls

Maximum number of droplet parcells	10000
Maximum droplet trajectory size (MB)	400
Maximum droplet tracking time	100.0

Table 3.21: Wall interaction model options

Wall interaction model	Bai
Bai coefficient 1	1.0e-6
Bai coefficient 2	0.7
Bai coefficient 3	1320.0
Bs	1.0
Bl	1.0
Leidenfrost temperature (K)	1000
Thermal break up	activated
Web1	30.0
Web2	80.0

Droplet heat transfer was activated, but droplet boiling was not activated. The atomization model used was Huh[56]. The nozzle model used was EFFE, and the nozzle parameters specified in table 3.23 were used.

Because there are two injections, there have to be two injectors. The parameters of these injectors are the same and are given in table 3.24

Table 3.24: Injection options

Injection temperature [K]	360
Hole diameter [m]	0.000313
Pintle hap [m]	deactivated
Mass flow by tab	activated
Number of parcels per injection	1e8

Initialization

The initialization options of the cylinder was selected as follows: The velocity was defined at constant omega, and specified to be -3581 RPM with axis z. The absolute pressure defined by a table in image from the experiment with OME1. The temperature was also defined by a table in image from the same experiment. The RNG k-ϵ turbulence model[57], under the eddy viscosity turbulence model category, was used because its computational efficiency due to its simple treatment of the near-wall flow region for highly turbulent flows. The initial turbulence levels were specified in terms of turbulence kinetic energy and dissipation rate (K-E constant), with the turbulence kinetic energy of 24.59 m^2/s^2 and the dissipation rate of 5555.753 m^2/s^3. The local EGR was selected and specified to be 7.194. The turbulence and EGR values were taken from earlier calculations that used a full engine model. The *compute MF* button was used to compute the initial mass fraction.

Boundary conditions

As the boundary wall temperature was not known, the thermal boundary condition was set to fixed for the combustion dome regions, the piston crown regions and cylinder wall regions. The temperature in kelvin was set to 500, 450 and 420 respectively. The optional thermal resistance parameter was not specified. The *extra regions* option was not activated. The global boundary conditions were set to default options.

Post-setup

The post-setup options were left to default. The Post-setup Global settings that were selected are given in table 3.25:

Table 3.25: Post-setup: Global settings and Cylinder settings that were activated

Global settings	Cylinder setting
Boundary quantities	Turbulence
Curtain flow, 4 sectors	Scalars
Droplets	Droplet details
Heat release	Air/fuel ratio
Pistion work	Velocity magnitude
Heat transfer, Yplus 100, storage interval 1	Monitoring position
PISO correctors	Swirl (definition 1)
Time step size	Swirl (definition)
Summary report	Valve lift

Time step control

The simulations were started at 595 CAD and were set to end at 780 CAD.The time steps are defined in the table 3.26. The numbers in parentheses are for the run with the Sun2016 mechanism.

Table 3.26: CFD time step options

Start angle [CAD]	Stop angle [CAD]	step size [CAD]
595	711(710)	0.02
711(710)	745(750)	0.005
745(750)	760(765)	0.01
760(765)	780	0.02

Write data

The default options were selected before the write data button was selected. The model was then set up for pro-STAR.

3.2.2 Set-up in pro-STAR

By using the *Resize*, *Model*, and *Events* macros from the es-ice panel created in es-ice, the model was loaded in prostar. The "mech" and the "therm" inputfiles are converted into different files with a different format when using the *model* macro in pro-STAR, these new files are called InputRedKinMec.txt and InputRedKinTherm.txt. However, when the inputfiles are converted in pro-STAR, the new files are not generated properly. DARS also have the option to convert the original mech

and therm input files into the new version, DARS does this without problems. So for each mechanism that was simulated in STAR-CD, the inputfiles generated by STAR-CD had to be replaced by the inputfiles generated from DARS.

Since the main set-up was done in es-ice, only a few parts have to be changed in pro-star: The reaction type in the scheme definition was changed to Unpremixed/Diffusion and Detailed Chemistry is chosen as the reaction model .

In the solver parameters for the primary variables, the residual tolerance for the momentums, the pressure, and the turbulence was decreased by a factor of 10. The differential scheme for temperature was changed to the monotone advection and reconstruction scheme (MARS) for a more stable calculation process.

MARS was also used as the differencing scheme for additional scalars (the species). Transport was the solution method with an under-relaxation factor of 0.7.

The model, the problem file and the geometry files were then saved, the latter with a scale factor of 0.001. Finally the problem was run in STAR. Most cases were run with 45 cores on a workstation, but some cases were run on the TUM computer cluster.

Table 3.27: CFD simulations of OME_3:Computational time

Combustion model	Mechanism	Total time steps	Total time used	Average time per time step
Detailed chemistry	Lin2019	8092	70057 s	8.7 s
Detailed chemistry	Huang2019	15100	272093 s	18.0 s
Detailed chemistry	Ren2019	15100	261868 s	17.3 s
Detailed chemistry	Sun2016	16000	1056593 s	70.0 s

Table 3.28: CFD simulations of OME_1:Computational time

Combustion model	Mechanism	Total time steps	Total time used	Average time per time step
Detailed chemistry	Lin2019	—	—	—
Detailed chemistry	Huang2019	16000	254521 s	15.9 s
Detailed chemistry	Ren2019	16000	311488 s	19.5 s
Detailed chemistry	Sun2016	10050	467667 s	46.5 s
ECFM-3Z	—	12600	231976 s	18.4 s

4 Results and discussions

In this chapter the results are presented and discussed. The reaction kinetics of OME_3 was simulated using the available OME3 mechanisms in the different models in DARS that were introduced in chapter 2.3.1. The results will be presented and compared with experimental data in chapter 4.1. The combustion of both OME_1 and OME_3 was simulated in STAR-CD with the available mechanisms. The results from the simulations will be presented in chapter 4.2.

4.1 Validation of the mechanisms

The ignition delay times, laminar flame speeds, species concentrations, and HCCI combustion results from the simulations in DARS will be presented, compared, and discussed in this section. Experimental data from the various experiments will be used to compare against.

4.1.1 Ignition delay time

The ignition delay time was defined as the time it took until the temperature had risen 400 K above the initial temperature, as previously defined in Huang et al.[33], Ren et al.[28], and Lin et al.[29]. Figure 4.1a, 4.1b, and 4.1c show the results from the ignition delay time simulations that were simulated using the constant volume reactor in DARS.

The Lin2019 mechanism's prediction of the ignition delay time is satisfactory for the measured ignition delay times for $\phi = 0.5$ and for $\phi = 1.0$. For $\phi = 1.5$. The prediction is agreeing well in the medium and high temperature regions. In the low temperature region however, there is a little overprediction in the ignition delay time. All in all the Lin2019 mechanism predicts the ignition delay times measured in the experiment reasonable well.

The Ren2019 prediction the ignition delay time is agreeing well for all equivalence ratios when the pressure is 10 bar. However, the ignition delay time tends to get overpredicted when the pressure is 15 bar. Nonetheless, the Ren2019 mechanism prediction of ignition delay time fits well with the experimental data.

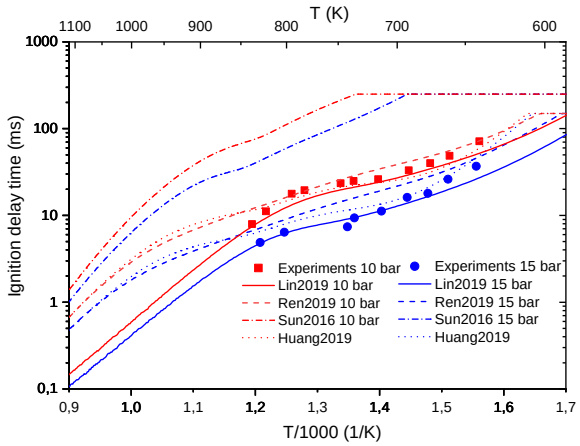

(a) $\phi = 0.5$

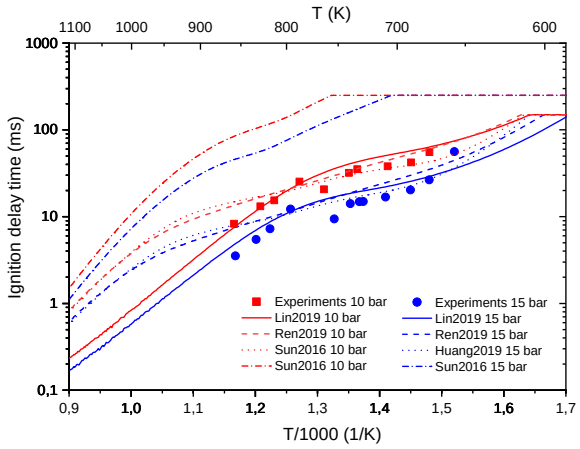

(b) $\phi = 1.0$

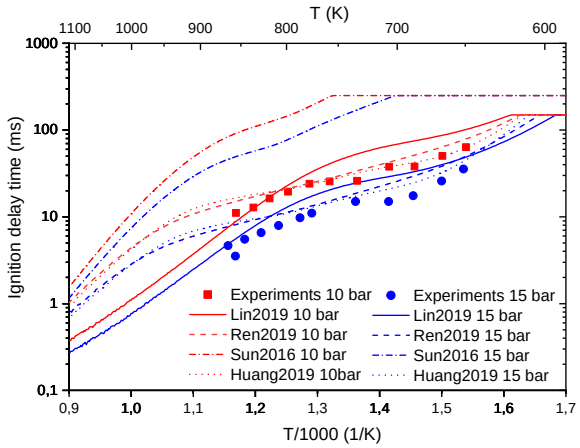

(c) $\phi = 1.5$

Figure 4.1: Ignition delay times for OME_3 with both experimental data and the preditctions of the mechanisms.

The Huang2019 mechanism predicts the ignition delay time satisfactory in all cases. As the temperature increases over 850 K, the correspondence between the mechanism and the experimental results decrease. Nonetheless, the correspondence is still satisfactory.

The Sun2016 mechanism overpredicts the ignition delay time measured in the experiments in all cases.

4.1.2 Laminar flame speed

The results from the laminar flame speed simulations performed by the Premixed Freely Propagating Flame Model in DARS are shown in figure 4.2. The results show that the mechanisms predicts the laminar flame speeds fairly well under lean to near stoichiometric conditions, but as the fuel mixture gets richer the flame speed predictions get worse and reach deviations of up to over 50%.

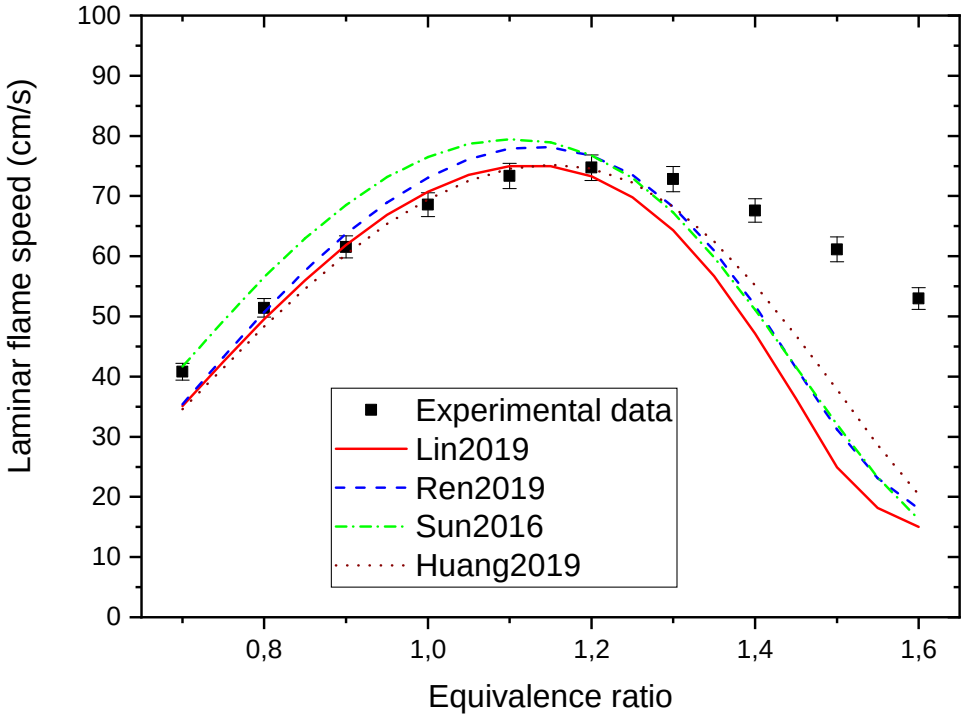

Figure 4.2: Laminar flame speed for OME_3 with both experimental data and the predictions of the mechanisms.

However, in previous released literature these mechanisms have predicted the experiment fairly well under all equivalence ratios. This discrepancy of results between released literature and the result above is most probably due to a difference in the software used to simulate the experiment. Published literature has used CHEMKIN, while the results from the figure above are produced in the premixed burner freely propagating model in DARS.

4.1.3 Species concentration

The figures 4.3a, 4.3b, 1.1, 4.3d, 4.3e, and 4.3f show the major species profiles from the simulations using the Premixed Stabilized Flame Model in DARS.

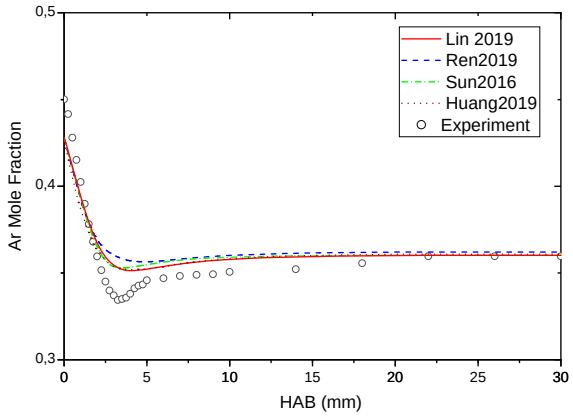

(a) Ar

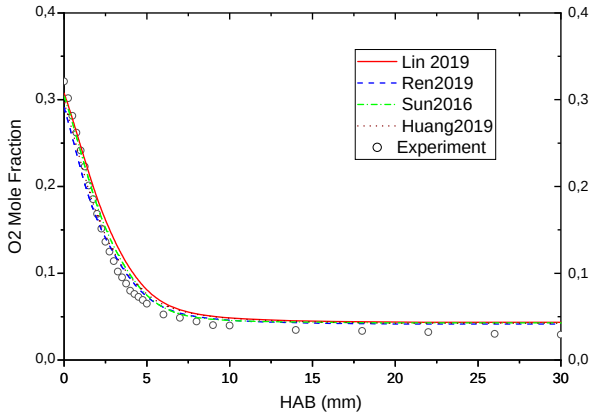

(b) O_2

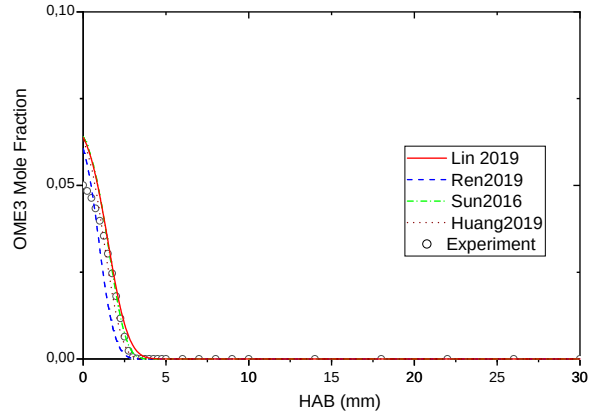

(c) OME_3

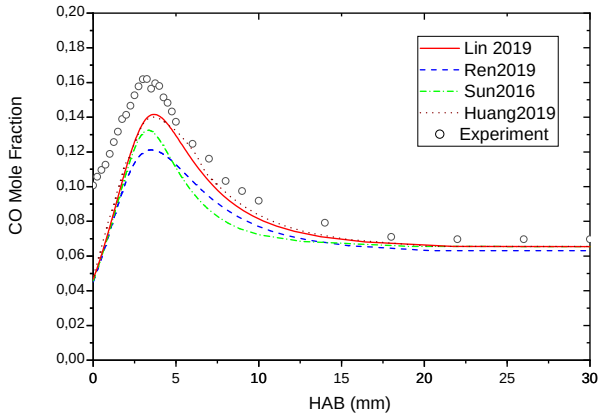

(d) CO

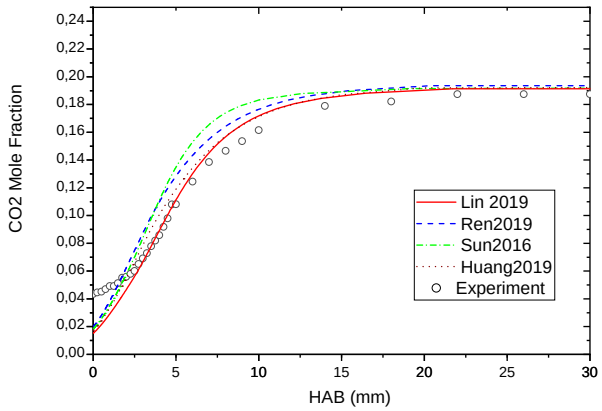

(e) CO_2

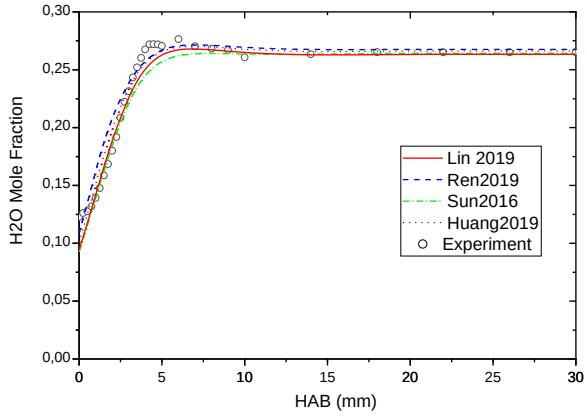

(f) H_2O

Figure 4.3: Species concentrations for major species with a OME_3 flame. Both experimental data and the preditctions of the mechanisms are included.

The major species are predicted fairly well, with the exception of CO. The initial CO and CO_2 concentration is underpredicted in the flame zone (HAB < 3 mm), this may be caused by probe perturbation and measurement errors in the experiments. The major species results may be summarized as follows:

- **CO_2**: the initial value is wrongly predicted. However, the rest of the values is predicted reasonable well. The Sun2016 mechanism, and to some extent the Ren2019 mechanism, overpredicts the CO_2 molefraction from 5-15 mm above the burner, but the final values are well predicted.
- **CO**: From the initial value to around 20 mm above the burner, the value is wrongly predicted most likely due to errors in the experiments.
- OME_3: Initial value is a bit overpredicted (which probably comes from the uncertanties in the experiments), but the mechanisms follow the experimental data nonetheless satisfactory.
- **Ar**: The argon concentration in the flame zone is overpredicted for all mechanisms, this is probably because of the uncertainties in the experiments. Otherwise, the results are adequate for all mechanisms.
- **H_2O** and O_2: The prediction of H_2O and O_2 by the mechanisms show satisfactory agreement with the experimental data.

The figures 4.4a, 4.4b, 4.4c, 4.4d, and 4.4e show the minor species profiles from the simulations using the Premixed Stabilized Flame Model in DARS.

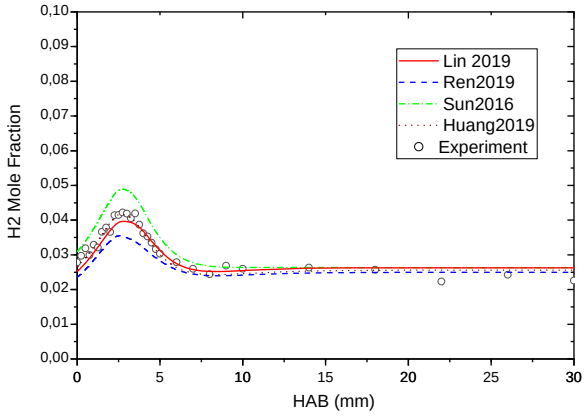

(a) H_2

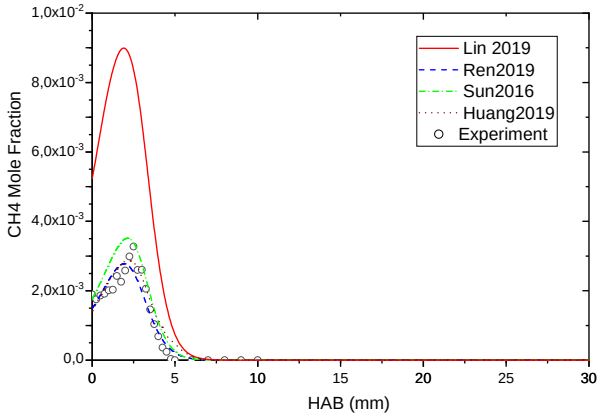

(b) CH_4

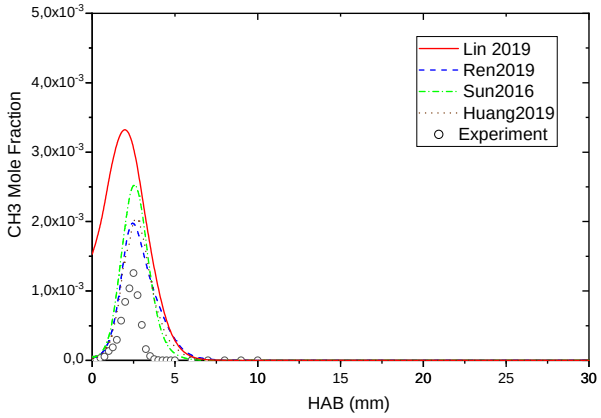

(c) CH_3

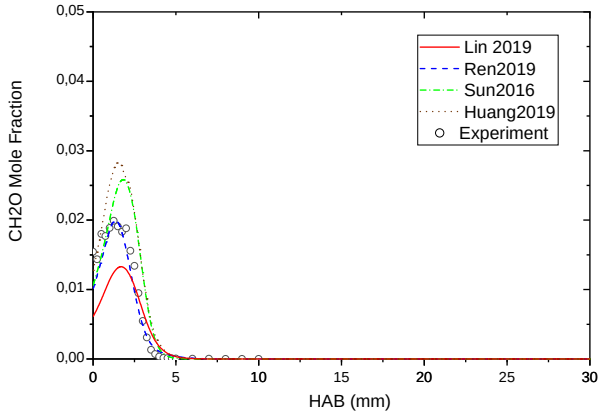

(d) CH_2O

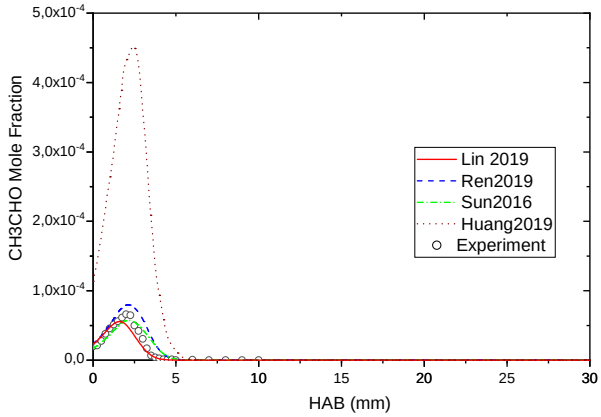

(e) CH_3CHO

Figure 4.4: Species concentrations for minor species with a OME_3 flame. Both experimental data and the preditctions of the mechanisms are included.

The minor species are also mostly predicted faily well. However, every mechanism have at least one species that is not predicted adequately. The results are summarized as follows:

- **H_2**: The H_2 concentration is slightly underpredicted by Ren2019 and slightly overpredicted by Sun2016. Huang2019 predicts this very well, and Lin's prediction is satisfactory.
- **CH_4**: The Ren2019, Huang2019, and Sun2016 mechanisms predict the concentration satisfactory, the Lin2019 mechanism overpredicts by a factor of 3.
- **CH_3**: The CH_3 concentration gets somewhat overpredicted by every mecha-

nism, Lin2019 more than the others.

- **CH_2O**: The Ren2019 mechanisms prediction of the CH_2O concentration is fitting very well with the experiments. The Lin2019 mechanism underpredicts while the Sun2016 and the Huang2019 overpredicts the concentration.

- **CH_3CHO**: Adequate prediction of every mechanism except of the Huang2019 mechanism which overpredicts by a factor of 5.

The figures 4.5a, 4.5b, and 4.5c show the species profiles of the soot precursors C_2H_2, C_2H_4, and C_2H_6 simulated using the Premixed Stabilized Flame Model in DARS against experimental data.

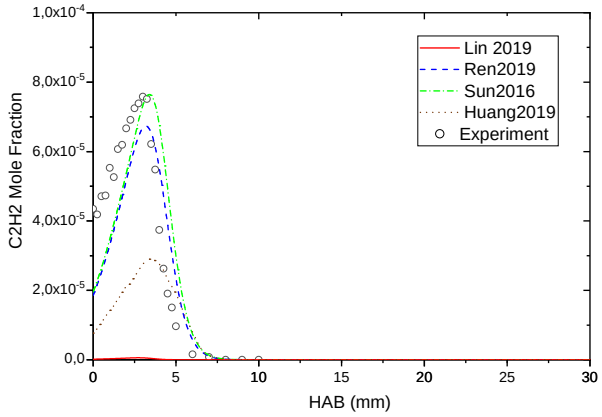

(a) C_2H_2

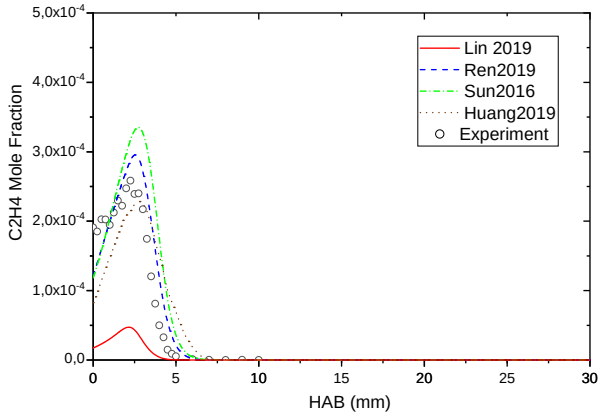

(b) C_2H_4

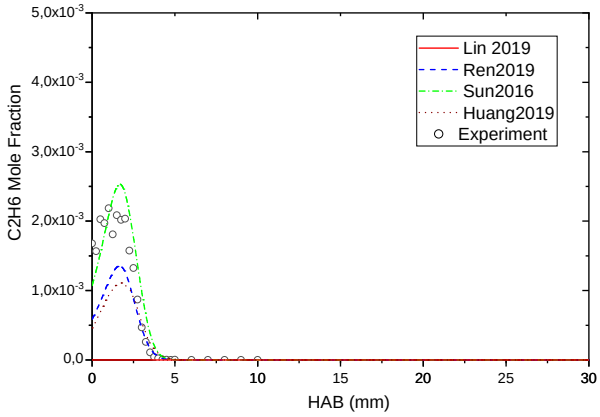

(c) C_2H_6

Figure 4.5: Species concentrations for soot precursors with a OME_3 flame. Both experimental data and the preditctions of the mechanisms are included.

The soot precursors are predicted reasonable well in the Sun2016, Ren2019 and Huang2019. The initial concentration of the soot precursors are predicted wronly, this may be caused by uncertainties in the experiment. Due to the removal of emission predictions, these species are not predicted adequatley in the Lin2019 mechanism. The simulations result of the soot precursor species are summarized as follows:

- $\mathbf{C_2H_2}$: The Huang2019 underpredicts the peak concentration of C_2H_2 by over a factor of 2. The Ren2019 and Sun2019 mechanisms predictions fit satisfactory to the experimental data.
- $\mathbf{C_2H_4}$: The Sun2016 mechanism overpredicts the concentration by a little, while Huang2019 slighly underpredicts the peak concentration, and slighly overpredicts the duration of the species. The Ren2019 mechanism is adequately fitting.
- $\mathbf{C_2H_6}$: The Sun2016 mechanism fits satisfactory to the experimental data. The Ren2019 and Huang2019 underpredicts the concentration.

4.1.4 HCCI combustion

The results from the HCCI combustion simulations (without EGR) performed by the Stochastic HCCI Reactor Model in DARS are shown in the figures 4.6a, 4.6b, 4.6c, and 4.6d. Two more figures, for $\phi = 0.18$ and $\phi = 0.21$, are found in the appendix A.

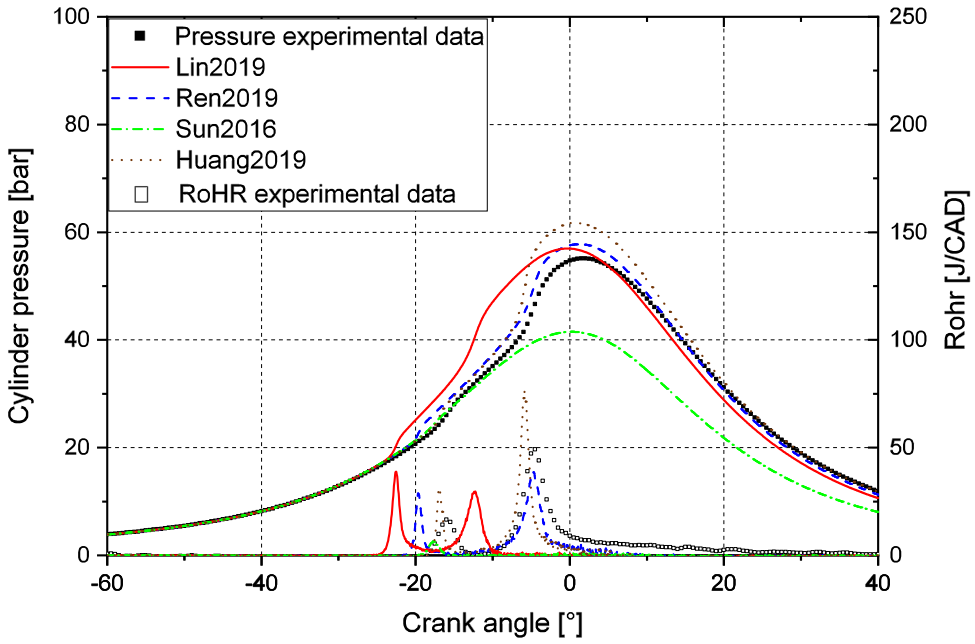

(a) $\phi = 0.24$

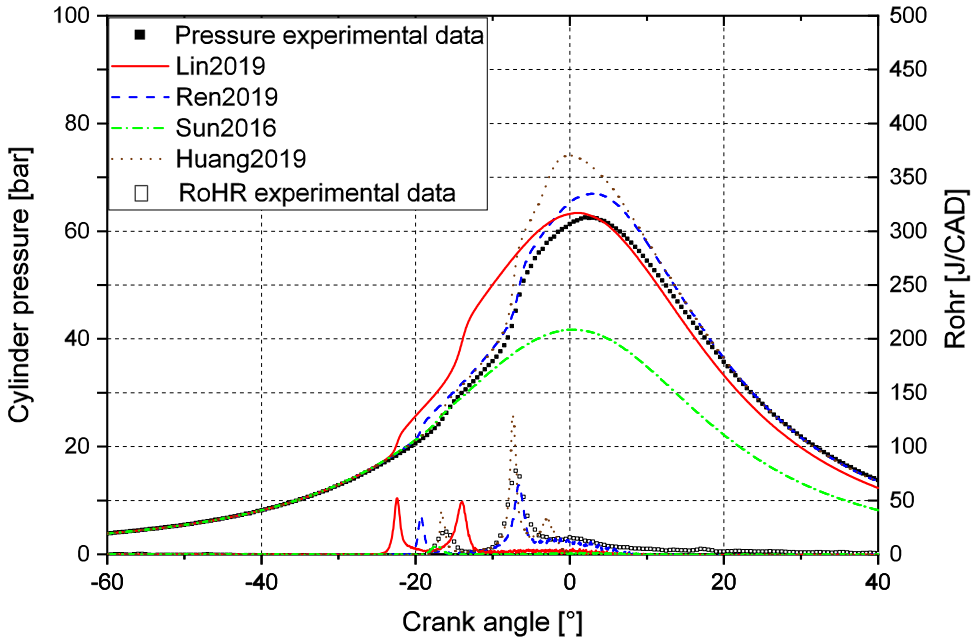

(b) $\phi = 0.28$

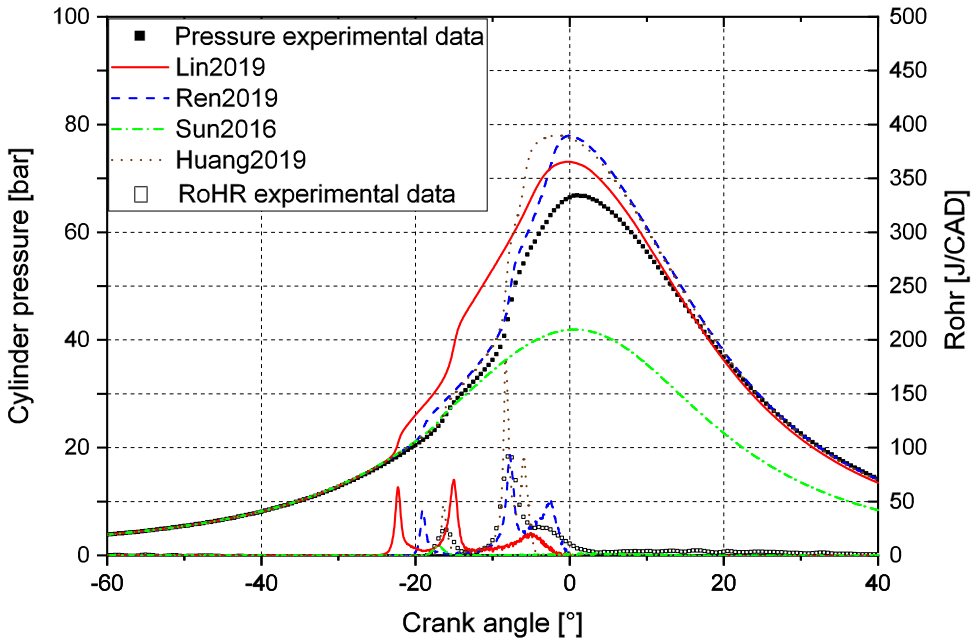

(c) $\phi = 0.31$

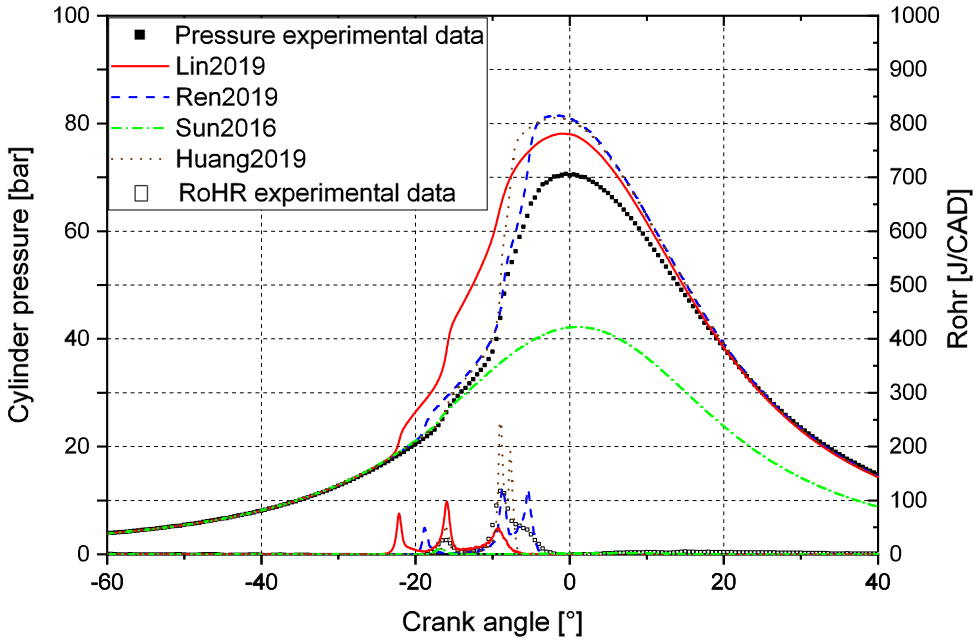

(d) $\phi = 0.34$

Figure 4.6: HCCI combustion with OME_3 as fuel. Both experimental data and the mechanisms' preditctions of the pressure profile and heat release are included.

The HCCI combustion results from the Lin2019 mechanism tends to predict the low-temperature heat release about 5 degrees of crank angle too early and too steep. The high-temperature heat release as also about 5 degrees of crank angle and is not as large as from the experiments. The predicted pressure curve differs from the experiments due to the early pressure rise caused by the early ignition and early heat releases.

The general trend in the HCCI combustion prediction by the Ren2019 mechanism is that the low-temperature heat release is about 2-3 crank angle degrees too early, and a little too steep. The timing of the high-temperature heat release is usually predicted satisfactory. The shape of the high-temperature heat release for $\phi \leq 0.28$ is acceptable, but the amount of heat released in the high-temperature heat release of lower than the experimental data.

For $\phi \geq 0.31$ the two stages of the high-temperature heat release is captured, but the second stage is nonetheless overpredicted. The predicted pressure curve follows the shape of the experimental pressure curve adequate for $\phi \leq 0.28$, and would be a realistic representation if it was not for the early prediction of low-temperature heat release. The difference between the predicted pressure peaks and the pressure peaks from the experiments , when $\phi \leq 0.28$, are normally under 4 bar. For $\phi \geq 0.31$ the difference in the pressure peaks are over 10 bars, this is caused by the overprediction of the second stage of the high-temperature heat release.

The timings of the low-temperature and the high-temperature heat releases predicted by the Huang2019 mechanism are in great correspondence with the experimental data in all cases except for the case with EGR = 52% . However, the heat release rates is too steep and the duration too short. The two-stage heat release of the high-temperature heat release is already predicted at $\phi = 0.28$, in the experiments the third heat release is only observed at $\phi \geq 0.31$.

At $\phi \geq 0.31$, the second stage of the high-temperature heat release is predicted 1-2 crank angle degrees too early, is too steep, and the duration is to short compared to the experimental data. Due to the steep heat releases, the pressure peaks are overpredicted by around 5 bars for the cases with $\phi \leq 0.24$. For the cases with $\phi \geq 0.28$ the preassure peak is overpredicted by more than 10 bars.

The Sun2016 mechanism experiences hardly any heat release in the low-temperature heat release, and apparently no high-temperature heat release. There is no main combustion process in any of the cases, as can be read from the pressure curves. This can be explained by the poor low- and intermediate temperature region (<800K and 800-1200 K) of the Sun2016 mechanism.

While the figures 4.7a and 4.7b show the results from the HCCI combustion (with EGR) simulations using the Homogeneous HCCI Reactor Model. The result from the simulation of HCCI combustion with EGR = 42% is found in appendix A

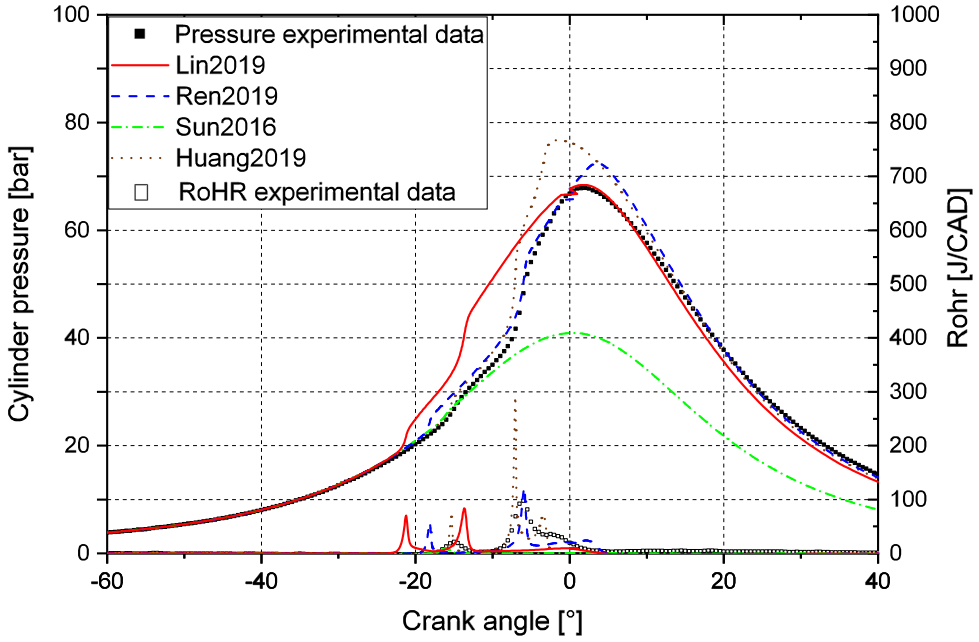

(a) $\phi = 0.34$ EGR=26%

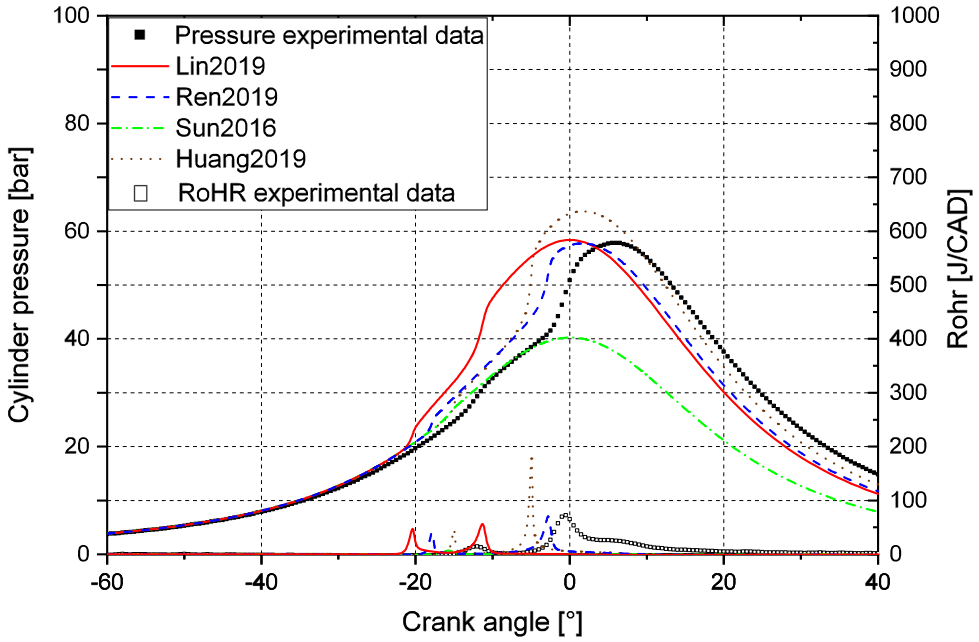

(b) $\phi = 0.34$ EGR=52%

Figure 4.7: HCCI combustion with EGR with OME_3 as fuel. Both experimental data and the mechanisms' preditctions of the pressure profile and heat release are included.

4.2 Implementation of the mechanisms in STAR-CD

The pressure diagram, temperature diagram, RoHR, and the species concentrations results from STAR-CD will be presented, compared, and discussed in this section. A comprehensive OME_3 mechanism should be able to adequately predict the combustion of OME_1, thus simulations using OME_1 as fuel is included. Experimens performed by an engine with the same engine data using OME_1 with an additive (OME_{1b}) will be used to compare against. The Lin2019 mechanism did not include OME_1 as a species, therefore the combustion of OME_1 were only simulated by the Ren2019, Huang2019, and the Sun2016 mechanism. An earlier simulation of OME_1 in the same engine model using the ECFM-3Z combustion model will also be used in the comparison of the OME_1 results. An earlier simulation of OME_3 using the ECFM-3Z combustion model does unfortunately not exist.

4.2.1 Combustion of OME_3

Figure 4.8 shows the pressure diagram and the RoHR from the OME_3 combustion simulation performed in STAR-CD. The squares are experimental data from the combustion of OME_{1b}.

Based on the cetane number, the ignition delay time should be smaller for OME_3 than for OME_{1b}. However, OME_{1b} evaporates more readily and the time it takes from droplets to vapour is lower than that of OME_3. This could be an explanation of the late ignition predicted by the mechanisms, compared to the experimental data. The injected mass in the CFD simulation is the same as in the experiment. Because the lower heating value of OME_3 is lower than the lower heating value of OME_{1b}, the heat release and the pressure peak is not as high in the simulations of OME_3 as the experimental data. As shown in figure 4.8. However, the differnce in heating value is not so significant that the difference in the pressure peaks are 15 bars.

The Lin2019 mechanism diverged during the main injection at 722.46 CAD. This was when the drop in heat release, as predicted by the other mechanisms, could have started. It is suspected that the mechanism is missing some reactions in the combustion process, and as a result it becomes unstable. However, the available data of the pressure profile and the RoHR show that the Lin2019 mechanism predicts the start of ignition slightly ahead of the Ren2019 and Huang2019 mechanisms. Apart from that, they are very similiar.

The Ren2019 and Huang2019 mechanisms have nearly identical predictions of the pressure profile and the RoHR. This may be related to the common relation to the

He2018 mechanism. Both mechanisms predict a drop in the heat release around 724 CAD, this drop in heat release is not physically realistic and is a deficiency in the mechanisms. The same drop in heat release can be seen with the Sun2016 mechanism at 730 CAD. The rest of the RoHR might be a little overpredicted, but the shape looks fitting. The many spikes in the RoHR is likely to be from the stiffness of the chemical equations used in the computation of heat release. By reducing the time step size, these spikes might be gone.

The Sun2016 mechanism ignited around five CAD later than the others and the RoHR was much steeper, this was due the mechanism's poor performance ignition prediction as seen in the ignition delay time section. After the injection, the ROHR looks like the prediction of Huang2019 and Ren2019 mechanisms.

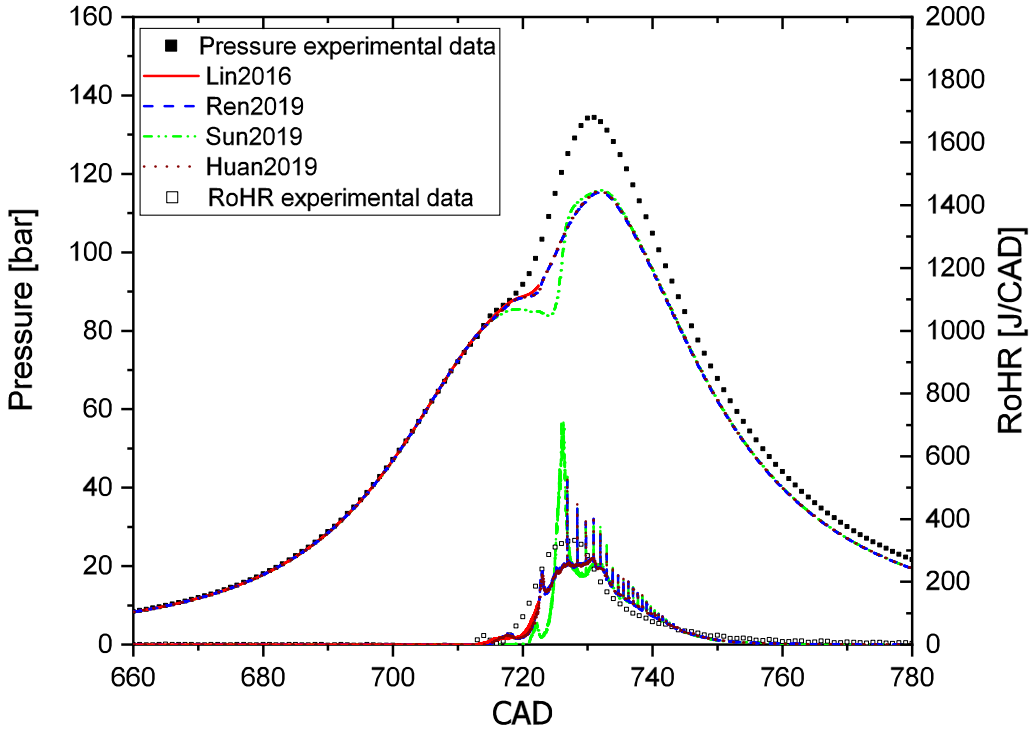

Figure 4.8: Pressure and RoHR diagram of the different mechanisms for OME_3.

Figure 4.9 shows the temperature diagram from the OME_3 combustion simulation performed in STAR-CD. The squares are experimental data from the combustion of OME_{1b}. It also shows the injection rate of the two injections.

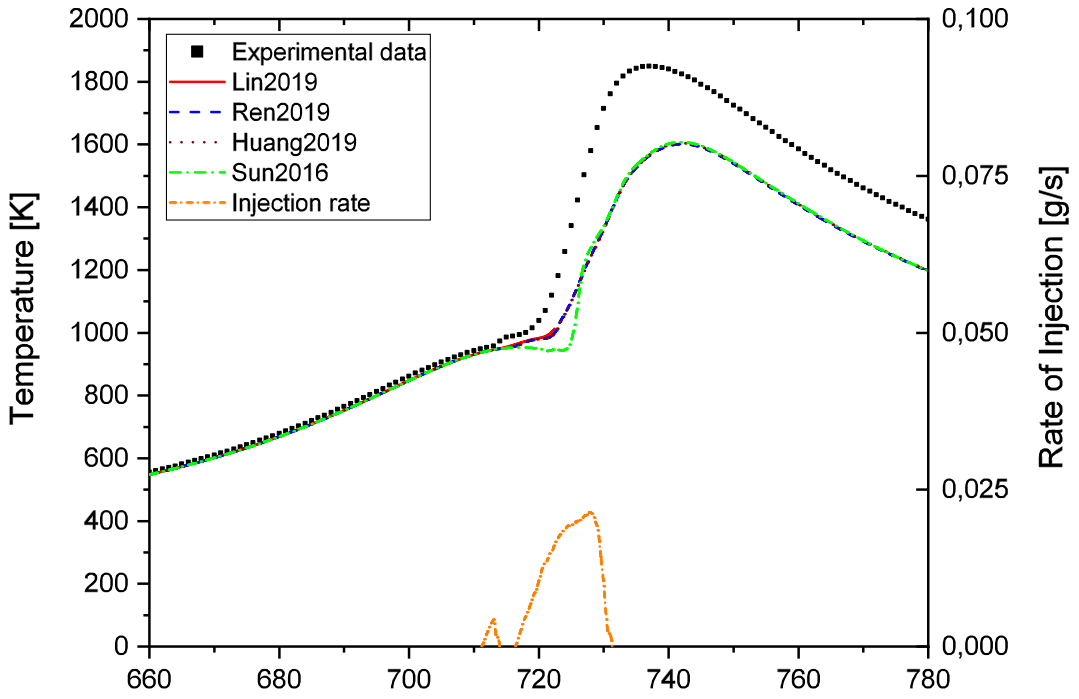

Figure 4.9: Temperature diagram of the different mechanisms for OME_3. The fuel injection rateis included.

All the mechanisms show somewhat unrealistic predictions of the temperature profile. It was expected to be a little lower than the experimental data. However, 250 °C is unrealistic given the small difference in the heating values of the fuels. Nonetheless, the Lin2019, Ren2019, and Huang2019 have a more realistic prediction of the temperature profile compared to the Sun2016 mechanism. The Sun2016 mechanism shows a late temperature increase, this is due to the poor ignition predictions.

The figures 4.10a, 4.10b, and 4.10c show the major species' profiles from the OME_3 combustion simulation performed in STAR-CD. The Lin2019 mechanism's major species is found in appendix A.

Due to the late ignition of the Sun2016 mechanism, the O_2 reacts later and therefore depletes later than for the O_2 predicted in the Sun2016 and Ren2019 mechanisms. At 725 CAD, the O_2 reacts faster compared to the Ren2019 and Huang2019 mechanisms. This is also visible in the other major species; the production of CO, CO_2, and H_2O starts, and the depletion of OME_3 starts. This late and fast reaction is the reason for the late, but steep pressure and temperature rise in figures 4.8 and 4.9.

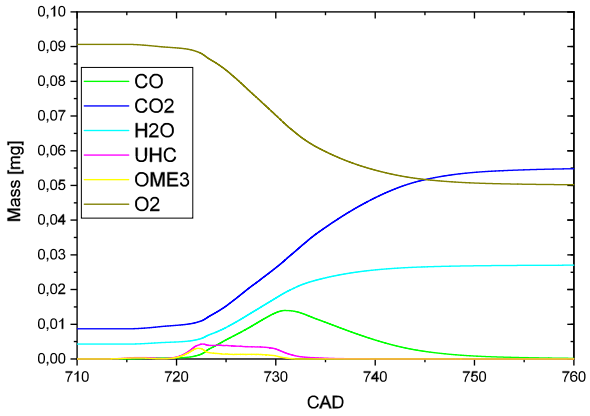

(a) Ren2019 Major species

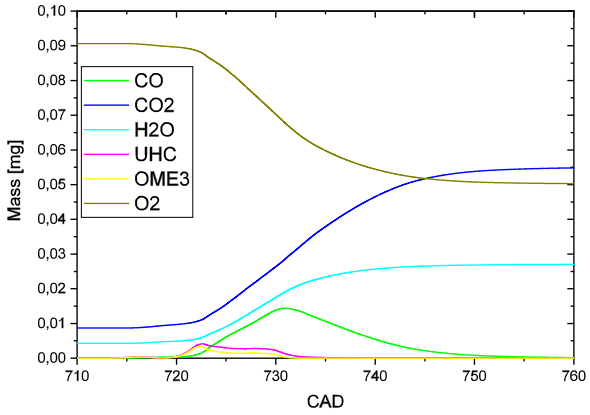

(b) Huang2019 Major species

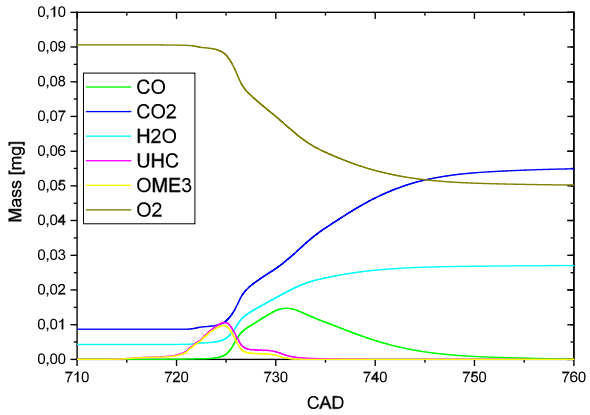

(c) Sun2016 Major species

Figure 4.10: Species concentrations for the major and minor species of the CFD simulation using OME_3 as fuel.

The major species mass profiles of the simulation with the Ren2019 and Huang2019 mechanisms are nearly identical. The only noticeable difference (on the plot) is in the mass of UHC and CO. The Ren2019 mechanism predicts a slightly higher UHC mass than Huang2019, while the Huang2019 mechanism's prediction of the CO mass during the main injection is barely higher than the Ren2019 mechanism's prediction.

The figures 4.11a, 4.11b, and 4.11c show the minor species' profiles from the OME_3 combustion simulation performed in STAR-CD. The Lin2019 mechanism's minor species is found in appendix A.

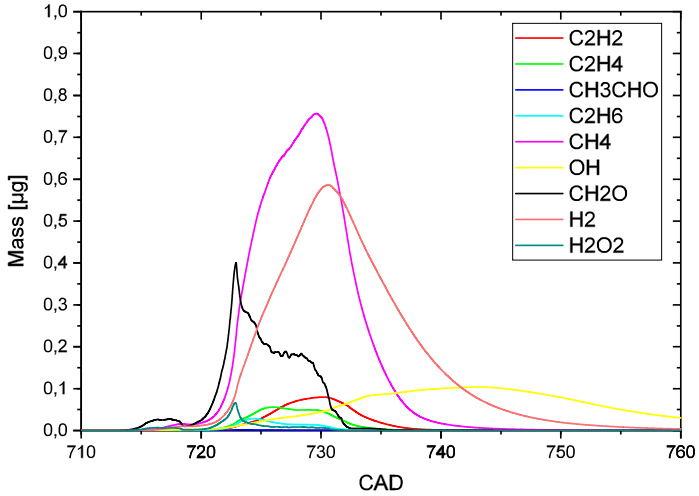

(a) Ren2019 Minor species

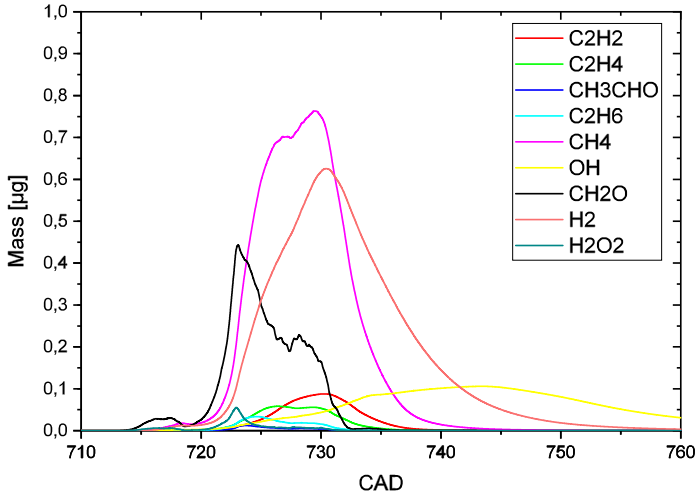

(b) Huang2019 Minor species

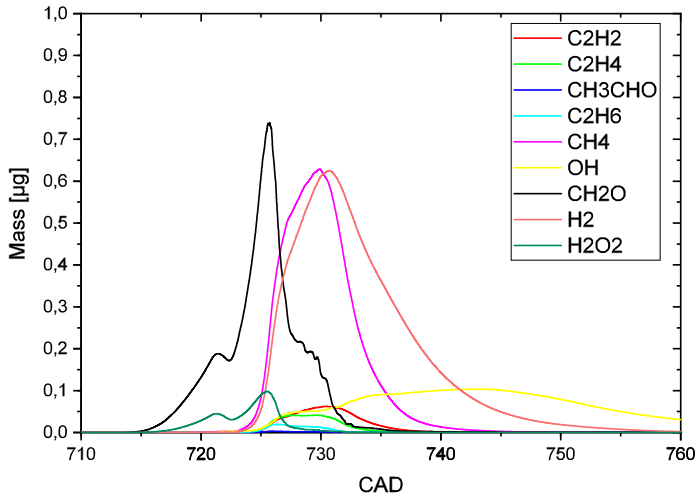

(c) Sun2016 Minor species

Figure 4.11: Species concentrations for the major and minor species of the CFD simulation using OME_3 as fuel.

The minor species mass profiles of the simulation with the Ren2019 and Huang2019 mechanisms are quite similiar although there exists some tiny differences. The major difference is in the CH_3CHO species. The Huang2019 mechanism's prediction of the mass of CH_3CHO reaches up to almost a magnitude difference in the mass prediction of the Ren2019 mechanism. Another difference in the mechanisms is that mass of $CH2_2O$ is alike and is increasing until just before 723 CAD. Then the $CH2_2O$ starts depleting in the Ren2019 mechanism. The depletion of $CH2_2O$ doesn't start in the Huang2019 mechanism until half a CAD later. The $CH2_2O$ is mass is then dissimilar. There is also a little difference in the mass of CH_4 and H_2. Other than that, there exists minor differences in the other species, with exception of OH. The mass OH is virtually the same according to the graphs.

The minor species predicted by Sun2016 is also quite different than the predictions of the other mechanisms. The major difference is the CH_2O mass profile. Both the first and the second production of CH_2O is predicted a little later than the other mechanisms, and more mass is predicted. Another major difference is that the H_2O_2 species has two production phases and more mass is predicted than for the other mechanisms. The production of CH_4, H_2, CH_3CHO, OH, and the soot precursos are also later due to the late ignition. The predicted mass of CH_4 is less compared to the other mechanisms. Other than that, the mass are similiar.

4.2.2 Combustion of OME_1

Figure 4.12 shows the pressure diagram and the RoHR from the OME_1 combustion simulation performed in STAR-CD. The squares are experimental data from the combustion of OME_{1b}.

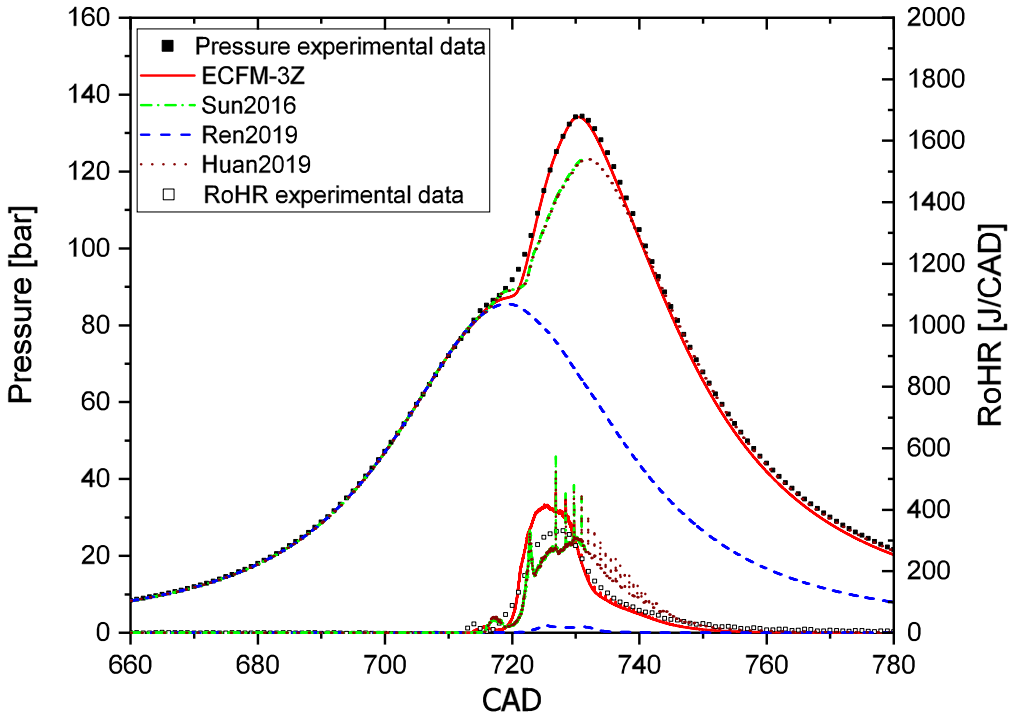

Figure 4.12: Pressure and RoHR diagram of the different mechanisms for OME_1.

The simulation of the Sun2016 mechanism reached 731.5 CAD before the results had to be extracted because of the deadline. However, the pilot injection and the main injection were both covered; hence, some important results can be presented.

Because the cetane number of OME_1 is lower than that of OME_{1b}, as seen table 3.17, the simulations should have a slightly delayed ignition compared to the experimental data. As expected, both the detailed chemistry combustion model using the mechanisms and the ECFM-3Z combustion model predicts the start of ignition later than the experimental data. Apart from that, the ECFM-3Z combustion model's prediction of the pressure curve is satisfactorily fitting after around 724 CAD. On the contrary, the detailed chemistry combustion model, underpredicts the pressure curve with every mechanism, thus giving a poor recreation of the experimental pressure curve. The Ren2019 mechanism did not ignite properly.

The ECFM-3Z combustion model predicts underpredicts the magnitude of first heat release, but the timing is fitting to an extent. The magnitude of the second heat release gets overprediced. Apart from that, the shape of the RoHR curve is fitting well with the experimental data. The heat release predicted by the Sun2016 and the Huang2019 mechanisms are virtually identical. The first heat release gets overpredicted and the timing is around two CAD too late. The same drop in heat release observed for the OME_3 simulation is observed here as well. This drop is inhibits the pressure curve from following the experimental pressure curve. Other than that, the RoHR is a bit overpredicted and not fitting that well with the experimental data. The Ren2019 mechanism did not ignite properly, although some reactions happened and gave off heat.

Figure 4.13 shows the temperature diagram from the OME_1 combustion simulation performed in STAR-CD. The squares are experimental data from the combustion of OME_{1b}. It also shows the injection rate of the two injections.

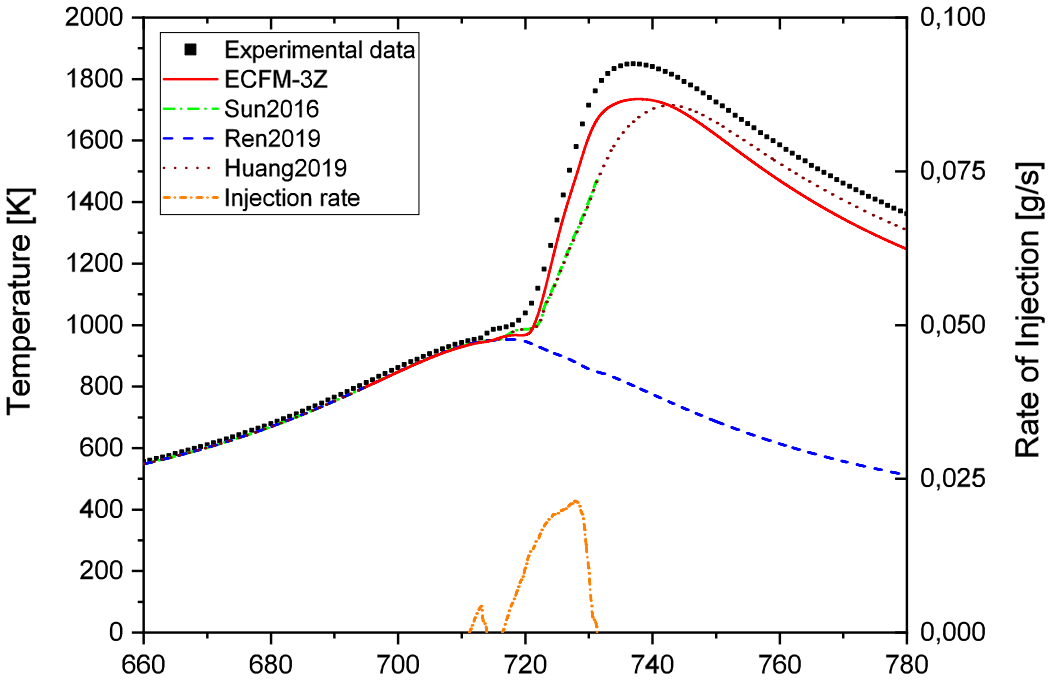

Figure 4.13: Temperature diagram of the different mechanisms for OME_1. The fuel injection rateis included.

The ECFM-3Z combustion model poor prediction of the first heat release is clear from the temperature profile. The second heat release was initially overpredicted and later more fitting to the experimental data. This can be seen on the temperature gradient, although it is larger in some places, it does not reach the high temperatures of the experimental data. The Huang2019 and Sun2016 mechanisms prediction of the magnitude and timing of the first heat release is visible in the temperature profile. The second heat release is not as steep as neither the experimental data nor the ECFM-3Z combustion model. The duration of the temperature increase is also longer than the experimental data, thus making the prediction more fitting to the experimental data. All things considered, both combustion models does not give a good recreation of the temperature profile.

The figures 4.14a, 4.14b, and 4.14c show the major species' profiles from the OME_3 combustion simulation performed in STAR-CD. The Lin2019 mechanism's major species is found in appendix A.

The Huang2019 and Sun2016 mechanisms prediction of the major species are virtually the same. On the other hand, the ECFM-3Z combustion model's prediction of the major species is very different. The only similar prediction of a species is OME_3. The major differences are listed listed below:

- For ECFM-3Z, the oxygen is depleted much faster, and the oxygen mass at the end is a tiny bit lower than for Huang2019.
- For Huang2019 UHC is computed, this was not computed for ECFM-3Z.
- The CO_2 and the H_2O were produced faster for ECFM-3Z than for the Huang2019 mechanism. The mass of both species were also both a tiny bit higher for the ECFM-3Z combustion model.
- The CO mass profile prediction of the Huang2019 mechanism is significantly larger than that of the ECFM-3Z combustion model.

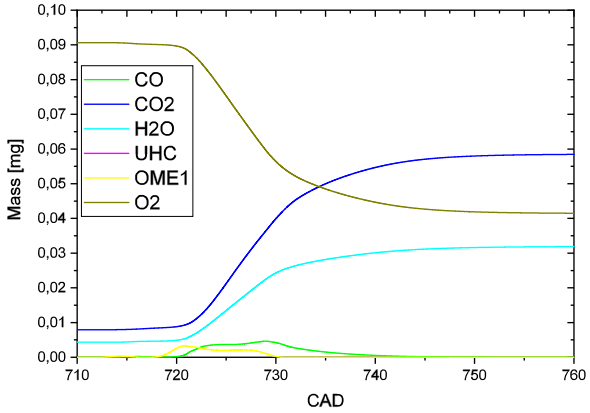

(a) ECFM-3Z Major species

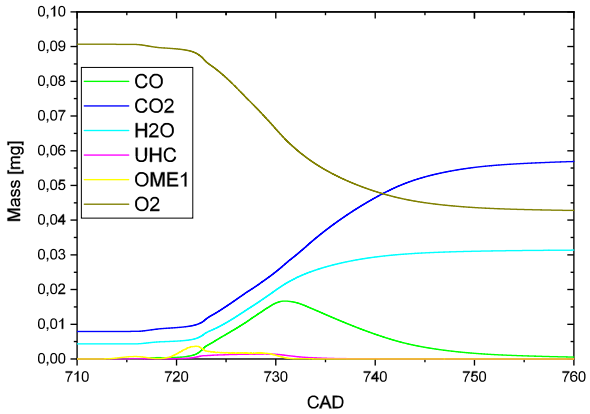

(b) Huang2019 Major species

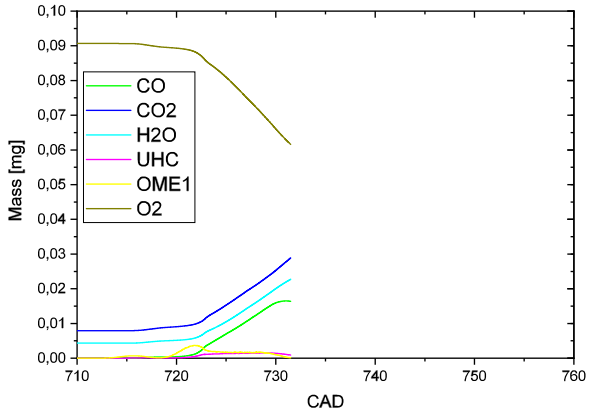

(c) Sun2016 Major species

Figure 4.14: Species concentrations for the major and minor species of the CFD simulation using OME_1 as fuel.

The figures 4.15a, 4.15b, and 4.15c show the minor species' profiles from the OME_3 combustion simulation performed in STAR-CD. The Lin2019 mechanism's minor species is found in appendix A.

The minor species mass profiles of the simulation with the Sun2016 and Huang2019 mechanisms are very similiar, only tiny differences exist; The shape of the mass profile of CH_4 and H_2 is alike, but the Sun2016 mechanism predicts a little higher production of CH_4 than the Huang2019 mechanism. And the Huang2019 mechanism predicts a little higher production of H_2 than the Sun2016 mechanism.

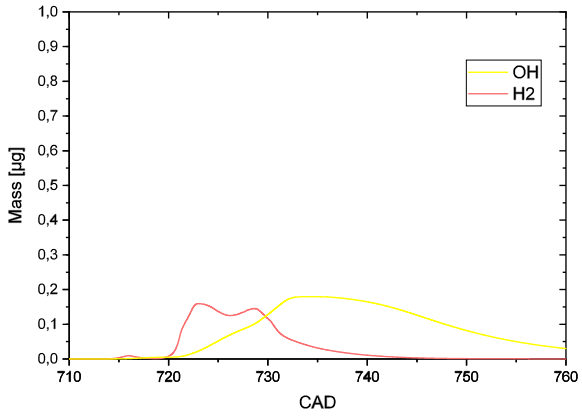

(a) ECFM-3Z Minor species

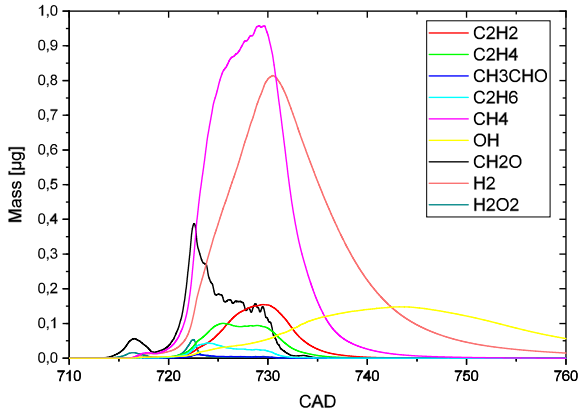

(b) Huang2019 Minor species

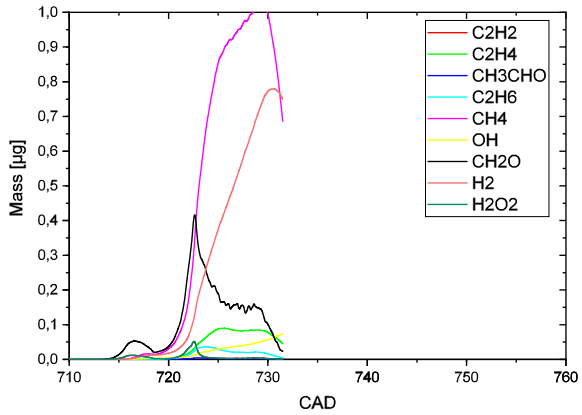

(c) Sun2016 Minor species

Figure 4.15: Species concentrations for the major and minor species of the CFD simulation using OME_1 as fuel.

The simulation of the ECFM-3Z combustion model only includes the mass profile of the minor species H_2 and OH. The highest H_2 mass predicted by ECFM-3Z is less than the prediction by the Huang2019 mechanism by over a factor of five. The production of OH starts the same time for both the ECFM-3Z combustion model and the Huang2019 mechanism. The OH mass predicted by ECFM-3Z is a bit higher than the prediction by the Huang2019 mechanism, but after around 744 CAD, the Huang2019 mechanism predicts a higher OH than the ECFM-3Z does.

5 Conclusion

The combustion characteristics of OME_3 were investigated using available OME_3 mechanisms in the 0D/1D simulation software, DARS. The OME_3 mechanisms were then implemented in 3D-CFD combustion simulations using the detailed chemistry combustion model in STAR-CD. The combustion of both OME_3 and OME_1 were simulated. This chapter will present the evaluation of the results.

The ignition delay time, species profile, laminar flame speed, and 0-D HCCI combustion results from the simulations in DARS showed satisfactory agreement with experimental data. The model used to simulate laminar flame speed were unfortunately unsuccessful in creating a realistic representation of the experimental data. However, the other models used gave satisfactory representations of the experimental data, with the exception of the Sun2016 mechanism's prediction of ignition delay time and HCCI combustion. The most accurate mechanisms based on the comparison of 0D and 1D simulations performed in DARS and the experiments, starting with the most accurate mechanism, are as follows: Ren2019, Huang2019, Lin2019, and Sun2016.

The mechanisms were then implemented in the 3D-CFD combustion simulation of OME_3 in STAR-CD. The Lin2019 mechanism diverged at 722.46 CAD, the suspected cause was the mechanism's lack of reactions that under the given conditions caused the unstability in the solver. The Sun2016 mechanism performed poorly compared to the Ren2019 and the Huang2019 mechanisms both in terms of computational cost and in terms of realistic results. However, the Ren2019 and Huang2019 mechanisms were found to underpredict the pressure- and the temperature diagram, thus giving an unrealistic representation of the combustion using OME_3 as fuel. Because there were no OME_3 engine test to compared against, this needs to be confirmed.

It was desired that the OME_3 mechanisms could also accurately predict the combustion of OME_1, thus OME_1 combustion simulations were also performed. Using the Sun2016, Huang2019 mechanisms in the detailed chemistry combustion model ignition was achieved, but they were unsuccessful in providing an accurate depiction of the experimental data. The ECFM combustion model showed more physically realistic results. The Ren2019 mechanism did not ignite properly, and the Lin2019 mechanism did not contain OME_1. Therefore, the ECFM-3Z combustion model is a better alternative for the simulation of the combusiton of OME_1 than the detailed chemistry model using the OME_3 mechanisms evaluated in this thesis.

6 Future work

The issues listed below could be used as a starting point for further investigations:

- Engine tests using OME_3 as fuel should be performed and compared to the simulated results of the 3D-CFD combustion of OME_3 using the OME_3 mechanisms in the detailed combustion model. The combustion of OME_3 using the ECFM-3Z combustion model should also be compared.
- A closer look into the 3D-CFD results and into the species profiles should be undertaken. The reactions taking place could then be predicted by looking at the change in the different species and comparing that to sensitivity analyses performed in DARS. The reaction(s) responsible for the drop in RoHR in the CFD simulations are especially interesting for improving the reaction mechanisms.
- It would be interesting to see how much the DMZ method would effect the 3D-CFD combustion results as the computational time could be substantially reduced.
- A closer look into the cause of the Lin2019 mechanism's divergence in the 3D-CFD simulation should be undertaken to perhaps make the mechanism compatible with the simulation.

Reference list

[1] W. W. T. R. Patrick R. Schmidt, Werner Zittel, "Renewables in transport 2050 – empowering a sustainable mobility future with zero emission fuels from renewable electricity – europe and germany.," tech. rep., FVV.

[2] W. Maus, E. Jacob, M. Härtl, P. Seidenspinner, and G. Wachtmeister, "Synthetic fuels - ome1: a potentially sustainable diesel fuel," *Internationales wiener motorensymposium*, vol. 777, pp. 325–347, 01 2014.

[3] U. Kramer, D. Goericke, and R. Thee, "Energy paths for road transport in the future," *MTZ worldwide*, vol. 80, pp. 18–25, May 2019.

[4] H. Liu, Z. Wang, J. Wang, and X. He, "Improvement of emission characteristics and thermal efficiency in diesel engines by fueling gasoline/diesel/PODEn blends," *Energy*, vol. 97, pp. 105–112, Feb. 2016.

[5] E. Jacob and W. Maus, "Oxymethylene ether as potentially carbon-neutral fuel for clean diesel engines part 2: Compliance with the sustainability requirement," *MTZ worldwide*, vol. 78, pp. 52–57, Mar 2017.

[6] K. Gaukel, P. Dworschak, D. Pélerin, M. Härtl, and G. Wachtmeister, "Combustion process optimization for oxymethylene ether fuels in a heavy-duty application," 02 2019.

[7] M. Härtl, P. Seidenspinner, E. Jacob, and G. Wachtmeister, "Oxygenate screening on a heavy-duty diesel engine and emission characteristics of highly oxygenated oxymethylene ether fuel OME1," *Fuel*, vol. 153, pp. 328–335, Aug. 2015.

[8] K. Gaukel, D. Pélerin, M. Härtl, G. Wachtmeister, J. Burger, W. Maus, and E. Jacob, "Der kraftstoff ome2: Ein beispiel für den weg zu emissionsneutralen fahrzeugen mit verbrennungsmotor," 04 2016.

[9] M. Härtl, K. Gaukel, D. Pélerin, and G. Wachtmeister, "Oxymethylene ether as potentially co2-neutral fuel for clean diesel engines part 1: Engine testing," *MTZ worldwide*, vol. 78, pp. 52–59, Feb 2017.

[10] D. Wang, G. Zhu, Z. Li, and C. Xia, "Polyoxymethylene dimethyl ethers as clean diesel additives: Fuel freezing and prediction," *Fuel*, vol. 237, pp. 833–839, Feb. 2019.

[11] "Ns-en 590," in *Automotive fuels - Diesel - Requirements and test methods, volume = 1, address = Oslo,No, author = SN/K 032 url="https://www.drivkraftnorge.no/siteassets/dokumenter–filer/diverse-dokumenter/bransjestandard-revidert-februar-2018.pdf"*, Jan. 2017.

[12] S. E. Iannuzzi, C. Barro, K. Boulouchos, and J. Burger, "POMDME-diesel blends: Evaluation of performance and exhaust emissions in a single cylinder heavy-duty diesel engine," *Fuel*, vol. 203, pp. 57–67, Sept. 2017.

[13] D. Pélerin, K. Gaukel, M. Härtl, and G. Wachtmeister, "Simplifying of the fuel injection system and lowest emissions with the alternative diesel fuel oxymethylene ether," in *16th Conference "The Working Process of the Internal Combustion Engine"*, Institute of Internal Combustion Engines and Thermodynamics, Graz University of Technology, 2017.

[14] J. Burger, M. Siegert, E. Ströfer, and H. Hasse, "Poly(oxymethylene) dimethyl ethers as components of tailored diesel fuel: Properties, synthesis and purification concepts," *Fuel*, vol. 89, pp. 3315–3319, Nov. 2010.

[15] L. Pellegrini, M. Marchionna, R. Patrini, C. Beatrice, N. D. Giacomo, and C. Guido, "Combustion behaviour and emission performance of neat and blended polyoxymethylene dimethyl ethers in a light-duty diesel engine," in *SAE Technical Paper Series*, SAE International, Apr. 2012.

[16] C. A. Daly, J. M. Simmie, P. Dagaut, and M. Cathonnet, "Oxidation of dimethoxymethane in a jet-stirred reactor," *Combustion and Flame*, vol. 125, pp. 1106–1117, May 2001.

[17] W. A. Kopp, L. C. Kröger, M. Döntgen, S. Jacobs, U. Burke, H. J. Curran, K. A. Heufer, and K. Leonhard, "Detailed kinetic modeling of dimethoxymethane. part i: Ab initio thermochemistry and kinetics predictions for key reactions," *Combustion and Flame*, vol. 189, pp. 433–442, Mar. 2018.

[18] S. Jacobs, M. Döntgen, A. B. Alquaity, W. A. Kopp, L. C. Kröger, U. Burke, H. Pitsch, K. Leonhard, H. J. Curran, and K. A. Heufer, "Detailed kinetic modeling of dimethoxymethane. part II: Experimental and theoretical study of the kinetics and reaction mechanism," *Combustion and Flame*, vol. 205, pp. 522–533, July 2019.

[19] T. Fleisch and R. Sills, "Large-scale gas conversion through oxygenates: beyond GTL-FT," in *Studies in Surface Science and Catalysis*, pp. 31–36, Elsevier, 2004.

[20] B. Lumpp, D. Rothe, C. Pastötter, R. Lämmermann, and E. Jacob, "Oxymethylene ethers as diesel fuel additives of the future," *MTZ worldwide eMagazine*, vol. 72, pp. 34–38, Mar 2011.

[21] L. Pellegrini, M. Marchionna, R. Patrini, and S. Florio, "Emission performance of neat and blended polyoxymethylene dimethyl ethers in an old light-duty diesel car," in *SAE Technical Paper Series*, SAE International, Apr. 2013.

[22] Z. Wang, H. Liu, X. Ma, J. Wang, S. Shuai, and R. D. Reitz, "Homogeneous charge compression ignition (HCCI) combustion of polyoxymethylene dimethyl ethers (PODE)," *Fuel*, vol. 183, pp. 206–213, Nov. 2016.

[23] H. Liu, Z. Wang, J. Wang, X. He, Y. Zheng, Q. Tang, and J. Wang, "Performance, combustion and emission characteristics of a diesel engine fueled with polyoxymethylene dimethyl ethers (PODE3-4)/ diesel blends," *Energy*, vol. 88, pp. 793–800, Aug. 2015.

[24] W. Sun, G. Wang, S. Li, R. Zhang, B. Yang, J. Yang, Y. Li, C. K. Westbrook, and C. K. Law, "Speciation and the laminar burning velocities of poly(oxymethylene) dimethyl ether 3 (POMDME 3) flames: An experimental and modeling study," *Proceedings of the Combustion Institute*, vol. 36, no. 1, pp. 1269–1278, 2017.

[25] T. He, Z. Wang, X. You, H. Liu, Y. Wang, X. Li, and X. He, "A chemical kinetic mechanism for the low- and intermediate-temperature combustion of polyoxymethylene dimethyl ether 3 (PODE3)," *Fuel*, vol. 212, pp. 223–235, Jan. 2018.

[26] S. Ren, S. L. Kokjohn, Z. Wang, H. Liu, B. Wang, and J. Wang, "A multicomponent wide distillation fuel (covering gasoline, jet fuel and diesel fuel) mechanism for combustion and PAH prediction," *Fuel*, vol. 208, pp. 447–468, Nov. 2017.

[27] T. He, H. ye Liu, Y. Wang, B. Wang, H. Liu, and Z. Wang, "Development of surrogate model for oxygenated wide-distillation fuel with polyoxymethylene dimethyl ether," *SAE International Journal of Fuels and Lubricants*, vol. 10, Oct. 2017.

[28] S. Ren, Z. Wang, B. Li, H. Liu, and J. Wang, "Development of a reduced polyoxymethylene dimethyl ethers (PODEn) mechanism for engine applications," *Fuel*, vol. 238, pp. 208–224, Feb. 2019.

[29] Q. Lin, K. L. Tay, D. Zhou, and W. Yang, "Development of a compact and robust polyoxymethylene dimethyl ether 3 reaction mechanism for internal combustion engines," *Energy Conversion and Management*, vol. 185, pp. 35–43, Apr. 2019.

[30] Y. Chang, M. Jia, Y. Li, Y. Liu, M. Xie, H. Wang, and R. D. Reitz, "Development of a skeletal mechanism for diesel surrogate fuel by using a decoupling methodology," *Combustion and Flame*, vol. 162, pp. 3785–3802, Oct. 2015.

[31] Y.-D. Liu, M. Jia, M.-Z. Xie, and B. Pang, "Enhancement on a skeletal kinetic model for primary reference fuel oxidation by using a semidecoupling methodology," *Energy & Fuels*, vol. 26, pp. 7069–7083, Nov. 2012.

[32] H. Song, C. Liu, F. Li, Z. Wang, X. He, S. Shuai, and J. Wang, "A comparative study of using diesel and PODEn as pilot fuels for natural gas dual-fuel combustion," *Fuel*, vol. 188, pp. 418–426, Jan. 2017.

[33] H. Huang, Y. Chen, J. Zhu, Y. Chen, D. Lv, Z. Zhu, L. Wei, and Y. Wei, "Construction of a reduced PODE3/nature gas dual-fuel mechanism under enginelike conditions," *Energy & Fuels*, vol. 33, pp. 3504–3517, Apr. 2019.

[34] H. Huang, D. Lv, J. Zhu, Z. Zhu, Y. Chen, Y. Pan, and M. Pan, "Development of a new reduced diesel/natural gas mechanism for dual-fuel engine combustion and emission prediction," *Fuel*, vol. 236, pp. 30–42, Jan. 2019.

[35] S. R. Turns, *An Introduction to Combustion: Concepts and Applications*. McGraw-Hill Education, 2011.

[36] J. D. Anderson, "Governing equations of fluid dynamics," in *Computational Fluid Dynamics*, pp. 15–51, Springer Berlin Heidelberg, 1992.

[37] D. A. Goussis and U. Maas, *Model Reduction for Combustion Chemistry*, pp. 193–220. Dordrecht: Springer Netherlands, 2011.

[38] C. Dopazo, "Relaxation of initial probability density functions in the turbulent convection of scalar fields," *Physics of Fluids*, vol. 22, no. 1, p. 20, 1979.

[39] C. Dopazo, "Recent developments in pdf methods," *Turbulent reacting flows*, pp. 375–474, 1994.

[40] J. Janicka, W. Kolbe, and W. Kollmann, "Closure of the transport equation for the probability density function of turbulent scalar field," *Journal of Non Equilibrium Thermodynamics*, vol. 4, 10 1979.

[41] R. Curl, "Dispersed phase mixing: I. theory and effects in simple reactors," *AIChE Journal*, vol. 9, 03 1963.

[42] H. A. Wouters, P. Nooren, T. Peeters, and D. Roekaerts, "Effects of micromixing in gas-phase turbulent jets," *International Journal of Heat and Fluid Flow - INT J HEAT FLUID FLOW*, vol. 19, pp. 201–207, 04 1998.

[43] G. Woschni, "A universally applicable equation for the instantaneous heat transfer coefficient in the internal combustion engine," in *SAE Technical Paper Series*, SAE International, Feb. 1967.

[44] R. Bellanca, *BlueBellMouse. A Tool for Kinetic Model Development*. PhD thesis, Lund University, 2004.

[45] O. Colin and A. Benkenida, "The 3-zones extended coherent flame model (ecfm3z) for computing premixed/diffusion combustion," *Oil & Gas Science and Technology*, vol. 59, pp. 593–609, Nov. 2004.

[46] R. Reitz, "Modeling atomization processes in high-pressure vaporizing sprays," *Atomisation Spray Technology*, vol. 3, pp. 309–337, 01 1987.

[47] J. C. Beale and R. Reitz, "Modeling spray atomization with the kelvin-helmholtz/rayleigh-taylor hybrid model," *Atomization and Sprays*, vol. 9, pp. 623–650, 11 1999.

[48] C. Bai and A. D. Gosman, "Development of methodology for spray impingement simulation," in *SAE Technical Paper Series*, SAE International, Feb. 1995.

[49] G. ROSA N., P. Villedieu, D. J, and G. Lavergne, "A new droplet-wall interaction model," 10 2008.

[50] J. Senda, T. Kanda, M. Al-Roub, P. V. Farrell, T. Fukami, and H. Fujimoto, "Modeling spray impingement considering fuel film formation on the wall," in *SAE Technical Paper Series*, SAE International, Feb. 1997.

[51] K. Ashida, T. Takahashi, T. Tanaka, J.-K. Yeom, J. Senda, and H. Fujimoto, "Spray-wall interaction model considering superheating degree of the wall surface," *Transactions of the Japan Society of Mechanical Engineers Series B*, vol. 66, 02 2000.

[52] J. Senda and H. G. Fujimoto, "Multidimensional modeling of impinging sprays on the wall in diesel engines," *Applied Mechanics Reviews*, vol. 52, no. 4, p. 119, 1999.

[53] L. Liang, J. G. Stevens, and J. T. Farrell, "A dynamic multi-zone partitioning scheme for solving detailed chemical kinetics in reactive flow computations," *Combustion Science and Technology*, vol. 181, pp. 1345–1371, Nov. 2009.

[54] H. J. Curran, "Developing detailed chemical kinetic mechanisms for fuel combustion," *Proceedings of the Combustion Institute*, vol. 37, no. 1, pp. 57–81, 2019.

[55] H. Di, X. He, P. Zhang, Z. Wang, M. S. Wooldridge, C. K. Law, C. Wang, S. Shuai, and J. Wang, "Effects of buffer gas composition on low temperature ignition of iso-octane and n-heptane," *Combustion and Flame*, vol. 161, pp. 2531–2538, Oct. 2014.

[56] H. K.Y. and G. A.D., "A phenomenological model of diesel spray atomisation," in *Proceedings of The International Conference on Multiphase Flows, Tsukuba, Japan, September 24-27*, Sept. 1991.

[57] V. Yakhot, S. A. Orszag, S. Thangam, T. B. Gatski, and C. G. Speziale, "Development of turbulence models for shear flows by a double expansion technique," *Physics of Fluids A: Fluid Dynamics*, vol. 4, pp. 1510–1520, July 1992.

Bibliography

Stephen R. Turns, *An Introduction to Combustion: Concepts and Applications*, McGraw-Hill Education, 2011.

C. K. Law, *Combustion Physics*, Cambridge University Press, 2006.

H. Versteeg and W. Malalasekera, *An Introduction to Computational Fluid Dynamics*, 2nd edition. Pearson, 2007.

J. M. Simmie, *Detailed chemical kinetic models for the combustion of hydrocarbon fuels*, *Progress in Energy and Combustion Science*, vol. 29, pp 599-634, Jan. 2003.

J. Heywood, *Internal Combustion Engine Fundamentals*. McGraw-Hill Education, 1988.

Siemens PLM Software, *Manual - Thermodynamics and Chemical Kinetics in DARS*, DARS Version 4.30, 2018.

Siemens PLM Software, *Manual - Engine In-Cylinder Reactor Models*, DARS Version 4.30, 2018.

Siemens PLM Software, *Manual - Flames*, DARS Version 4.30, 2018.

Siemens PLM Software, *Manual - Homogeneous Reactor Models*, DARS Version 4.30, 2018

Siemens PLM Software, *User Guide - es-ice*, DARS Version 4.30, Jan. 2019.

Siemens PLM Software, *STAR METHODOLOGY - For Internal Combustion Engine Applications*, Version 4.30, Jan. 2019.

Appendices

A Additional figures

A.1 HCCI combustion

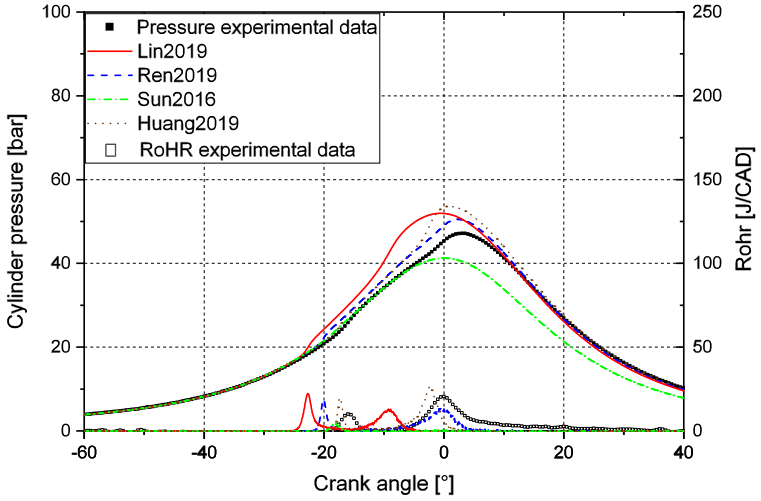

(a) $\phi = 0.18$

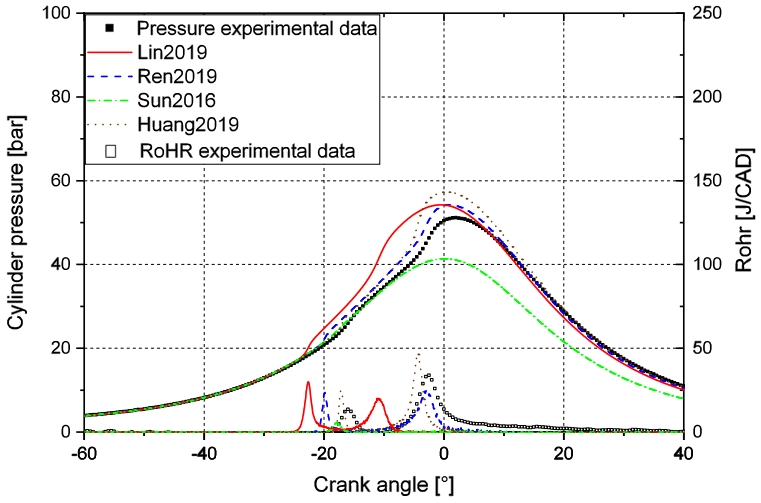

(b) $\phi = 0.21$

Figure A.1: HCCI combustion with OME_3 as fuel. Both experimental data and the mechanisms' preditctions of the pressure profile and heat release are included.

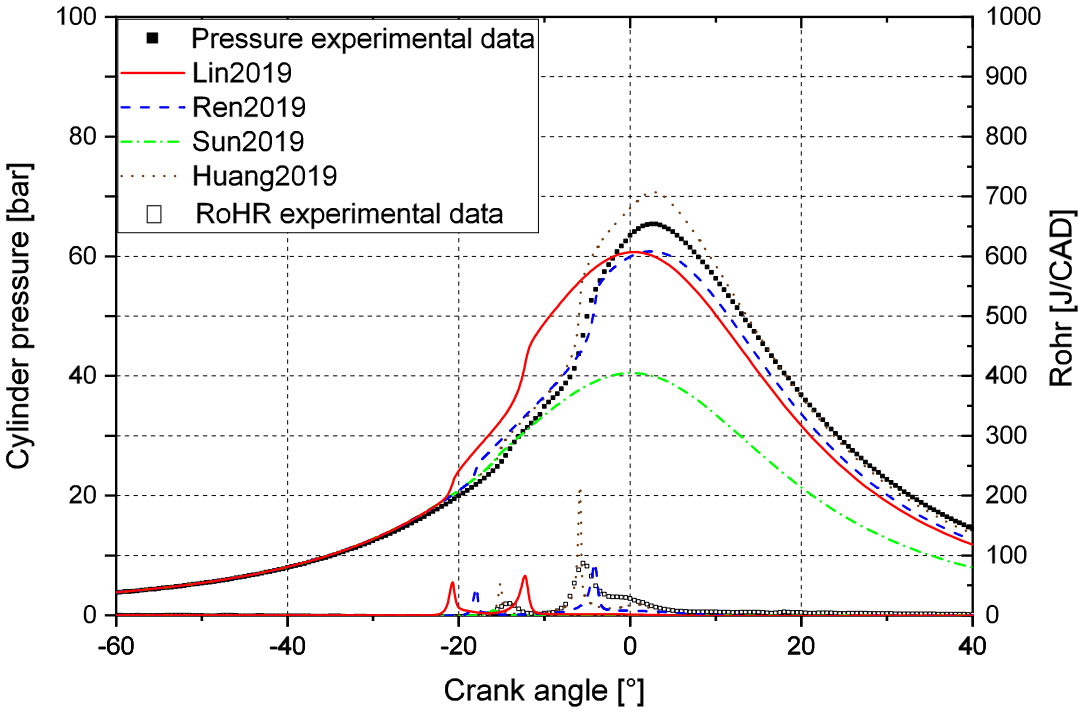

Figure A.2: $\phi = 0.34$ EGR=42%

Figure A.3: HCCI combustion with EGR with OME_3 as fuel. Both experimental data and the mechanisms' preditctions of the pressure profile and heat release are included.

A.2 Combustion of OME_3

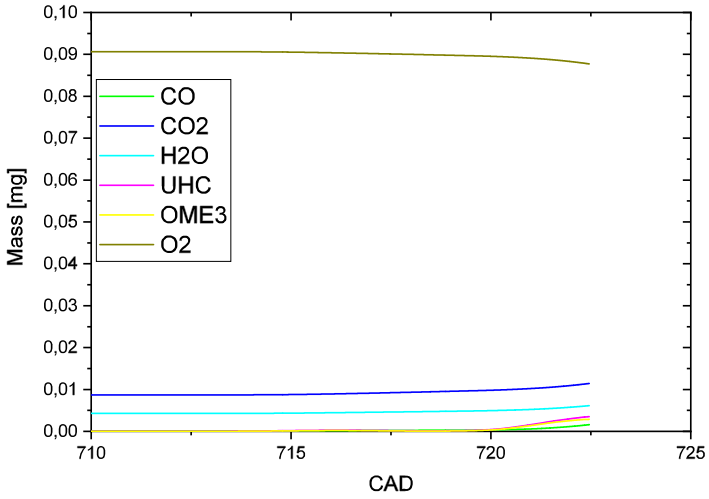

(a) Lin2019 Major species

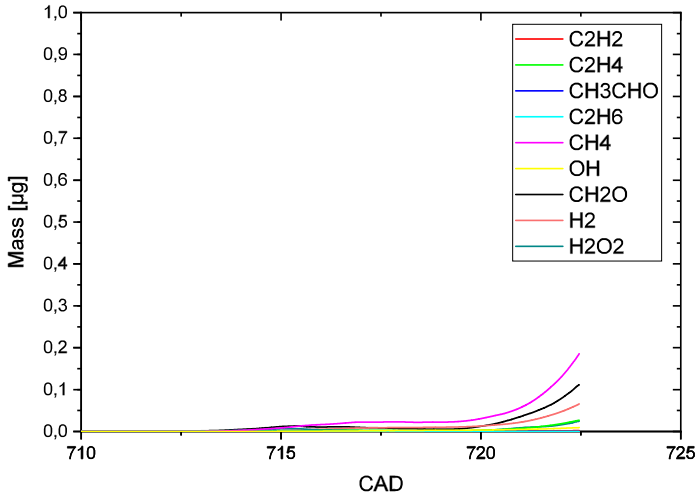

(b) Lin2019 Minor species

A.3 Combustion of OME_1

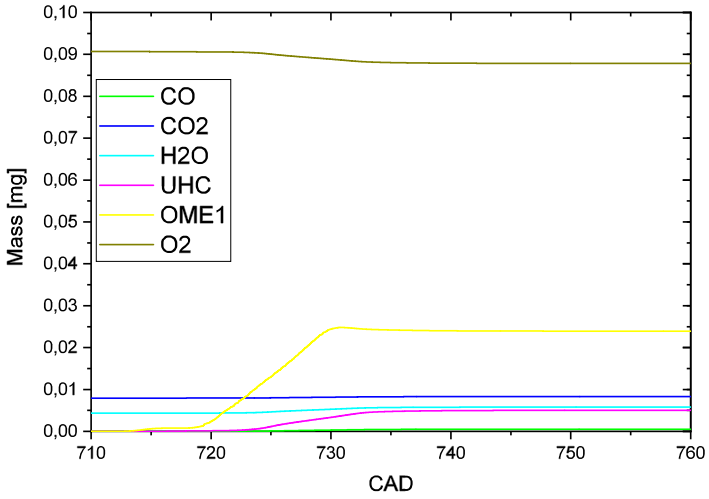

(a) Ren2019 Major species

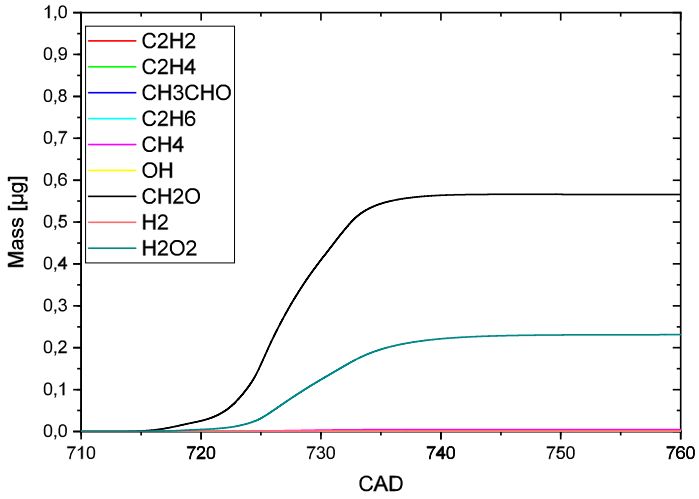

(b) Ren2019 Minor species

B Mechanism Files

B.1 Lin2019 mechanism file

```
!*****************************************************************************
!Development of a compact and robust PODE3 reaction mechanism for
 internal combustion engines
!Qinjie Lin, Kun Lin Tay, Wenming Yang
!Department of Mechanical Engineering, National University of Singapore
!*****************************************************************************!
ELEMENTS
C  H   O   N   AR   HE
END
SPECIES
C7H16 C8H18 DMM3
HE     AR     O2     N2     CO2     H2O     CO
H2     OH     H2O2   HO2    H       O       CH4
CH3O   CH2O   HCO    CH3    CH2OH   CH3OH   CH3CHO
C2H2   CH2CO  C2H3   C2H4   C2H5    HCCO    CH2CHO
CH3CO  C2H6   C3H4   C3H5   C3H6    C3H7
  C8H17   C8H17OO  C8H16OOH  OOC8H16OOH C8KET   C6H13CO
C8H16
   C7H15   C7H15O2  C7H14OOH  O2C7H14OOH
C7KET   C5H11CO  C7H14
   DMM3B   DMM3BO2  DMM3_OOH3_5  DMM3_OOH3_OO5  DMM3_KET35
CH3OCOO  COCOC*O  CH3OCH2OCH2  CH3OCHO  CH3OCO

END
REACTIONS

! N-HEPTANE
!(taken from Energy Fuels 2012, 26, 7069−7083)

C7H16   + O2    = C7H15   + HO2          1.000E+16  0.00  46000.0
 REV                        / 1.000E+12  0.00    0.0 /
C7H16   + OH    =>C7H15   + H2O          5.000E+13  0.00   3000.0
C7H16   + HO2   =>C7H15   + H2O2         1.000E+13  0.00  16950.0
C7H15   + O2    = C7H15O2               3.000E+12  0.00    0.0
 REV                        / 2.510E+13  0.00  27400.0 /
C7H15O2         = C7H14OOH              1.510E+11  0.00  19000.0
 REV                        / 1.000E+11  0.00  11000.0 /
C7H14OOH  + O2    = O2C7H14OOH          6.160E+10  0.00    0.0
 REV                        / 2.510E+13  0.00  27400.0 /
O2C7H14OOH      =>C7KET   + OH          8.910E+10  0.00  17000.0
C7H15   + O2    = C7H14   + HO2         3.160E+11  0.00   6000.0
 REV                        / 3.160E+11  0.00  19500.0 /
```

```
C7KET          =>C5H11CO  + CH2O  + OH       3.980E+15  0.00  43000.0
C5H11CO   + O2     =>C3H7    + C2H3  + CO   + HO2 3.160E+13  0.00  10000.0
C7H14    + O2     =>C3H6    + C2H5  + CH2O + HCO 3.160E+13  0.00  10000.0
C7H15          =>C3H6    + C2H5    + C2H4    6.500E+12  0.00  28810.0

!iso-octane sub-mechanism

C8H18    +O2     <=>C8H17   +HO2            5.000E+15  0.00  46000.0
 REV                          / 1.000E+12  0.00     0.0 /
C8H18    +OH      =>C8H17   +H2O            8.000E+13  0.00   3000.0
C8H18    +HO2     =>C8H17   +H2O2           2.300E+13  0.00  16950.0
C8H17    +O2     <=>C8H17OO                3.000E+11  0.00     0.0
 REV                          / 5.510E+13  0.00  27400.0 /
C8H17OO         <=>C8H16OOH                2.000E+11  0.00  21800.0
REV                           / 1.000E+11  0.00  11000.0 /
C8H16OOH  +O2     <=>OOC8H16OOH              3.000E+11  0.00     0.0
 REV                          / 5.510E+13  0.00  27400.0 /
OOC8H16OOH       =>C8KET   +OH             8.910E+10  0.00  17000.0
C8KET          =>C6H13CO  +CH2O+OH          6.000E+14  0.00  43000.0
C6H13CO   +O2     =>C3H7    +C3H5+CO+HO2       3.160E+13  0.00  10000.0
C8H17    +O2     <=>C8H16   +HO2            3.160E+11  0.00   6000.0
 REV                          / 3.160E+11  0.00  19500.0 /
C8H16    +O2     =>C3H7    +C3H6+CH2O+HCO     3.160E+13  0.00  10000.0
C8H17          =>C3H7    +C3H6+C2H4         1.117E+17 -1.27  29700.0

!PODE3 sub-mechanism by Lin Qinjie
DMM3+O2 = DMM3B+HO2                                  6.660E+16  0.00  43540.0
DMM3+OH = DMM3B+H2O                                  3.785E+04  2.72  -1243.9
DMM3+H => DMM3B+H2                                   7.400E+12  0.00   3170.0
DMM3+HO2 = DMM3B+H2O2                                4.000E+15  0.00  16500.0
DMM3B + O2 = DMM3BO2                                 3.000E+13  0.00     0.0
 REV                          / 2.510E+13  0.00  27400.0 /
DMM3BO2 = DMM3_OOH3_5                                1.044E+03  2.33  11363.0
DMM3_OOH3_5 + O2 = DMI       3.000E+16  0.00     0.0
 REV                          / 2.510E+13  0.00  27400.0 /
DMM3_OOH3_OO5 = DMM:   1.044E+03    11363.0
DMM3_KET35 => CH3OCOO + COCOC*O + OH            5.000e+15  0.00  40000.0
CH3OCOO = CO2 + CH3O                             1.606E+14  0.09  16350.0
COCOC*O+O2 => CH3O+CH2       2.000E+13  0.00  49700.0
DMM3B = CH3OCH2OCH2+CH3OCHO                          2.483E+11  0.54  12805.6
CH3OCH2OCH2 => CH3+CH2       5.567E+1  24633.9
CH3OCHO+OH<=>CH3OCO+H2O                              1.580E+07  1.80   934.0
CH3OCHO+H<=>CH3OCO+H2                                6.500E+05  2.40   4471.0
CH3OCO<=>CH3O+CO                                 2.825E+28 -3.44  23592.4
CH3OCO<=>CH3+CO2                                     8.690E+17 -1.81  13656.7

!C2-C3 sub-mechanism
C3H7           <=>C2H4     +CH3            5.600E+14   0.00   30950.0
C3H7           <=>C3H6     +H             1.250E+14   0.00   36900.0
```

```
C3H6    +OH    <=>C3H5    +H2O           1.970E+006 2.200   540.0
C3H6    +H     <=>C3H5    +H2            1.730E+005 2.500  2492.0
C3H5    +H(+M) <=>C3H6(+M)               7.000E+012 0.000     0.0
LOW/                                  1.330E+060 -12.00 5967.8/
TROE/ 2.000E-002 1.097E+003 1.097E+003 6.860E+003/
H2/ 2.00/ H2O/ 6.00/ CH4/ 2.00/ CO/ 1.50/ CO2/ 2.00/
C2H6/ 3.00/ AR/ 0.70/
C2H3   +CH3(+M) <=>C3H6(+M)               2.500E+013 0.000     0.0
LOW/                                  4.270E+058 -11.940 9769.8/
TROE/ 1.750E-001 1.341E+003 6.000E+004 1.014E+004/
C3H6    +CH3   <=>C3H5    +CH4           9.000E+12   0.00  8480.0
C3H5    +O2    <=>C3H4    +HO2           6.000E+11   0.00 10000.0
C3H4    +O     <=>C2H4    +CO            2.000E+07   1.800  1000.0
C3H4    +OH    <=>C2H3    +CH2O          3.000E+12   0.00     0.0
C3H4    +OH    <=>C2H4    +HCO           1.000E+12   0.00     0.0
C2H5    +H     <=>C2H4    +H2            2.000E+012  0.000    0.0
C2H5    +O2    <=>C2H4    +HO2           2.094E+009  0.490  -391.4
DUP
C2H5    +O2    <=>C2H4    +HO2           6.609E+000  3.510 14160.0
DUP
CH3     +C2H5  <=>CH4     +C2H4          1.180E+004  2.450 -2921.0
C2H4    +C2H4  <=>C2H5    +C2H3          4.820E+014  0.000 71530.0
C2H4    +H(+M) <=>C2H5(+M)               9.569E+008  1.463  1355.0
LOW/                                  1.419E+039 -6.642  5769.0/
TROE/ -5.690E-001 2.990E+002 -9.147E+003 1.524E+002/
H2/ 2.00/ H2O/ 6.00/ CH4/ 2.00/ CO/ 1.50/ CO2/ 2.00/
C2H6/ 3.00/ AR/ 0.70/
C2H4    +OH    <=>CH2O    +CH3           1.000E+14   0.00   960.0
C2H4    +OH    <=>C2H3    +H2O           8.020E+13   0.00  5955.0
C2H3    +O2    <=>CH2O    +HCO           1.700E+029 -5.312  6503.1
C2H3    +O2    =>H      +CO+CH2O         5.190E+015 -1.260  3312.6
C2H3    +HCO   <=>C2H4    +CO            6.034E+13   0.00     0.0
C3H5          <=>C2H2    +CH3           6.397E+48  -9.90  8.208E+04
 REV   / 2.610E+46  -9.82  3.695E+04  /
C2H4(+M)       <=>C2H2    +H2(+M)         1.800E+13   0.00  7.600E+04
 LOW   / 1.500E+15   0.00  5.544E+04  /
C2H3    +O2    <=>C2H2    +HO2           2.120E-06   6.00  9.484E+03
 REV   / 1.114E-07   6.33  1.757E+04  /
C2H3    +H     <=>C2H2    +H2            2.000E+13   0.00  2.500E+03
 REV   / 1.331E+13   0.00  6.808E+04  /
C2H2    +H(+M) <=>C2H3(+M)               3.110E+11   0.58  2.589E+03
 LOW     / 2.254E+40  -7.269    6577.  /
 TROE/ 1.0 1.E-15 675. 1.E+15/
 H2/2/ H2O/5/ CO/2/ CO2/3/
C2H2    +O2    <=>HCCO    +OH            2.000E+08   1.50  3.010E+04
 REV   / 2.232E+05   1.50  2.540E+04  /
C2H2    +O     <=>HCCO    +H             3.930E+08   2.00  1.900E+03
 REV   / 2.021E+05   2.00  1.331E+04  /
C2H2    +OH    <=>CH2CO   +H             2.190E-04   4.50 -1.000E+03
 REV   / 2.161E-03   4.50  1.966E+04  /
```

```
CH2CO    +H    <=>CH3    +CO           1.100E+13   0.00  3.400E+03
 REV   / 2.400E+12   0.00  4.020E+04 /
CH2CO    +O    <=>HCCO    +OH          1.000E+13   0.00  8.000E+03
 REV   / 1.432E+10   0.00 -1.255E+03 /
CH2CO    +OH   <=>HCCO    +H2O          1.000E+13   0.00  2.000E+03
 REV   / 1.412E+11   0.00  9.995E+03 /
CH2CO    +H    <=>HCCO    +H2          2.000E+14   0.00  8.000E+03
 REV   / 6.522E+11   0.00  8.400E+02 /
HCCO     +OH   <=>HCO     +HCO          1.000E+13   0.00  0.000E+00
 REV   / 2.411E+14   0.00  4.036E+04 /
HCCO     +O    <=>H      +CO+CO        8.000E+13   0.00  0.000E+00
 REV   / 0.000E+00   0.00  0.000E+00 /
HCCO     +O2   <=>CO2    +HCO          2.400E+11   0.00 -8.540E+02
 REV   / 1.474E+14   0.00  1.336E+05 /
C2H5     +O    <=>CH3CHO  +H           1.1E14      0.0   0.0E0
C2H5     +O2   <=>CH3CHO  +OH           8.265E2     2.41  5.285E3
C2H4     +OH   <=>CH3CHO  +H           2.937E9     0.89  1.253E4
CH3CHO(+M)      <=>CH3    +HCO(+M)       2.45E22    -1.74  8.636E4
   LOW/1.03E59 -1.13E1 9.591E4/
   TROE/2.49E-3 7.181E2 6.089E0 3.78E3/
CH3CHO   +H    <=>CH3CO   +H2           1.31E5      2.58  1.22E3
CH3CHO   +H    <=>CH2CHO  +H2           2.72E3      3.1   5.21E3
CH3CHO   +O    <=>CH3CO   +OH           5.94E12     0.0   1.868E3
CH3CHO   +OH   <=>CH3CO   +H2O          3.37E12     0.0  -6.19E2
CH3CHO   +O2   <=>CH3CO   +HO2          3.01E13     0.0   3.915E4
CH3CHO   +HO2  <=>CH3CO   +H2O2         3.01E12     0.0   1.192E4
CH3CHO   +OH   <=>CH2CHO  +H2O          1.72E5      2.4   8.15E2
CH2CHO(+M)      <=>CH2CO   +H(+M)        1.43E15    -0.15  4.56E4
   LOW/6.0E29 -3.8E0 4.342E4/
   TROE/9.85E-1 3.93E2 9.8E9 5.0E9/
CH2CHO(+M)      <=>CH3    +CO(+M)        2.93E12     0.29  4.03E4
   LOW/9.52E33 -5.07E0 4.13E4/
   TROE/7.13E-17 1.15E3 4.99E9 1.79E9/
CH2CHO   +O2   <=>CH2CO   +HO2          7.05E7      1.63  2.529E4
CH3CO(+M)       <=>CH3    +CO(+M)        1.07E12     0.63  1.69E4
   LOW/5.65E18 -9.7E-1 1.46E4/
   TROE/6.29E-1 8.73E9 5.52E0 7.6E7/
CH3CO    +H    <=>CH2CO   +H2           2.0E13      0.0   0.0E0
CH3CO    +O    <=>CH2CO   +OH           2.0E13      0.0   0.0E0
CH3CO(+M)       <=>CH2CO   +H(+M)        9.413E7     1.917  4.499E4
   LOW/1.516E51 -1.027E1 5.539E4/
   TROE/6.009E-1 8.103E9 6.677E2 5.0E9/

!H2/O2 sub-mechanism

H+O2 = O+OH                    1.04E+14   0.00  1.5286E+04
O+H2 = H+OH                    3.818E+12   0.00  7.948E+03
DUPLICATE
O+H2 = H+OH                    8.792E+14   0.00  1.917E+04
  DUPLICATE
```

```
H2+OH = H2O+H                     0.216E+09   1.51  0.343E+04
OH+OH = O+H2O                      3.34E+04   2.42  -1.93E+03
H2+M = H+H+M                      4.577E+19  -1.40  1.0438E+05
  H2/2.5/ H2O/12/
  CO/1.9/ CO2/3.8/
  AR/0.0/ HE/0.0/
H2+AR = H+H+AR                     5.840E+18 -1.10  1.0438E+05
H2+HE = H+H+HE                     5.840E+18 -1.10  1.0438E+05
O+O+M = O2+M                       6.165E+15 -0.50  0.000E+00
  H2/2.5/ H2O/12/
  AR/0.0/ HE/0.0/
  CO/1.9/ CO2/3.8/
O+O+AR = O2+AR                     1.886E+13  0.00 -1.788E+03
O+O+HE = O2+HE                     1.886E+13  0.00 -1.788E+03
O+H+M = OH+M                       4.714E+18 -1.00  0.000E+00
  H2/2.5/  H2O/12/
  AR/0.75/ HE/0.75/
  CO/1.9/  CO2/3.8/
H2O+M = H+OH+M                       6.064E+27 -3.322 1.2079E+05
  H2/3.0/  H2O/0.0/
  HE/1.10/ N2/2.00/
  O2/1.5/
  CO/1.9/ CO2/3.8/
 H2O+H2O = H+OH+H2O                    1.006E+26 -2.44  1.2018E+05
H+O2(+M) = HO2(+M)                   4.65084E+12  0.44  0.000E+00
  LOW/6.366E+20 -1.72  5.248E+02/
  TROE/0.5  1E-30  1E+30/
  H2/2.0/ H2O/14/ O2/0.78/ CO/1.9/ CO2/3.8/ AR/0.67/ HE/0.8/
HO2+H = H2+O2                      2.750E+06  2.09 -1.451E+03
HO2+H = OH+OH                       7.079E+13  0.00  2.950E+02
HO2+O = O2+OH                      2.850E+10  1.00 -7.2393E+02
HO2+OH = H2O+O2                      2.890E+13  0.00 -4.970E+02
HO2+HO2 = H2O2+O2                     4.200E+14  0.00  1.1982E+04
  DUPLICATE
HO2+HO2 = H2O2+O2                     1.300E+11  0.00 -1.6293E+03
  DUPLICATE
H2O2(+M) = OH+OH(+M)                    2.00E+12  0.90  4.8749E+04
  LOW/2.49E+24 -2.30 4.8749E+04/
  TROE/0.43 1E-30 1E+30/
  H2O/7.5/ CO2/1.6/
  N2/1.5/  O2/1.2/
  HE/0.65/ H2O2/7.7/
  H2/3.7/ CO/2.8/
H2O2+H = H2O+OH                     2.410E+13  0.00  3.970E+03
H2O2+H = HO2+H2                     4.820E+13  0.00  7.950E+03
H2O2+O = OH+HO2                     9.550E+06  2.00  3.970E+03
H2O2+OH = HO2+H2O                     1.740E+12  0.00  3.180E+02
  DUPLICATE
H2O2+OH = HO2+H2O                     7.590E+13  0.00  7.270E+03
  DUPLICATE
```

```
!methanol sub-mechanism

CO+O(+M)=CO2(+M)                    1.80E+10  0.00  2384.
  LOW/1.55E+24 -2.79  4191./
  H2/2.5/ H2O/12/ CO/1.9/ CO2/3.8/
CO+O2=CO2+O                       0.253E+13  0.00  0.477E+05
CO+HO2=CO2+OH                       3.01E+13  0.00   2.30E+04
CO+OH=CO2+H                        2.229E+05  1.89   -1158.7
HCO+M=H+CO+M                        5.7485E+11  0.659 1.4874E+04
H2/2.5/ H2O/6/ CO/1.9/ CO2/3.8/
HCO+O2=CO+HO2                       0.758E+13  0.00  0.410E+03
HCO+H=CO+H2                        0.723E+14  0.00  0.000E+00
HCO+O=CO+OH                        0.302E+14  0.00  0.000E+00
HCO+OH=CO+H2O                       0.302E+14  0.00  0.000E+00
HCO + O = CO2 + H                  3.000E+13  0.00  0.000E+00
HCO + HO2 = CO2 + OH + H              3.000E+13  0.00  0.000E+00
HCO + CH3 = CO + CH4                1.200E+14  0.00  0.000E+00
HCO + HCO = H2 + CO + CO              3.000E+12  0.00  0.000E+00
HCO + HCO = CH2O + CO                 3.0E+13  0.00  0.00
CH2O + M = HCO + H + M                3.3E+39  -6.3  9.99E+04
H2/2.5/ H2O/12.0/ CO/1.9/ CO2/3.8/
CH2O + M = CO + H2 + M                3.1E+45  -8.0  9.751E+04
H2/2.5/ H2O/12.0/ CO/1.9/ CO2/3.8/
CH2O + H = HCO + H2                   5.74E+07  1.9  2.7486E+03
CH2O + O = HCO + OH                1.810E+13  0.00  3.080E+03
CH2O + OH = HCO + H2O               3.430E+09  1.18 -4.470E+02
CH2O + O2 = HCO + HO2               1.23E+6  3.00    52000.
CH2O + HO2 = HCO + H2O2             4.11E+4   2.5     10210.
CH2O+CH3 = HCO+CH4                 3.636E-06   5.42  9.980E+02
CH2O+H(+M)<=>CH2OH(+M)          5.400E+011  0.454    3600.0
LOW/                      1.270E+032  -4.820    6530.0/
TROE/  7.187E-001  1.030E+002  1.291E+003  4.160E+003/
H2/ 2.00/ H2O/ 6.00/ CO/ 1.50/ CO2/ 2.00/ CH4/ 2.00/ C2H6/ 3.00/
CH3 + O = CH2O + H                8.430E+13    0.00  0.000E+00
CH3 + O2 = CH3O + O               1.990E+18   -1.57  2.923E+04
CH3 + O2 = CH2O + OH              3.74E+11     0.0   14640.
CH3+HO2<=>CH3O+OH                   1.000E+012   0.269    -687.5
CH3+HO2<=>CH4+O2                  1.160E+005   2.230   -3022.0
CH3+H(+M)<=>CH4(+M)               1.270E+016  -0.630    383.0
LOW/                      2.477E+033  -4.760    2440.0/
TROE/  7.830E-001  7.400E+001  2.941E+003  6.964E+003/
H2/ 2.00/ H2O/ 6.00/ AR/ 0.70/ CO/ 1.50/ CO2/ 2.00/ CH4/ 2.00/
C2H6/ 3.00/ HE/ 0.70/
CH4 + H = CH3 + H2                5.470E+07  1.97  1.121E+04
CH4 + O = CH3 + OH                3.150E+12  0.50    10290.0
CH4 + OH = CH3 + H2O               5.720E+06  1.96  2.639E+03
CH4 + HO2 = CH3 + H2O2            1.810E+11  0.00  1.858E+04
CH2OH + H = CH2O + H2             6.000E+12  0.00  0.000E+00
CH2OH + H = CH3 + OH              9.635E+13  0.00  0.000E+00
```

```
CH2OH + O = CH2O + OH           4.200E+13  0.00  0.000E+00
CH2OH + OH = CH2O + H2O         2.400E+13  0.00  0.000E+00
CH2OH + O2 = CH2O + HO2         2.410E+14  0.00  5.017E+03
  DUP
CH2OH + O2 = CH2O + HO2         1.510E+15 -1.00  0.000E+00
  DUP
CH2OH + HO2 = CH2O + H2O2       1.200E+13  0.00  0.000E+00
CH2OH + HCO = CH3OH + CO        1.000E+13  0.00  0.000E+0
CH2OH + HCO = CH2O + CH2O       1.500E+13  0.00  0.000E+00
 2CH2OH = CH3OH + CH2O          3.000E+12  0.00  0.000E+00
 CH2OH + CH3O = CH3OH + CH2O    2.400E+13  0.00  0.000E+00
CH3O + M = CH2O + H + M         8.300E+17 -1.20  1.550E+04
CH3O + H = CH3 + OH             3.200E+13  0.00  0.000E+00
CH3O + O = CH2O + OH            6.000E+12  0.00  0.000E+00
CH3O + OH = CH2O + H2O          1.800E+13  0.00  0.000E+00
CH3O + O2 = CH2O + HO2          9.033E+13  0.00  1.198E+04
 DUP
CH3O + O2 = CH2O + HO2          2.200E+10  0.00  1.748E+03
 DUP
CH3O + HO2 = CH2O + H2O2        3.000E+11  0.00  0.000E+00
CH3O + CO = CH3 + CO2           1.600E+13  0.00  1.180E+04
CH3O + HCO = CH3OH + CO         9.000E+13  0.00  0.000E+00
2CH3O = CH3OH + CH2O            6.000E+13  0.00  0.000E+00
OH+CH3(+M)<=>CH3OH(+M)       2.790E+18  -1.430   1330.00
   LOW  /  4.000E+36  -5.920  3140.00/
   TROE/  .4120  195.0  5900.00  6394.00/
H2/2.00/ H2O/6.00/ CH4/2.00/ CO/1.50/ CO2/2.00/
H+CH2OH(+M)<=>CH3OH(+M)       1.055E+12    .500     86.00
   LOW  /  4.360E+31  -4.650  5080.00/
   TROE/  .600  100.00  90000.0  10000.0 /
H2/2.00/ H2O/6.00/ CH4/2.00/ CO/1.50/ CO2/2.00/
H+CH3O(+M)<=>CH3OH(+M)        2.430E+12    .515     50.00
   LOW  /  4.660E+41  -7.440  14080.0/
   TROE/  .700  100.00  90000.0 10000.00 /
H2/2.00/ H2O/6.00/ CH4/2.00/ CO/1.50/ CO2/2.00/
CH3OH + H = CH2OH + H2          3.200E+13  0.00  6.095E+03
CH3OH + H = CH3O + H2           8.000E+12  0.00  6.095E+03
CH3OH + O = CH2OH + OH          3.880E+05  2.50  3.080E+03
CH3OH+OH<=>CH2OH+H2O           3.080E+004  2.650   -806.7
CH3OH+OH<=>CH3O+H2O            1.500E+002  3.030   -763.0
CH3OH + O2 = CH2OH + HO2        2.050E+13  0.00  4.490E+04
CH3OH + HCO = CH2OH + CH2O      9.635E+03  2.90  1.311E+04
CH3OH + HO2 = CH2OH + H2O2      3.980E+13  0.00  1.940E+04
CH3OH + CH3 = CH2OH + CH4       3.190E+01  3.17  7.172E+03
CH3O + CH3OH = CH3OH + CH2OH    3.000E+11  0.00  4.060E+03
END
```

B.2 Lin2019 transport file

```
HE          0   10.200    2.576    0.000    0.000    0.000
AR          0  136.500    3.330    0.000    0.000    0.000
O2          1  107.400    3.458    0.000    1.600    3.800
N2          1   97.530    3.621    0.000    1.760    4.000
CO2         1  244.000    3.763    0.000    2.650    2.100
H2O         2  572.400    2.605    1.844    0.000    4.000
CO          1   98.100    3.650    0.000    1.950    1.800
H2          1   38.000    2.920    0.000    0.790  280.000
OH          1   80.000    2.750    0.000    0.000    0.000
H2O2        2  107.400    3.458    0.000    0.000    3.800
HO2         2  107.400    3.458    0.000    0.000    1.000
H           0  145.000    2.050    0.000    0.000    0.000
O           0   80.000    2.750    0.000    0.000    0.000
CH4         2  141.400    3.746    0.000    2.600   13.000
CH3O        2  417.000    3.690    1.700    0.000    2.000
CH2O        2  498.000    3.590    0.000    0.000    2.000
HCO         2  498.000    3.590    0.000    0.000    0.000
CH3         1  144.000    3.800    0.000    0.000    0.000
CH2OH       2  417.000    3.690    1.700    0.000    2.000
CH3OH       2  481.800    3.626    0.000    0.000    1.000
C2H3        2  265.300    3.721    0.000    0.000    1.000
C2H4        2  238.400    3.496    0.000    0.000    1.500
C2H5        2  247.500    4.350    0.000    0.000    1.500
C2H6        2  247.500    4.350    0.000    0.000    1.500
C2H2        1  265.300    3.721    0.000    0.000    2.500
CH2CO       2  436.000    3.970    0.000    0.000    2.000
HCCO        2  150.000    2.500    0.000    0.000    1.000
CH3CO       2  436.0      3.97     0.0      0.0      2.0
CH2CHO      2  436.0      3.97     0.0      0.0      2.0
CH3CHO      2  436.0      3.97     0.0      0.0      2.0
C3H4        1  324.800    4.290    0.000    0.000    1.000
C3H5        2  316.000    4.220    0.000    0.000    1.000
C3H6        2  307.800    4.140    0.000    0.000    1.000
C3H7        2  303.400    4.810    0.000    0.000    1.000
C8H18       2  458.5      6.414    0.0      0.0      1.0
C8H17       2  458.5      6.414    0.0      0.0      1.0
C8H16       2  485.6      6.440    0.3      0.0      1.0
C8H16OOH    2  581.3      6.506    2.0      0.0      1.0
C8H17OO     2  581.3      6.506    2.0      0.0      1.0
OOC8H16OOH  2  581.3      6.506    2.0      0.0      1.0
C8KET       2  581.3      6.506    2.0      0.0      1.0
C6H13CO     2  581.3      6.506    2.0      0.0      1.0
!PODE3
DMM3 2 600.600 6.190 0.079 0.000 1.000
DMM3B 2 600.600 6.190 0.079 0.000 1.000
DMM3BO2 2 523.2 5.664 1.7 0.0 1.0
DMM3_OOH3_5 2 523.2 5.664 1.7 0.0 1.0
DMM3_OOH3_OO5 2 523.2 5.664 1.7 0.0 1.0
DMM3_KET35 2 523.2 5.664 1.7 0.0 1.0
CH3OCOO 2 395.0 4.037 1.3 0.0 1.0
```

```
COCOC*O 2 414.260 5.770 3.766 0.000 1.000
CH3OCH2OCH2 2 435.5 4.860 2.9 0.0 1.0
CH3OCHO 2 395.0 4.037 1.3 0.0 1.0
CH3OCO 2 395.0 4.037 1.3 0.0 1.0
! N-HEPTANE
C7H16          2   459.6      6.253    0.0      0.0      1.0 !   TCPC
C7H15          2   459.6      6.253    0.0      0.0      1.0 !   WJP
C7H15O2          2   561.0      6.317    1.7      0.0      1.0 !   WJP
C7H14OOH         2   561.0      6.317    1.7      0.0      1.0 !   WJP
O2C7H14OOH       2   600.6      7.229    1.8      0.0      1.0 !   NC10H22O WJP
C7KET          2   581.3      6.506    2.0      0.0      1.0 !   1C8H17OH WJP
C5H11CO          2   498.6      6.009    2.0      0.0      1.0 !   C2H5COC3H7-N WJP
C7H14          2   457.8      6.173    0.3      0.0      1.0 !   WJP, 1C7H14, TCPC
```

B.3 Lin2019 thermochemical file

```
THERMO
  300.000  1000.000  5000.000
H               L 6/94H   1    0    0    0G   200.000  6000.00  1000.00      1
 0.25000000E+01 0.00000000E+00 0.00000000E+00 0.00000000E+00 0.00000000E+00    2
 0.25473660E+05-0.44668285E+00 0.25000000E+01 0.00000000E+00 0.00000000E+00    3
 0.00000000E+00 0.00000000E+00 0.25473660E+05-0.44668285E+00 0.26219035E+05    4
H2              TPIS78H   2    0    0    0G   200.000  6000.00  1000.00      1
 2.93286575E+00 8.26608026E-04-1.46402364E-07 1.54100414E-11-6.88804800E-16    2
-8.13065581E+02-1.02432865E+00 2.34433112E+00 7.98052075E-03-1.94781510E-05    3
 2.01572094E-08-7.37611761E-12-9.17935173E+02 6.83010238E-01 0.00000000E+00    4
O               L 1/90O   1    0    0    0G   200.000  6000.00  1000.00      1
 2.54363697E+00-2.73162486E-05-4.19029520E-09 4.95481845E-12-4.79553694E-16    2
 2.92260120E+04 4.92229457E+00 3.16826710E+00-3.27931884E-03 6.64306396E-06    3
-6.12806624E-09 2.11265971E-12 2.91222592E+04 2.05193346E+00 2.99687009E+04    4
OH              IU3/03O   1 H  1    0    0G   200.000  6000.00  1000.00      1
 2.83853033E+00 1.10741289E-03-2.94000209E-07 4.20698729E-11-2.42289890E-15    2
 3.69780808E+03 5.84494652E+00 3.99198424E+00-2.40106655E-03 4.61664033E-06    3
-3.87916306E-09 1.36319502E-12 3.36889836E+03-1.03998477E-01 4.48613328E+03    4
H2O             L 5/89H   2 O  1    0    0G   200.000  6000.00  1000.00      1
 0.26770389E+01 0.29731816E-02-0.77376889E-06 0.94433514E-10-0.42689991E-14    2
-0.29885894E+05 0.68825500E+01 0.41986352E+01-0.20364017E-02 0.65203416E-05    3
-0.54879269E-08 0.17719680E-11-0.30293726E+05-0.84900901E+00-0.29084817E+05    4
O2              RUS 89O   2    0    0    0G   200.000  6000.00  1000.00      1
 3.66096065E+00 6.56365811E-04-1.41149627E-07 2.05797935E-11-1.29913436E-15    2
-1.21597718E+03 3.41536279E+00 3.78245636E+00-2.99673416E-03 9.84730201E-06    3
-9.68129509E-09 3.24372837E-12-1.06394356E+03 3.65767573E+00 0.00000000E+00    4
HO2             T 1/09H   1O   2    0    0G   200.000  5000.00  1000.00      1
 4.17228741E+00 1.88117627E-03-3.46277286E-07 1.94657549E-11 1.76256905E-16    2
 3.10206839E+01 2.95767672E+00 4.30179807E+00-4.74912097E-03 2.11582905E-05    3
-2.42763914E-08 9.29225225E-12 2.64018485E+02 3.71666220E+00 1.47886045E+03    4
H2O2            T 8/03H   2O   2    0    0G   200.000  6000.00  1000.00      1
 4.57977305E+00 4.05326003E-03-1.29844730E-06 1.98211400E-10-1.13968792E-14    2
-1.80071775E+04 6.64970694E-01 4.31515149E+00-8.47390622E-04 1.76404323E-05    3
-2.26762944E-08 9.08950158E-12-1.77067437E+04 3.27373319E+00-1.63425145E+04    4
N2              G 8/02N   2    0    0    0G   200.000  6000.00  1000.00      1
 2.95257637E+00 1.39690040E-03-4.92631603E-07 7.86010195E-11-4.60755204E-15    2
-9.23948688E+02 5.87188762E+00 3.53100528E+00-1.23660988E-04-5.02999433E-07    3
 2.43530612E-09-1.40881235E-12-1.04697628E+03 2.96747038E+00 0.00000000E+00    4
AR              G 5/97AR  1 0    0     0G   200.000  6000.00  1000.00      1
 2.50000000E+00 0.00000000E+00 0.00000000E+00 0.00000000E+00 0.00000000E+00    2
-7.45375000E+02 4.37967491E+00 2.50000000E+00 0.00000000E+00 0.00000000E+00    3
 0.00000000E+00 0.00000000E+00-7.45375000E+02 4.37967491E+00 0.00000000E+00    4
HE              G 5/97HE 1    0    0    0 G   200.000  6000.00  1000.00      1
 2.50000000E+00 0.00000000E+00 0.00000000E+00 0.00000000E+00 0.00000000E+00    2
-7.45375000E+02 9.28723974E-01 2.50000000E+00 0.00000000E+00 0.00000000E+00    3
 0.00000000E+00 0.00000000E+00-7.45375000E+02 9.28723974E-01 0.00000000E+00    4
CO              RUS 79C   1O   1    0    0G   200.000  6000.00  1000.00      1
 0.30484859E+01 0.13517281E-02-0.48579405E-06 0.78853644E-10-0.46980746E-14    2
-0.14266117E+05 0.60170977E+01 0.35795335E+01-0.61035369E-03 0.10168143E-05    3
 0.90700586E-09-0.90442449E-12-0.14344086E+05 0.35084093E+01-0.13293628E+05    4
```

```
CO2             L 7/88C   1O   2    0    0G   200.000  6000.00  1000.00      1
 0.46365111E+01 0.27414569E-02-0.99589759E-06 0.16038666E-09-0.91619857E-14    2
-0.49024904E+05-0.19348955E+01 0.23568130E+01 0.89841299E-02-0.71220632E-05    3
 0.24573008E-08-0.14288548E-12-0.48371971E+05 0.99009035E+01-0.47328105E+05    4
CH3             IU0702C  1 H  3    0    0 G   200.000  6000.00  1000.00      1
 0.29781206E+01 0.57978520E-02-0.19755800E-05 0.30729790E-09-0.17917416E-13    2
 0.16509513E+05 0.47224799E+01 0.36571797E+01 0.21265979E-02 0.54583883E-05    3
-0.66181003E-08 0.24657074E-11 0.16422716E+05 0.16735354E+01 0.17643935E+05    4
CH2OH           IU2/03C  1 H  3 O  1    0 G   200.000  6000.00   1000.00     1
 5.09314370E+00 5.94761260E-03-2.06497460E-06 3.23008173E-10-1.88125902E-14    2
-4.03409640E+03-1.84691493E+00 4.47834367E+00-1.35070310E-03 2.78484980E-05    3
-3.64869060E-08 1.47907450E-11-3.50072890E+03 3.30913500E+00-2.04462770E+03    4
CH2O            T 5/11H   2C   1O   1    0G   200.000  6000.00  1000.00      1
 3.16952665E+00 6.19320560E-03-2.25056366E-06 3.65975660E-10-2.20149458E-14    2
-1.45486831E+04 6.04207898E+00 4.79372312E+00-9.90833322E-03 3.73219990E-05    3
-3.79285237E-08 1.31772641E-11-1.43791953E+04 6.02798058E-01-1.31293365E+04    4
CH3O            IU1/03C  1 H  3 O  1    0 G   200.000  6000.00  1000.00      1
 4.75779238E+00 7.44142474E-03-2.69705176E-06 4.38090504E-10-2.63537098E-14    2
 3.78111940E+02-1.96680028E+00 3.71180502E+00-2.80463306E-03 3.76550971E-05    3
-4.73072089E-08 1.86588420E-11 1.29569760E+03 6.57240864E+00 2.52571660E+03    4
CH3OH           T06/02C   1H  4 O  1    0 G   200.000  6000.00  1000.00      1
 3.52726795E+00 1.03178783E-02-3.62892944E-06 5.77448016E-10-3.42182632E-14    2
-2.60028834E+04 5.16758693E+00 5.65851051E+00-1.62983419E-02 6.91938156E-05    3
-7.58372926E-08 2.80427550E-11-2.56119736E+04-8.97330508E-01-2.41746056E+04    4
CH4             G 8/99C  1 H  4    0    0 G   200.000  6000.00  1000.00      1
 1.65326226E+00 1.00263099E-02-3.31661238E-06 5.36483138E-10-3.14696758E-14    2
-1.00095936E+04 9.90506283E+00 5.14911468E+00-1.36622009E-02 4.91453921E-05    3
-4.84246767E-08 1.66603441E-11-1.02465983E+04-4.63848842E+00-8.97226656E+03    4
HCO             T 5/03C  1 H  1 O  1    0 G   200.000  6000.00  1000.00      1
 3.92001542E+00 2.52279324E-03-6.71004164E-07 1.05615948E-10-7.43798261E-15    2
 3.65342928E+03 3.58077056E+00 4.23754610E+00-3.32075257E-03 1.40030264E-05    3
-1.34239995E-08 4.37416208E-12 3.87241185E+03 3.30834869E+00 5.08749163E+03    4
C2H5      8/ 4/ 4 THERMC   2H   5    0    0G   300.000  5000.000 1387.000      1
 5.88784390E+00 1.03076793E-02-3.46844396E-06 5.32499257E-10-3.06512651E-14    2
 1.15065499E+04-8.49651771E+00 1.32730217E+00 1.76656753E-02-6.14926558E-06    3
-3.01143466E-10 4.38617775E-13 1.34284028E+04 1.71789216E+01                  4
C2H4            G 1/00C  2 H  4    0    0 G   200.000  6000.00  1000.00      1
 3.99182724E+00 1.04833908E-02-3.71721342E-06 5.94628366E-10-3.53630386E-14    2
 4.26865851E+03-2.69081762E-01 3.95920063E+00-7.57051373E-03 5.70989993E-05    3
-6.91588352E-08 2.69884190E-11 5.08977598E+03 4.09730213E+00 6.31426266E+03    4
C2H3            ATCT/AC  2 H  3    0    0 G   200.000  6000.00  1000.00      1
 4.15026763E+00 7.54021341E-03-2.62997847E-06 4.15974048E-10-2.45407509E-14    2
 3.38566380E+04 1.72812235E+00 3.36377642E+00 2.65765722E-04 2.79620704E-05    3
-3.72986942E-08 1.51590176E-11 3.44749589E+04 7.91510092E+00 3.56701718E+04    4
C2H6            G 8/88C   2H 6    0     0G   200.000  6000.00  1000.00      1
 4.04666411E+00 1.53538802E-02-5.47039485E-06 8.77826544E-10-5.23167531E-14    2
-1.24473499E+04-9.68698313E-01 4.29142572E+00-5.50154901E-03 5.99438458E-05    3
-7.08466469E-08 2.68685836E-11-1.15222056E+04 2.66678994E+00-1.00849652E+04    4
C2H2            G 1/91C  2 H  2    0    0 G   200.000  6000.00  1000.00      1
 4.65878489E+00 4.88396667E-03-1.60828888E-06 2.46974544E-10-1.38605959E-14    2
```

```
 2.57594042E+04-3.99838194E+00 8.08679682E-01 2.33615762E-02-3.55172234E-05    3
 2.80152958E-08-8.50075165E-12 2.64289808E+04 1.39396761E+01 2.74459950E+04    4
CH2CO               H  2C  2O  1    0G    300.00  5000.00 1000.00      1
 5.35869367E+00 6.95641586E-03-2.64802637E-06 4.65067592E-10-3.08641820E-14    2
-7.90294013E+03-3.98525731E+00 1.81422511E+00 1.99008590E-02-2.21416008E-05    3
 1.45028521E-08-3.98877068E-12-7.05394926E+03 1.36079359E+01                  4
HCCO           T 4/09H  1 C  2 O  1    0 G   200.000  6000.00  1000.00      1
 5.91479333E+00 3.71408730E-03-1.30137010E-06 2.06473345E-10-1.21476759E-14    2
 1.93596301E+04-5.50567269E+00 1.87607969E+00 2.21205418E-02-3.58869325E-05    3
 3.05402541E-08-1.01281069E-11 2.01633840E+04 1.36968290E+01 2.14444387E+04    4
CH3CHO          L-8-88H   4O   1C   2     G     200.0    6000.0  1000.0      1
   5.4041108E0   1.1723059E-2  -4.2263137E-6  6.8372451E-10 -4.0984863E-14    2
  -2.2593122E4   -3.4807917E0   4.7294595E0  -3.1932858E-3   4.7534921E-5    3
  -5.7458611E-8  2.1931112E-11   -2.1572878E4   4.1030159E0                  4
CH3CO           IU2-03H   3O   1C   2     G     200.0    6000.0  1000.0      1
   5.3137165E0   9.1737793E-3  -3.3220386E-6  5.3947456E-10 -3.2452368E-14    2
  -3.6450414E3   -1.6757558E0   4.0358705E0   8.7729487E-4   3.071001E-5    3
  -3.9247565E-8  1.5296869E-11   -2.6820738E3   7.8617682E0                  4
CH2CHO          T03-10H   3O   1C   2     G     200.0    6000.0  1000.0      1
  6.53928338E0  7.80238629E-3 -2.76413612E-6 4.42098906E-10 -2.6295429E-14    2
 -1.18858659E3  -8.72091393E0    2.795026E0  1.01099472E-2  1.61750645E-5    3
 -3.10303145E-8 1.39436139E-11   1.62944975E2   1.23646657E1                  4
C3H5            BUR 92C   3H   5O   0N   0G   200.000  6000.000 1000.00      1
 6.54761132E+00 1.33152246E-02-4.78333100E-06 7.71949814E-10-4.61930808E-14    2
 1.72714707E+04-9.27486841E+00 3.78794693E+00 9.48414335E-03 2.42343368E-05    3
-3.65604010E-08 1.48592356E-11 1.86261218E+04 7.82822499E+00 2.03259122E+04    4
C3H6      5/27/97 THERMC   3H   6    0    0G   300.000  5000.000 1388.000     1
 8.01595958E+00 1.37023634E-02-4.66249733E-06 7.21254402E-10-4.17370126E-14    2
-1.87821271E+03-2.00160668E+01 3.94615444E-01 2.89107662E-02-1.54886808E-05    3
 3.88814209E-09-3.37890352E-13 1.06688164E+03 2.19003736E+01                  4
C3H7            120186C   3H   7        G  0300.00   5000.00  1000.00      1
 0.08063369E+02 0.01574488E+00-0.05182392E-04 0.07477245E-08-0.03854422E-12    2
 0.05313871E+05-0.02192647E+03 0.01713300E+02 0.02542616E+00 0.01580808E-04    3
-0.01821286E-06 0.08827710E-10 0.07535809E+05 0.01297901E+03                  4
C3H4            L12/92C   3H   4O   0N   0G   200.000  6000.000 1000.00      1
 6.31694869E+00 1.11336262E-02-3.96289018E-06 6.35633775E-10-3.78749885E-14    2
 2.01174617E+04-1.09718862E+01 2.61307487E+00 1.21223371E-02 1.85405400E-05    3
-3.45258475E-08 1.53353389E-11 2.15415642E+04 1.02503319E+01 2.29622672E+04    4
C7H8      5/19/93 THERMC   7H   8    0    0G   300.000  5000.000 1389.000     1
 1.63091542E+01 2.25331612E-02-7.84281827E-06 1.23200630E-09-7.20675043E-14    2
-2.75804095E+03-6.66759774E+01-4.08982289E+00 6.86477374E-02-4.74716566E-05    3
 1.67001205E-08-2.39578007E-12 4.49937542E+03 4.34582591E+01                  4
C6H5CH2         T08/90C   7H   7    0    0G   200.000  6000.000 1000.       1
 0.14043980E+02 0.23493873E-01-0.85375367E-05 0.13890841E-08-0.83614420E-13    2
 0.18564203E+05-0.51665589E+02 0.48111540E+00 0.38512832E-01 0.32861492E-04    3
-0.76972721E-07 0.35423068E-10 0.23307027E+05 0.23548820E+02                  4
C6H5CHO    2/25/94 THERMC   7H   6O   1    0G   300.000  5000.000 1382.000     1
 1.75038056E+01 1.87911370E-02-6.51897523E-06 1.02244104E-09-5.97629759E-14    2
-1.31835944E+04-6.88975598E+01-2.70517666E+00 6.46821582E-02-4.57286415E-05    3
 1.60322213E-08-2.23734122E-12-6.07344750E+03 4.00414090E+01                  4
```

```
C6H5OH    5/ 2/91 THERM C   6H   6O   1    0G   300.000  5000.000 1397.000    1
 1.71524986E+01 1.60438540E-02-5.46325607E-06 8.46545276E-10-4.90760276E-14    2
-1.94633414E+04-6.96841718E+01-4.48630945E+00 7.22845991E-02-6.19803619E-05    3
 2.67795393E-08-4.60013317E-12-1.26013373E+04 4.43727892E+01                   4
C6H6      5/2/91  THERMC   6H   6    0    0G   300.000  5000.000 1390.000    1
 1.38672847E+01 1.74152368E-02-6.08383755E-06 9.58140923E-10-5.61503296E-14    2
 2.59989001E+03-5.68524653E+01-5.18689051E+00 6.30511006E-02-4.82874623E-05    3
 1.89015490E-08-3.01017276E-12 9.09950343E+03 4.50744831E+01                   4
C6H5  PHENYL RAD  T04/02C   6H   5    0    0G   200.000  6000.000 1000.       1
 1.08444762E+01 1.73212473E-02-6.29233249E-06 1.02369961E-09-6.16216828E-14    2
 3.55598475E+04-3.53735134E+01 2.10306633E-01 2.04745507E-02 5.89743006E-05    3
-1.01534255E-07 4.47105660E-11 3.95468722E+04 2.52910455E+01                   4
C6H5CO    2/25/94 THERMC   7H   5O   1    0G   300.000  5000.000 1382.000    1
 1.77196103E+01 1.59990428E-02-5.54532150E-06 8.69582681E-10-5.08335220E-14    2
 4.57408086E+03-6.82553109E+01-1.93001550E+00 6.18799970E-02-4.60916515E-05    3
 1.70133701E-08-2.49869948E-12 1.13352170E+04 3.71779131E+01                   4
C6H5O     4/26/ 0HADAD C   6H   5O   1    0G   300.000  5000.000 1401.000    1
 1.59513173E+01 1.52837431E-02-5.26838909E-06 8.22485253E-10-4.79122756E-14    2
-1.56782534E+03-6.22003421E+01-4.56101748E+00 6.98936182E-02-6.18066353E-05    3
 2.76045454E-08-4.89409696E-12 4.83671356E+03 4.55069524E+01                   4
C5H5      5/ 2/91 THERMC   5H   5    0    0G   300.000  5000.000 1403.000    1
 1.35569720E+01 1.22914133E-02-4.25209533E-06 6.65536380E-10-3.88428452E-14    2
 2.21734660E+04-5.31109915E+01-5.44117341E+00 6.32470657E-02-5.71657025E-05    3
 2.57052547E-08-4.55247216E-12 2.80395761E+04 4.64652136E+01                   4
C5H4O     3/27/95 XIAN C   5H   4O   1    0G   300.000  5000.000 1397.000    1
 1.43779472E+01 1.19184228E-02-4.19444268E-06 6.63874349E-10-3.90411169E-14    2
-3.12321247E+03-5.61146171E+01-4.15438982E+00 6.11975086E-02-5.52982224E-05    3
 2.49740399E-08-4.46438553E-12 2.68411141E+03 4.12432368E+01                   4
C5H4OH    5/ 2/91     C   5H   5O   1    0G   300.000  5000.000 1409.000    1
 1.64571358E+01 1.14589263E-02-3.86643522E-06 5.95873719E-10-3.44277590E-14    2
 9.37609019E+02-6.38874692E+01-5.73477597E+00 7.32209786E-02-6.98649600E-05    3
 3.24462652E-08-5.84437946E-12 7.50649045E+03 5.15348696E+01                   4
C4H6      4/ 4/ 0 THERMC   4H   6    0    0g   300.000  5000.000 1398.000    1
 1.11633789e+01 1.37163965e-02-4.69715783e-06 7.29693836e-10-4.23486203e-14    2
 7.79039770e+03-3.69847949e+01-1.43095121e+00 4.78706062e-02-4.15446800e-05    3
 1.91549552e-08-3.57158507e-12 1.17551314e+04 2.90825833e+01                   4
C7H13     9/11/ 3     C   7H  13    0    0G   300.000  5000.000 1390.000    1
 2.06286628e+01 2.92376417e-02-1.00059274e-05 1.55393368e-09-9.01719819e-14    2
 5.70589927e+03-8.05911711e+01-1.54565686e+00 8.07549368e-02-5.62650639e-05    3
 2.07289386e-08-3.18615282e-12 1.34892129e+04 3.86890383e+01                   4
MCH       4/22/ 4 THERMC   7H  14    0    0G   300.000  5000.000 1391.000    1
 2.14785343E+01 3.32215917E-02-1.14861934E-05 1.79638933E-09-1.04761864E-13    2
-3.04164647E+04-9.93118588E+01-8.09426478E+00 1.00736150E-01-7.00859796E-05    3
 2.48687934E-08-3.59166681E-12-1.99875643E+04 6.00729224E+01                   4
MCHR      4/22/ 4     C   7H  13    0    0G   300.000  5000.000 1386.000    1
 2.07652473E+01 3.09626852E-02-1.06426808E-05 1.65847490E-09-9.64926483E-14    2
-6.65581961E+03-9.21194389E+01-6.88013903E+00 9.11808945E-02-5.87542615E-05    3
 1.82388338E-08-2.13977403E-12 3.31407004E+03 5.77907942E+01                   4
MCH2OO    8/12/ 4 THERMC   7H  13O   2    0G   300.000  5000.000 1383.000    1
 2.58827836E+01 3.24519738E-02-1.14135201E-05 1.80554171E-09-1.06137166E-13    2
```

```
-2.71371529E+04-1.16714756E+02-6.82417761E+00 1.03611740E-01-6.86743010E-05    3
 2.19845246E-08-2.72032601E-12-1.52772798E+04 6.07675141E+01                   4
MCHOOH    8/12/ 4 THERMC   7H  13O   2    0G   300.000  5000.000 1384.000     1
 2.76662374e+01 3.02147433e-02-1.05829460e-05 1.67032446e-09-9.80560118e-14    2
-2.16774193e+04-1.24644963e+02-7.02615514e+00 1.04852686e-01-6.83054910e-05    3
 2.02241594e-08-2.06687837e-12-9.15755876e+03 6.36699862e+01                   4
MOOCHOOH  10/ 3/ 4 THERMC   7H  13O   4    0G   300.000  5000.000 1366.000     1
 3.43294088e+01 2.76848470e-02-9.93604540e-06 1.59312148e-09-9.45309022e-14    2
-4.30671915e+04-1.57671070e+02-4.23342371e+00 1.10402406e-01-7.35609590e-05    3
 2.18475735e-08-2.20234682e-12-2.91316898e+04 5.17331597e+01                   4
MOOCHO    10/ 3/ 4 THERMC   7H  12O   3    0G   300.000  5000.000 1378.000     1
 2.90497680e+01 2.96809666e-02-1.05377274e-05 1.67749776e-09-9.90421629e-14    2
-5.87922569e+04-1.30886773e+02-6.95573363e+00 1.10748964e-01-7.90481497e-05    3
 2.75519806e-08-3.79343557e-12-4.60428241e+04 6.34719691e+01                   4
C5H11CO    2/29/96     C   6H  11O   1    G   300.000  5000.000           1
 1.94783812E+01 2.50466029E-02-8.54861346E-06 1.32557944E-09-7.68503296E-14    2
-2.07923937E+04-7.21995578E+01 2.14479069E+00 6.17863563E-02-3.74134690E-05    3
 1.13283795E-08-1.36917698E-12-1.43451172E+04 2.23128045E+01                   4
C8H18     7/27/95 THERMC   8H  18    0    0G   300.000  5000.000 1396.00     1
 2.71373590E+01 3.79004890E-02-1.29437358E-05 2.00760372E-09-1.16400580E-13    2
-4.07958177E+04-1.23277495E+02-4.20868893E+00 1.11440581E-01-7.91346582E-05    3
 2.92406242E-08-4.43743191E-12-2.99446875E+04 4.49521701E+01                   4
C8H17               C   8H  17O   0    G  0300.00   5000.00  1000.00     1
 1.65781000E+01 4.79568000E-02-1.58330000E-05 2.45887000E-09-1.47904000E-13    2
-1.13886000E+04-5.77977000E+01-2.45792000E+00 1.00416000E-01-5.52412000E-05    3
 8.18171000E-10 7.48841000E-12-6.56307000E+03 3.95814000E+01                   4
C8H17OO             C   8H  17O   2    G  0300.00   5000.00  1000.00     1
 2.61790E+01   4.02621E-02  -1.21840E-05   1.77416E-09  -1.01822E-13     2
-3.13354E+04  -1.06205E+02  -1.33130E+00   1.07392E-01  -5.66082E-05     3
-2.14473E-09   8.62014E-12  -2.33465E+04   3.80377E+01                   4
C8H16OOH            C   8H  17O   2    G  0300.00   5000.00  1000.00     1
 2.59673E+01   3.94986E-02  -1.17491E-05   1.69063E-09  -9.62759E-14     2
-2.86414E+04  -1.02359E+02   4.63771E+00   7.70682E-02   5.46587E-06     3
-6.02176E-08   2.84759E-11  -2.20723E+04   1.22966E+01                   4
OOC8H16OOH          C   8H  17O   4    G  0300.00   5000.00  1000.00     1
 3.12917E+01   3.92720E-02  -1.14955E-05   1.63072E-09  -9.17048E-14     2
-4.28382E+04  -1.25286E+02   7.66149E-01   1.15621E-01  -6.49312E-05     3
 3.70399E-10   8.77610E-12  -3.41337E+04   3.41493E+01                   4
C8KET               C   8H  16O   3    G  0300.00   5000.00  1000.00     1
 2.34007E+01   4.58018E-02  -1.53548E-05   2.41072E-09  -1.46115E-13     2
-5.82798E+04  -8.43852E+01  -1.22819E+00   1.10258E-01  -6.32868E-05     3
 2.95991E-09   7.38667E-12  -5.15453E+04   4.31889E+01                   4
C6H13CO             C   7H  13O   1    G  0300.00   5000.00  1000.00     1
 1.94783812E+01 2.50466029E-02-8.54861346E-06 1.32557944E-09-7.68503296E-14    2
-2.07923937E+04-7.21995578E+01 2.14479069E+00 6.17863563E-02-3.74134690E-05    3
 1.13283795E-08-1.36917698E-12-1.43451172E+04 2.23128045E+01                   4
C8H16     7/27/95 THERMC   8H  16    0    0G   300.000  5000.000 1394.00     1
 2.56756746E+01 3.41801998E-02-1.16002952E-05 1.79195478E-09-1.03613002E-13    2
-2.62458324E+04-1.13928273E+02-2.79610447E+00 1.00836172E-01-7.12250651E-05    3
 2.60659824E-08-3.90031814E-12-1.64002496E+04 3.88854068E+01                   4
```

```
!PODE3
DMM3               C   5H  12O   4    G   298.150  2500.000 1000.000    01
 1.9899747e+01  3.9912973e-02 -1.9118063e-05  4.4929191e-09 -4.2155413e-13    2
-8.9675988e+04 -7.0685846e+01 -1.6150180e+01  2.3867562e-01 -4.2010835e-04    3
 3.5798712e-07 -1.1574661e-10 -8.4652677e+04  9.1070915e+01                  4
DMM3B              C   5H  11O   4    G   298.150  2500.000 1000.000    01
 1.6885976e+01  4.1324388e-02 -2.0654958e-05  5.0923485e-09 -5.0302753e-13    2
-6.5496155e+04 -5.0214796e+01  1.5268705e+00  1.2871427e-01 -2.0109926e-04    3
 1.6703455e-07 -5.4089407e-11 -6.3452228e+04  1.8130904e+01                  4
DMM3BO2            C   5H  11O   6    G   298.150  2500.000 1000.000    01
 2.4473306e+01  4.5892739e-02 -2.7164652e-05  7.8546091e-09 -8.9585300e-13    2
-8.9522562e+04 -9.4552796E+01  2.1309925e+00  8.9447827e-02 -1.2941324e-05    3
-6.5648336e-08  3.7244195e-11 -8.2950607e+04  2.4079063E+01                  4
DMM3_OOH3_5        C   5H  11O   6    G   298.150  2500.000 1000.000    01
 2.4849602e+01  5.6588735e-02 -3.8463450e-05  1.2083490e-08 -1.4506133e-12    2
-8.7168936e+04 -1.0452389E+02 -4.2450226e+00  1.4242685e-01 -1.2546997e-04    3
 4.3007198e-08 -2.1393463e-12 -7.9583632e+04  4.3983059E+01                  4
DMM3_OOH3_OO5      C   5H  11O   8    G   298.150  2500.000 1000.000    01
 1.3988307e+01  9.4310680e-02 -6.7482323e-05  2.1700190e-08 -2.6325162e-12    2
-1.0426262e+05 -4.4569320E+01  3.2047056e+00  1.2631886e-01 -1.1933429e-04    3
 7.2709205e-08 -2.3165685e-11 -1.0084371e+05  1.1970511E+01                  4
DMM3_KET35         C   5H  10O   7    G   298.150  2500.000 1000.000    01
 2.7335763e+01  5.0811514e-02 -3.3587285e-05  1.0325317e-08 -1.2192514e-12    2
-1.3519561e+05 -1.1583013E+02 -1.4116019e+01  1.9166882e-01 -2.0664093e-04    3
 9.7109079e-08 -1.4333133e-11 -1.2556044e+05  9.0525847E+01                  4
CH3OCOO            C   2H   3O   3    G   298.150  2500.000 1000.000    01
 5.2122772e+00  2.1084249e-02 -1.2461744e-05  3.5659004e-09 -4.0127044e-13    2
-4.4108532e+04  1.9589275e+00  2.7514800e+00  2.0098991e-02  7.1328653e-06    3
-2.3651992e-08  1.0678485e-11 -4.3097950e+04  1.6447646e+01                  4
COCOC*O            C   3H   6O   3    G   298.150  2500.000 1000.000    01
 5.5886834e+00  3.6123007e-02 -2.1421355e-05  6.0996212e-09 -6.8107806e-13    2
-6.5417405e+04  3.4337833e-01  3.1822698e+00  2.8631843e-02  1.9613409e-05    3
-4.5295558e-08  1.9601359e-11 -6.4151095e+04  1.6000165e+01                  4
CH3OCH2OCH2        C   3H   7O   2    G   298.150  2500.000 1000.000    01
 9.3491155e+00  2.5414404e-02 -1.2924765e-05  3.2615078e-09 -3.3082920e-13    2
-2.3085072e+04 -1.8940430e+01  1.4709681e+00  5.7243832e-02 -6.1378826e-05    3
 3.6009358e-08 -8.5731528e-12 -2.1508726e+04  1.9021809e+01                  4
CH3OCHO         T 6/08C  2 H  4 O  2    0 G   200.000  6000.00  1000.00     1
 6.33360880E+00 1.34851485E-02-4.84305805E-06 7.81719241E-10-4.67917447E-14    2
-4.68316521E+04-6.91542601E+00 5.96757028E+00-9.38085425E-03 7.07648417E-05    3
-8.29932227E-08 3.13522917E-11-4.55713267E+04 7.50341113E-01-4.37330508E+04    4
CH3OCO    5/ 8/ 3 THERMC   2H   3O   2    0G   300.000  5000.000 1601.000    21
 9.73659803E+00 7.42432713E-03-2.65641779E-06 4.25031143E-10-2.51824924E-14    2
-2.36015721E+04-2.36353471E+01 4.16215406E+00 1.38037511E-02-3.08486109E-07    3
-4.56430814E-09 1.46909632E-12-2.10130301E+04 8.64301044E+00                  4
!
!n-heptane
C7H16          P10/95C   7H  16    0    0G   300.000  5000.000  1391.000    1
 2.22148969E+01 3.47675750E-02-1.18407129E-05 1.83298478E-09-1.06130266E-13    2
-3.42760081E+04-9.23040196E+01-1.26836187E+00 8.54355820E-02-5.25346786E-05    3
```

```
 1.62945721E-08-2.02394925E-12-2.56586565E+04 3.53732912E+01              4
C7H15     2/10/95     C   7H  15    0    0G   300.000  5000.000  1391.000    1
 2.17940709E+01 3.26280243E-02-1.11138244E-05 1.72067148E-09-9.96366999E-14    2
-9.20938221E+03-8.64954311E+01-4.99570406E-01 8.08826467E-02-5.00532754E-05    3
 1.56549308E-08-1.96616227E-12-1.04590223E+03 3.46564011E+01              4
C7H15O2    7/23/98     C   7H  15O   2    G   300.000  5000.000           1
 2.49023689E+01 3.50716920E-02-1.20440306E-05 1.87464822E-09-1.08947791E-13    2
-2.82976050E+04-9.73923542E+01 2.37499334E+00 8.34651906E-02-5.13897320E-05    3
 1.64217662E-08-2.19505216E-12-1.99237961E+04 2.53067342E+01              4
C7H14OOH   7/23/98     C   7H  15O   2    G   300.000  5000.000           1
 2.70028807E+01 3.22272216E-02-1.09366516E-05 1.68977918E-09-9.77321946E-14    2
-2.27229231E+04-1.06332170E+02 2.49875186E+00 8.32443344E-02-4.85933986E-05    3
 1.28927950E-08-1.09878385E-12-1.36530733E+04 2.73754005E+01              4
O2C7H14OOH   7/23/98    C   7H  15O   4    G   300.000  5000.000           1
 3.23937788E+01 3.33911097E-02-1.15672104E-05 1.81146023E-09-1.05739941E-13    2
-4.36321048E+04-1.32597311E+02 3.84933185E+00 9.45955097E-02-5.94934121E-05    3
 1.78836457E-08-2.00618696E-12-3.32051631E+04 2.25912030E+01              4
C7KET     2/10/95     C   7H  14O   3    G   300.000  5000.000 1382.000    1
 2.80512936E+01 3.27356029E-02-1.14107044E-05 1.79404506E-09-1.05002142E-13    2
-5.89640173E+04-1.11392338E+02 4.19023030E+00 8.43118237E-02-5.44315814E-05    3
 1.85837721E-08-2.72768938E-12-5.00570382E+04 1.85783455E+01              4
C5H11CO    2/29/96     C   6H  11O   1    G   300.000  5000.000           1
 1.94783812E+01 2.50466029E-02-8.54861346E-06 1.32557944E-09-7.68503296E-14    2
-2.07923937E+04-7.21995578E+01 2.14479069E+00 6.17863563E-02-3.74134690E-05    3
 1.13283795E-08-1.36917698E-12-1.43451172E+04 2.23128045E+01              4
C7H14     1/ 1/95 THERMC   7H  14    0    0G   300.000  5000.000 1392.00     1
 2.10164030E+01 3.15214597E-02-1.08073947E-05 1.68040191E-09-9.75892313E-14    2
-2.12117050E+04-8.63818785E+01-1.33081497E+00 8.21082352E-02-5.49123303E-05    3
 1.94284948E-08-2.88886541E-12-1.32021384E+04 3.43549746E+01              4

END
```

C Original description of the project

Lehrstuhl für Verbrennungskraftmaschinen
Fakultät für Maschinenwesen
Technische Universität München

Untersuchung von Reaktionsmechanismen zur 3D-CFD Verbrennungssimulation

Master-/Diplomarbeit (theoretisch / simulativ)

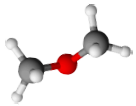

Dimethylether (DME)

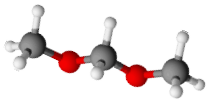

Oxymethylenether 1 (OME1)

Für die Berechnung der Verbrennung von Dimethylether (DME) und Oxymethylenether (OME1) sollen verschiedene reaktionskinetische Modelle aus der aktuellen Literatur verglichen und auf die Anwendung am Lehrstuhl abgestimmt werden. Insbesondere das Zündverhalten und die Abbildung der Emissionsentstehung stehen dabei im Vordergrund. Außerdem sollen Methoden zur Reduktion der Rechenzeit untersucht werden.

Zum Arbeitsumfang dieser Arbeit gehören:

- Einarbeitung in die 0D/1D Berechnung von Reaktionskinetik
- Einarbeitung in die 3D-CFD Simulationssoftware
- Erstellen eines reduzierten Zündmodells für DME & OME1
- Berechnung, Auswertung und Darstellung der Simulationsergebnisse
- Sorgfältige Dokumentation der Ergebnisse

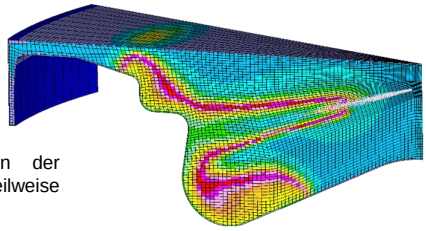

Temperaturfeld im Brennraum während der Verbrennung

Die Arbeit sollte hauptsächlich im Motorenlabor des Lehrstuhls in der Schragenhofstraße durchgeführt werden, nach Abstimmung ist auch eine teilweise Bearbeitung von zu Hause möglich.

Beginn: ab sofort / nach Absprache

Kontakt: Kai Gaukel, M.Sc. Tel: 089-289-24108 gaukel@lvk.mw.tum.de

Kai Gaukel, M.Sc. | Lehrstuhl für Verbrennungskraftmaschinen | Technische Universität München